



Master's Degree program
in Conservation Science and
Technology for Cultural Heritage

Final Thesis

Additive Manufacturing and Cultural Heritage:
chemical-mechanical characterisation and environmental sustainability
assessment of 3D printed Polylactic Acid treated with cold plasma source
at atmospheric pressure.

Supervisor

Ch. Prof. Elisabetta Zendri

Assistant supervisor

Dr. Dafne Cimino, PhD

Dr. Silvio Cristiano, PhD

Graduand

Veronica Monti

Matriculation Number: 855082

Academic Year 2020/2021

A Filippo, Virginia ed Emiliano

Aim of the thesis	6
Introduction	9
Chapter 1	12
1.1 Technologies for digital manufacturing	13
1.1.1 Additive techniques	14
1.1.2 Subtractive techniques	18
1.2 Advantages and disadvantages of Additive Manufacturing	20
1.3 Materials for 3D printing	21
1.3.1 Polymers and biopolymers	21
1.3.2 Printing materials	22
1.4 3D printing in Cultural Heritage	27
1.5 Plasma technology	29
1.6 Atmospheric plasma sources	32
1.7 Atmospheric pressure cold plasma technology and 3D integration in Cultural Heritage	37
1.8 Life Cycle Assessment	40
Chapter 2	43
2.1 Materials	44
2.1.1 Samples	44
2.1.2 Plasma torch	46
2.2 Methods of investigation	48
2.2.1 Attenuated Total Reflectance - Fourier Transform - Infrared Spectroscopy (ATR-FTIR)	48
2.2.2 Raman Spectroscopy	53
2.2.3 Thermogravimetric analysis (TG) and differential scanning calorimetry (DSC)	55
2.2.4 Colorimetric measurements	57
2.2.5 Accelerated ageing	58
2.2.6 Acid attack resistance tests	60
2.2.7 Dynamometric tests	62
Chapter 3	64
3.1 Filament and samples characterization	65
- ATR-FTIR Spectroscopy	66
- Raman Spectroscopy	68
- TG-DSC	70
- Colorimetric measurement	74
- Dynamometric tests	75
3.2 Accelerated ageing	78

- ATR-FTIR spectroscopy	78
- Raman spectroscopy	83
- TG-DSC	85
- Colourimetric measurements	87
3.1.6 Acid attack resistance tests	92
3.1.7 Dynamometric tests	94
Chapter 4. Life Cycle Assessment	100
4.1 Comparison between two case study	100
4.1.1 Unit function of the system	100
4.1.2 Boundaries of the system	100
4.2 Life Cycle Inventory	104
4.3 Life Cycle Impact Assessment	109
4.4 Life Cycle Interpretation	118
Chapter 5. Conclusion	120

Aim of the thesis

Three-dimensional fabrication and digitization of artefacts have opened new frontiers in the field of conservation, restoration and fruition of Cultural Heritage. These technologies are becoming valid alternatives for the accurate manufacturing of replicas of works of art or duplication of parts of them. Among the printing materials used for this purpose, poly-lactic acid (PLA) is often employed; it is a biodegradable thermoplastic polymer derived from the fermentation of natural products particularly rich in starch. It is a material that can be used not only for integrations within restoration treatments but also for the creation of pieces of contemporary art and objects with exhibition purposes, such as those located along inclusive museum paths. The use of 3D scanning technologies makes it possible to reproduce works of art and monuments to scale, providing an effective educational tool for didactic workshops, ensuring museum accessibility and learning opportunities for all categories of visitors. In fact, 3D printing makes to adopt solutions that foster direct contact with the artefact by visitors possible.

PLA is a polymer which, also for these reasons, has been the subject of much interest in recent years. Numerous studies have been conducted on its mechanical and chemical stability, the transformations that it can undergo when subjected to different environmental conditions and the processes to which it can be subjected to implement its properties.

This thesis aims at studying the behaviour of a promising material used in 3D printing, called ‘neutro-opalino’, based on PLA. The research will chemically and mechanically test it before and after accelerated ageing simulating outdoor conditions, the most critical environment where a 3D- print object made of a biodegradable material might be located. The treatment with a cold plasma source at atmospheric pressure will be evaluated as a possible way to improve its properties, thus its resistance outdoor. Concerning new technologies and new art materials, it is crucial to understand the extent of their impact on the environment, determining whether and how much it is worth using innovative digital technologies rather than traditional and established methods for the same case. For this reason, an evaluation in terms of sustainability (LCA) of the material under examination was performed, treated with atmospheric plasma technology, considering it in a generic case of integrative restoration and

placing its impact in relation to that given by some traditional materials commonly used for the realization of casts and artistic integrations, such as Araldite[®], epoxy resin and silicone rubber.

Introduction

3D reproduction technologies have been widely used for many years, especially in various fields of science and industry, but only recently they have moved from purely industrial use to the general public of makers and enthusiasts. Since 2009, with the expiry date of the patent on FDM technology (which will be largely introduced in the following pages), the cost of 3D printers has fallen considerably, making them, together with the materials used for 3D design, affordable.

An important factor in the spread in Italy of 3D printing has been the creation of FabLabs: laboratories open to the public with the needed equipment for digital fabrication, where ideas can be transformed into prototypes and concrete products [2].

In the field of Cultural Heritage, these technologies have spread as well, and are becoming valid alternatives not only for the integration of missing parts of art objects but also for the creation of replicas and for the creation of museum itineraries able to involve and facilitate the education of all users' categories.

Given the exponential increase in the application of these particular technologies in the conservation and restoration of works of art, many companies are working to adapt their expertise to the Cultural Heritage sector and implement their potential. However, despite possible applications and the encouragement given by various international organisations, the systematic use of 3D printing techniques in the field of Cultural Heritage has not yet become a widespread approach. There are several reasons, the most frequent being the preference for more traditional or established materials and methodologies, such as plaster casts with the addition of an acrylic binder and the difficulties given by the transposition from two-dimensional to three-dimensional level for 2D objects, like photographs and drawings.

In this context, digital technologies offer interesting solutions for the reproduction of 2D artworks using 3D printing techniques.

A suggestive example is the self-portrait of Rembrandt van Rijn, a Dutch painter who died in 1669. This painting was created, thanks to the collaboration of various professionals, including art historians and developers, through the computer analysis of all 346 paintings of the artist. The algorithm formulated allowed to identify the executive aspects of Rembrandt's

technique and to reproduce, using a 3D printer, all the surface characteristics of the paintings, such as the orientation and thickness of the brushstrokes [1].

Despite the reasons that may lead a user not to use digital technologies, the contribution that these can bring to the conservation, restoration, use and valorisation of a work of art is considerable; in fact, these are areas that have obtained multiple benefits from recent advances, increasingly experimenting and applying solutions borrowed from disciplines in other scientific sectors [2].

First, conservation and restoration should aim at a technological and scientific improvement of traditional methods of intervention, that up to now have provided, for the reproduction of artistic artefacts, the creation of moulds (often with silicone materials), on a 1:1 scale, lately used for the creation of plaster or resin copies. These are undoubtedly lengthy manual processes that are strongly influenced by the complexity of the shape of the work of art and sometimes risk to damage surfaces that are already considerably compromised [3]. 3D manufacturing technologies allow copies to be made on any scale and in a few hours, but it also provides an accurate image of the surface conformation using laser scanners; this methodology projects a blade of light onto the object for reconstructing it in the three-dimensional model based on the deformation the light underwent on the target surface. This method has a considerable advantage: it is non-invasive - meaning that it does not come into direct contact with the work, thus it allows even soft, fragile and small objects to be detected [4].

Enormous progress has been made not only in terms of instrumentations but of materials too. Research into polymers to be used with 3D printers is in rapid and continuous evolution.

One of the most widely used thermoplastic polymers used in 3D printing is poly-lactate (PLA), a material derived from plants such as corn, wheat or beet, naturally rich in starch. The latter is converted into lactic acid through a fermentation process and then into a polymer. PLA is a high- quality bio-plastic with excellent physical and mechanical properties and products are fully biodegradable material once used, this only if the polymer has not been loaded with additives that cannot be composted.

Given the brief introduction and the purpose of the research , this thesis will consist of four main sections:

- an overview of the different 3D printing technologies and materials (§ Chapter 1);
- the description of the experimental part aimed at determining the chemical and mechanical properties of neutro-opalino, the thermoplastic polymer selected for the study (§ Chapter 2);
- the evaluation of the results obtained together with considerations about the stability of the material and the effect of a surface and inter-layers treatment to improve it (§ Chapter 3);
- the evaluation of the sustainability of the application of 3D-printing technologies to the conservation field through LCA assessment (§ Chapter 4).

Chapter 1

1.1 Technologies for digital manufacturing

Digital fabrication is a design and manufacturing workflow in which digital data directly guide production tools to create the geometries of objects. Digital fabrication processes consist of three steps: the first, also known as 'design' involves input data being formulated by CAD (*Computer-Aided Design*), software which allows the creation of a virtual model of a specific design; after that, 'preparation' takes place, with the definition of production parameters and specific machine settings; finally with the conclusive step, known as 'manufacturing', the object is created: the data processed in the first phase is transferred to the CAM (*Computer-Aided Manufacturing*) software that gives directions and guides the processes of a specific machine, such as a 3D printer [5,6].

The term *3D Printing*, or *Additive Manufacturing*, refers to any robotic process in which a digital model is transformed into a solid three-dimensional object by the deposition of superimposed layers. The actual printing process starts with the construction of the support layer and, on top of this, all the others. Once the last one is complete, the overlapping of all layers has generated the desired object.

The production of solid 3D objects can be done either through 'additive' or 'subtractive' techniques. Additive manufacturing allows the creation of an object by superimposing multiple thin layers of material. The existing additive techniques differ according to the way the layers are deposited and the material that can be used. The main advantages of additive manufacturing are:

1. possibility of making truly complex and detailed shapes without the use of moulds or equipment, such as mills or cutters (which are necessary for subtractive manufacturing);
2. minimal material waste with, as a consequence, lower costs;
3. wide availability of materials, such as metal, ceramics, resins and polymers;
4. the objects produced do not, in most cases, require further finishing;
5. it uses less energy than subtractive production.

Subtractive techniques, on the other hand, are more specifically concerned with rapid prototyping techniques: automated production processes that allow solid 3D prototypes to be

produced quickly and efficiently by mechanically removing material from a block according to a 3D CAD file [7]. The most common technologies of this type are numerically controlled milling machines and laser cutters.

1.1.1 Additive techniques

Since the official birth of additive manufacturing, in 1982, a variety of different techniques have been developed. Each has several characteristics that make it different from the others, the most important of these include: the materials used for the printed component, the materials needed for the substrates, tolerances and surface roughness of the printed component, maximum printing volume and the ability to make final parts or just prototypes.

The strength of this methodology is the ability to go directly from CAD modelling to the production of the finished product, reducing time and costs not only of design but also of shaping and eventual assembly, which are necessary with traditional production processes. All this with a small number of operators. Additive manufacturing, therefore, develops in the same direction as the market demands, allowing the realisation of geometries that were previously unfeasible or difficult to realise and representing the best choice in the case of the production of complex and customised objects [8].

Depending on the technology, the 3D printer can deposit material, selectively melt and sinter powder or semicrystalline materials or polymerise liquid photopolymers.

Three types of processes can be distinguished: liquid-based, in which a resin is cured when exposed to an ultraviolet light source; solid-based, in which the material, whether molten, passes through the printer nozzle and start to solidify once deposited; and powder-based, in which a metal powder, arranged in a horizontal plane, is melted by lasers or electron beam in certain strategic areas, where compact material must be obtained for the construction of the three-dimensional component.

Based on these deposition techniques, we can distinguish different additive technologies.

Among the **liquid-based processes**, for example, are the following printing techniques:

- *StereoLithography Apparatus (SLA)*: a technology patented in the 1980s, which allows objects to be created thanks to photopolymerisation of the liquid resins used for printing; the process is promoted through the induction of energy emitted by sources of electromagnetic radiation, such as UV light. While maintaining the same basic concept of layer-on-layer printing, SLA technology can work in two ways: i) the first consists of progressively immersing the print base in the liquid resin to allow the laser to solidify the various layers of the product. Once the first layer has been created, the print base is lowered sufficiently for the object to be covered by the liquid resin; the laser then proceeds to print a new layer in contact with the first. ii) in the second method, the liquid material is collected inside a transparent containment tray, which delimits the working space of the machine. The ultraviolet laser is then positioned at the bottom and strikes the resin upwards, exploiting the transparency of the bottom of the tray. The resin solidifies on a platform positioned in the tray, which is then lifted so that the second layer can be created. Basically, while in the first method the laser at the top creates the layers by moving the part downwards, in the second method the process takes place with a laser positioned at the bottom solidifying an object that is progressively raised [9]. To obtain high-quality products, the size of the laser is important, since the smaller the diameter of the beam, the greater the precision. In fact, if the laser is not focused the quality of the product will suffer, since the resin will be well solidified where the laser is focused, but will be surrounded by a soft, less solid part where the laser cannot initialise the polymerisation providing enough energy [9,10]. It can be used to fabricate highly complex geometries. In addition, the material is no longer limited to conventional polymers, but it is possible to manufacture composites [11], as well as metallic [12] and ceramic [13] objects. In fact, the resins for SLA all have the same essential components, such as liquid precursors (substances that form the network when polymerised), photoinitiators (that initiate the reaction), hardeners (that catalyse the reaction and increase its speed accordingly), additives (such as thinners, surfactants or other stabilisers) and fillers (such as ceramics, metals and composites) [10]. However, it is a technology with lower printing time but higher costs;

- *Polyjet or Multijet (PJM/MJM)*: is a 3D printing technology which produces smooth and accurate objects with microscopic layer resolution and accuracy down to 0.014 mm [14]. Liquid photopolymers are layered by a printhead with one or more nozzles onto a build platform and then cured by irradiation with UV lamps. During this process, the printhead moves over the platform along paths predefined by a CAD model until a layer is printed. UV lamps are positioned directly on the printhead so the polymerisation starts as the resin has been applied. The intensity of the UV light is regulated in such a way that it does not completely harden the top layer, thereby creating a stable adhesion between the superimposed layers. As soon as the last layer has been printed, the UV lamps are passed over the entire object several times to complete the curing [15,16,17];
- *Digital Light Processing (DLP)*: this is a technique very similar to SLA, in which resins are polymerised by light but, in this case, the source is a LED or LCD projector. Machines using this printing solution are cheaper than stereolithography machines but cannot achieve comparable degrees of accuracy [18].

The **solid-base processes**, on the other hand, include technologies like:

- *Fusion Deposition Modelling (FDM) or Fused Filament Fabrication (FFF)*: it is a 3D printing technique that uses a continuous filament of thermoplastic polymer that is heated and deposited, layer by layer, onto a printing platform, to create an object. The main materials used include: ABS (acrylonitrile butadiene styrene), PLA (polylactic acid), PC (polycarbonate), PET (polyethylene terephthalate), TPU (thermoplastic polyurethane) and polyamide (known as Nylon). Having linear, non-cross-linked and poorly branched polymer chains, these materials have low softening temperatures and are excellent candidates for additive manufacturing.

The choice of the most suitable polymer depends on the type and characteristics of the object to be produced. It is therefore important to consider certain properties of the printing material, such as:

- *adhesion capacity between layers*: a measure of the ability of adhesion between different printing layers;
- *elongation at break*: maximum elongation of the material before breaking;

- *ease of printing*: measure of the difficulties encountered in printing the material (adhesion to the printing surface, maximum printing speed, accuracy, ease of loading, etc.);
- *visual quality*: related to the surface finishing and printing accuracy;
- *mechanical strength*: maximum load that the material can withstand before breaking;
- *heat resistance*: maximum temperature the object can bear before softening.

The material sold as filament collected in spools is pushed towards an extruder by gears or rollers; here it enters the heating chamber where its viscosity decreases enough to be directed towards a heated nozzle, with a smaller diameter than what was at the beginning. Once pushed out of the nozzle the polymer will have the appearance of a thin and viscous wire and will be deposited on a horizontal work surface. The laying of the material is a computerised process in which the nozzle is moved in both directions of the horizontal plane to build up the first layer of the object to be made by depositing the filament. Then the moulding platform is lowered and the process is reiterated to continue with the laying of the next layers [19].

The system continuously regulates the heat of the heating chamber by a thermal sensor located at the end of the extruder, that measures the difference between the desired and measured temperature values. The nozzle melts and keeps the material at a temperature just above its melting point so that once printed it solidifies immediately. This allows the material not to drip when deposited as solidification is almost instantaneous [20]. The main advantages of FDM/FFF are the low cost required as well as the simplicity and speed of the process. The costs of the machines can vary considerably depending on the degree of precision and quality that is desired. One disadvantage of the process is the generally low surface finish, which is closely related to the height and thickness of each deposited layer;

- *Laminated Object Manufacturing (LOM)*: rapid prototyping technology in which, during the printing process, layers of laminates of paper, plastic or metal are joined together by heat and pressure and then cut into the desired shape with a computer-controlled laser or blade. It is certainly not the most popular method of 3D printing, but it is one of the cheapest and fastest. The cost of printing is low because of cheap raw materials [21].

Among the **powder-based processes** are instead the following printing techniques:

- Selective Laser Sintering (SLS): unlike SLA technology, it does not start with a liquid photopolymer, but with an ultra-fine powder that can be a thermoplastic polymer or a metallic or ceramic material. During the printing process, a layer of powder is spread out and carefully rolled to create a uniform plane. Immediately afterwards, a laser provides the heat necessary where needed for the fabrication of the component, melting (in the case of thermoplastic polymer powders) or sintering (in the case of metal or ceramic powders). Finally, the build platform is lowered by the thickness of one layer and the process begins again [21,22]. The process is repeated until the last layer of the 3D model has been printed. Layer thicknesses are between 0.05 mm and 0.15 mm, depending on the resolution and the implant. The powders typically used can be ABS, Nylon, PVC, waxes and epoxy resins, as well as different types of metals, such as titanium, aluminium, magnesium and zinc [23];
- Direct Metal Laser Sintering (DMLS) and Selective Laser Melting (SLM): method by which metal powders can be melted and very high-density objects obtained. This technology, therefore, does not sinter but melts the metal powders into a solid, homogeneous mass using a very high-power laser, according to the 3D design entered. The operating scheme is almost entirely similar to that of the SLS [24, 25];
- Electronic Beam Melting (EBM): it is a technology whereby a high-energy source, consisting of a sufficiently concentrated and accelerated beam of electrons, strikes a material in micro-grain form, causing it to melt completely. This method can produce metal objects with an even higher density than SLS, which uses a high-power laser. It is not a particularly popular additive manufacturing technology, as it is slow and expensive [26,27].

1.1.2 Subtractive techniques

Nowadays, subtractive manufacturing processes mainly involve the use of CNC (*Computer Numerically Controlled*) equipment, in which the object is produced by controlled mechanical processing of material in the form of solid blocks – such as hard thermosets, thermoplastics (like polystyrene), metals, wood, glass and others - that are shaped by the removal of the outer material by cutting, drilling or grinding [28]. Subtractive manufacturing processes are ideal

for applications that require tight tolerances and geometries that are difficult to recreate. Unfortunately, CNC machines present a non-negligible number of geometric and kinetic constraints, mainly due to the tips used for engraving and the limited movements of the mechanical arm they are anchored to, making the use of this technology in Cultural Heritage not particularly widespread. To overcome these issues, more complex machines have been developed, with five or six axes, to acquire greater freedom of movement and recreate objects with more complex conformations, albeit with more delayed times and higher costs [29]. Subtractive production techniques are also expensive, because of the large amount of waste material that is taken away from the starting block [30,31].

Subtractive manufacturing encompasses a wide variety of process methods and materials. Lighter materials are much easier to mould than heavier ones; however, because of their fragility and lightness, usury will inevitably be faster.

Other subtractive manufacturing processes involve, for example, the use of:

- *Electrical Discharge Machining (EDM)*: an established machining technology to produce geometrically complex objects or parts made of hard materials that are particularly difficult to machine with conventional manufacturing processes, such as metals. It uses thermal energy to machine electrically conductive parts, regardless of their hardness [32];
- *Electric Water-jet Cutting Machining (EWCM)*: cutting technology that uses an ultra- high-pressure water jet to cut a wide range of materials, with thicknesses up to about 150 mm (15 cm), with high cutting precision. The pressure applied to the surface of the material determines the depth of the cut [33];
- *Laser Beam Machining (LBM)*: technology in which a laser beam interacts with the material to be processed. The laser beam is focused to melt and vaporise the unwanted material from the parent one. This technique is suitable for cutting geometrically complex profiles and it can be applied to a wide range of hard materials, such as metals and alloys [34].

1.2 Advantages and disadvantages of Additive Manufacturing

Each additive manufacturing method has its advantages and disadvantages, that depend on the specific characteristics of the production process itself, but, when compared to traditional techniques, several benefits and limitations can be identified within the category as a whole.

Among the main advantages there are:

- the possibility of making unlimited shapes with a single machine overcomes a great limitation, typical of moulding, where it is necessary to use a mould for each geometry to be obtained;
- the absence of tools or clamping systems, which are necessary for traditional machining techniques;
- the transition from the fabrication of one element to another is very short. This means that there is no downtime and production is optimised [35];
- operator intervention is minimal and specifically concerns the pre- and post-machining phases. This means that the operator can be occupied with other tasks during machining;
- the production time and cost depend mainly on the size of the object and not on its geometric complexity. In traditional techniques, however, the cost increases exponentially as the geometric complexity increases [36];
- high product customisation is an increasingly popular feature of the consumer market, and with 3D printing it is possible because, to produce different elements, it is enough to have the CAD model, without the need to change machine or machining equipment [37].

However, there are still several limitations associated with these innovative technologies, such as:

- the dimension of the objects to be produced is closely related to the size of the machine and the work volumes. A technique that makes it possible to exploit all the space made available by the machine is the Selective Laser Sintering technique, which can exploit the entire working volume [38,21];
- each machine is able to use a limited range of materials, thus limiting its production flexibility;

- the need to insert support structures to enable the object to be manufactured, especially if it has a complex geometry: this generates, in the areas of contact between the support and the piece, greater surface roughness and a subsequent treatment process to divide the two elements [39];
- the surface finish varies according to the different techniques, materials used and machinery, and post-treatment may therefore be necessary.

1.3 Materials for 3D printing

1.3.1 Polymers and biopolymers

Polymers are high molecular weight macromolecules made up of many structural units, called ‘monomers’, joined together by covalent bonds to form long chains that are linear, branched or cross-linked.

Depending on their origin, polymers can be classified as natural and synthetic. Natural polymers, also called ‘biopolymers’, are biological macromolecules that derive from living organisms. Synthetic polymers, on the other hand, consist of macromolecules produced through chemical reactions from monomers derived from hydrocarbons.

The term ‘biopolymer’ and ‘bioplastic’ are often mistakenly associated with the same type of material. The term ‘biopolymer’ refers to a material that is entirely bio-based and biodegradable. The term ‘bioplastic’, instead, does not necessarily refer to polymers derived from renewable and biodegradable sources but has a much broader meaning [40]. In fact, according to the *European Bioplastics*, the association representing the interests of the bioplastics industry in Europe, the term bioplastics refers to three families of polymers (Figure 1) [41]:

- polymers derived from renewable and biodegradable sources;
- polymers derived from renewable sources, but not biodegradable;
- polymers derived from non-renewable sources, but biodegradable.

Degradation is an irreversible process due to modifications in the structure of the material, commonly characterised by the loss of certain properties, such as integrity and mechanical strength. The rate of degradation depends on the environmental conditions where the material is placed and can occur in different ways: through exposure to UV-light - with the sun as the major source - (photo-degradation), mechanical stress (mechanical degradation), temperature changes (thermal degradation), oxygen (oxidative degradation), water which promotes hydrolysis reactions (hydrolytic degradation), or microorganisms and enzymes (biodegradation).

The norm UNI EN ISO 14855-2:2018 states that a biodegradable polymer is designed to undergo changes in chemical structure due to living organisms such as bacteria, fungi and algae, resulting in the loss of certain properties [42].

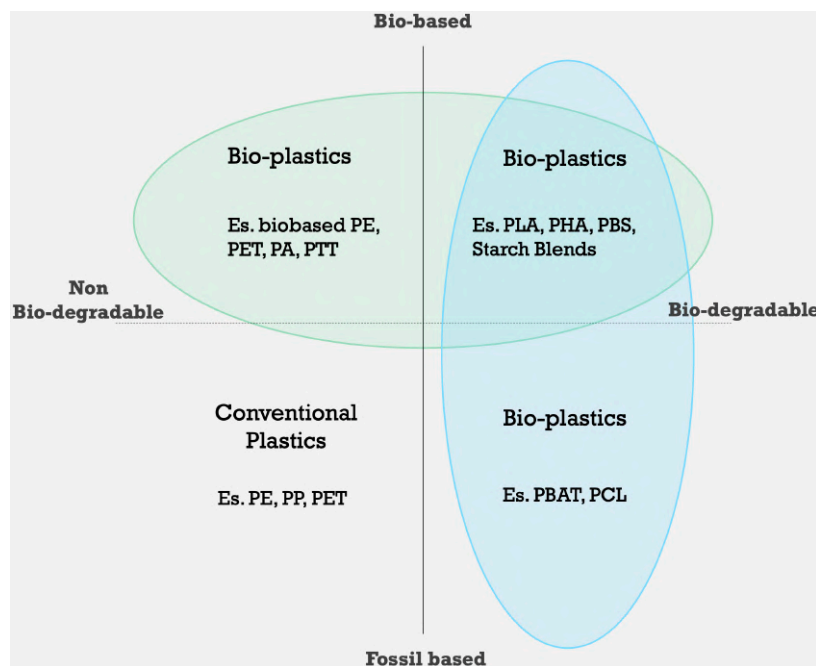


Figure 1. Bioplastics classification [40].

1.3.2 Printing materials

Nowadays, with the help of chemistry, a wide range of 3D printing filaments for the FDM technology is available on the prototyping market, differing not only in their constituent materials but also in their properties. The resulting quality of a 3D printed object varies

considerably depending on specific parameters that are essential to consider, such as resistance, durability, aesthetic performance and the need for post-processing after printing [11,39,43].

After years of intensive development, a wide range of materials possesses the required characteristics and properties to produce geometrically complex objects; materials that are available in different forms, such as powder, filaments, pellets, granules, resins, etc [44].

Some examples of the most commonly used materials in different additive manufacturing technologies are:

- **Polymers:** for additive manufacturing processes, polymeric materials can be used to produce objects with different printing techniques, such as SLA, SLS, MJM, and FDM. The most used are:

- *PLA*: polylactic acid, with chemical formula $(C_3H_4O_2)_n$, is a biodegradable polyester made from renewable sources (e.g. starch), that make it a viable 'bio' or environmentally friendly alternative to other synthetic polymers traditionally used [45].

PLA is produced by the polymerisation of lactic acid, a carboxylic acid that is easily available in nature and can be obtained by the fermentation mainly of corn, but also sugar cane and wheat [10]. It is a semicrystalline polymer that melts and reaches a low viscous state at a temperature of around 50÷60°C. It is, in fact, one of the easiest filaments for printing and is in some ways the precursor of materials for 3D printing. From the point of view of the performance, PLA is a material that adheres very easily to the work plane and the object surface can be finished with simple sandpaper. Over the years, 3D filament manufacturers have made several variants available on the market, both in terms of colouring and composition, as PLA can be enriched with additives and other materials as filler to confer peculiar aesthetical features, such as wood, marble or bronze powder. Once ground, the object takes on a slightly dull colour but regains its lustre when brought to extrusion temperature with a small flame and blowtorch. The extrusion temperature can vary between 190÷230°C. However, being a semicrystalline polymer, PLA does not enjoy great mechanical strength and its melting temperature is around 130÷180°C. This bioplastic is also biodegradable and

compostable, so it degrades rapidly once the necessary temperature and humidity conditions have been reached [43]. Once printing is complete, it is, therefore, advisable to store the spool of filament in a dry environment, at room temperature and away from direct sunlight. Table 1 summarises the optimal printing settings for a PLA filament.

Table 1. Optimal printing settings for PLA [43].

Aspects of printing	Optimal values
Nozzle temperature	200°÷230°
Print bed temperature	105°÷110°
Materials printing plate	Lokbuild, BuildTak, Blue tape
First layer speed	15÷20 mm/s
Printing speed	60÷90 mm/s
Retraction	0.8÷1.2 mm
Cooling fan	No
Printing chamber	Closed

- **ABS**: Acrylonitrile Butadiene Styrene, with chemical formula $(C_8H_8 \cdot C_4H_6 \cdot C_3H_3N)_n$, is one of the most popular thermoplastic materials for makers, but also one of the most difficult to achieve the right balance of print settings. It is a non-biodegradable material with considerable elasticity, flexibility and very good mechanical properties, that allow it to be used in the manufacture of durable parts requiring high resistance to impact and wear [44, 46]. It has good aesthetics - it can be painted and smoothed - and can withstand temperatures up to about 85°C without deformation or degradation. The extrusion temperature can vary between 240 and 260°C [47]. It is also resistant to water, aqueous salt and alkaline solutions, diluted acids, saturated hydrocarbons,

petrol, mineral oils, animal and vegetable fats. It has also sufficient resistance to ageing, but is not resistant to concentrated mineral acids, aromatic and chlorinated hydrocarbons, ethers and ketones. It is not an easy material to print because during the cooling phase it undergoes considerable deformation and requires finishing by solvents, including flammable ones, such as acetone. One of the undesirable effects most feared by makers: the *warping effect* [43].

This is a phenomenon in which the object being printed, especially if it has a large base, gradually bends due to a too fast-cooling step. The only solution to counteract this phenomenon, which inevitably compromises the printing, is to use ABS with a low warping rate and closed-chamber and temperature-controlled printers. Its characteristics make it suitable for the manufacture of small parts or for creating products that are resistant to impact and wear [44,48].

- *Nylon*: polyamide (PA) with chemical formula $C_{12}H_{22}N_2O_2$; is one of the most widely used and studied polymers in the SLS process, because it melts and binds to the laser better than other polymers. It is wear-resistant, elastic and colourable. When moulded, if it is used for thin structures, it is flexible, while, if thicknesses are increased, it increases in strength and robustness [49];
- *Thermoplastic elastomers*: another category of product, popular since the early 1950s, and they consist of a mixture of rubber and hard plastic [50]. Elastomers, in general, have excellent adherence to printing planes; in fact, objects can be created directly on the plane at temperatures between 230 and 250°C. Another characteristic that should not be underestimated is the resistance to impact and wear that this category of products presents, since they are essentially rubbers and, for this reason, very elastic. In fact, the moulded object allows it to be crushed and pulled without suffering persistent damage. However, if ABS is a difficult material to print - it requires a lot of care - elastomers are even more difficult, as they are extremely soft and difficult to introduce and control in the hot chamber of the nozzle [47]. Another particularly common problem with elastomers is stringing, which is generally due to an excessively high printing temperature that makes the material too liquid and causes it to run during extruder service movements;
- *PET (or PETG)*: polyethylene terephthalate (or polyethylene terephthalate glycol-modified), with monomeric unit $(C_{10}H_8O_4)_n$, is a member of the polyester family and is a thermoplastic resin. It is used for its chemical resistance, high-temperature

performance and rapidity of moulding. It decomposes at temperatures of 340°C, then it is processed at lower temperatures, specifically between 230 and 260°C. It is a fairly rigid and impact-resistant material [51];

- *PC*: polycarbonate is a thermoplastic resin. It has high tensile and flexural strength, making it ideal for complex prototypes, tools and elements. It is commonly used as an electrical insulator, used in many medical applications and for mechanical parts. It offers precision, durability and stability, creating parts that are also highly resistant to heat. It therefore has mechanical properties superior to ABS and most other thermoplastics. It is not brittle and if it is bent it tends to flex and deform like hard rubber until it breaks. The extrusion temperature is very high, from 240°C to 285°C, and it absorbs external moisture to an exaggerated degree [52];
- *TPU*: thermoplastic polyurethane has remarkable properties, such as elasticity, transparency and resistance to abrasion and cuts. It is moulded at high temperatures, which are between 240°C and 260°C [52];
- *PVA*: Polyvinyl Alcohol is a water-soluble material. It is generally used as a support material in dual extruder printers. The primary extruder deposits the material with which the object will be built, while the secondary extruder deposits PVA in the areas where support is needed. The extrusion temperature is in the range of 180 to 200°C [46,52];
- **Metals**: The variety of metals that are used in additive manufacturing is growing over time. While the first ones were aluminium, bronze and stainless steel, gold and silver have recently joined this group, with the resulting applications in the jewellery sector [44];
- **Ceramics**: they are mainly used for their resistance to high temperatures. However, this type of material is very brittle and this property does not make it the ideal choice in the construction of products with complex geometries. Alumina, Silica and Zirconia are the main materials used;
- **Other compounds**: these are heterogeneous materials, i.e. made up of two or more phases with different physical properties, which are much better than those of the constituent phases. Composite materials used in 3D printing are, for example, carbon and glass fiber [54].

1.4 3D printing in Cultural Heritage

Nowadays, more than ever before, Cultural Heritage is being redefined, no longer as the exclusive domain of scholars and professionals, but rather as a resource for the economic development of local communities, a way to rediscover one's cultural identity, a valuable educational tool, and much more. For this reason, great attention is currently being paid to digital technologies, such as virtual reality, rapid prototyping, three-dimensional models made with laser scanners, digital photogrammetry, photomodelling and 3D reconstruction, 2D virtual restoration and cataloguing, and digitisation for the online accessibility of archival heritage.

These new tools help scholars to manage and analyse scientific data and also allow the general public to have a better understanding of the past through interactive installations and highly realistic virtual environments [55]. Despite the initial difficulties in their introduction and diffusion, mainly due to high costs, and low-performance devices, scanning, modelling and 3D printing technologies have become a powerful tool to present and analyse works of art in virtual locations, such as the web, and real places, such as museums [56].

The main application of rapid prototyping is the production of copies that are very faithful to the original. More specifically to the world of Cultural Heritage, these copies can be useful as follows:

- I. *permanent or temporary replacement of original works of art*: a copy can take the place of any artefact which, for any reason, has been removed from its original location. The substitution can be temporary (limited, for example, to the duration of its restoration or loan) or permanent (to prevent the artwork from degradation or avoid further damage to an artefact already seriously compromised). In this way, the visitor can appreciate the work in an arrangement specifically designed and created to house it and, at the same time, the original is preserved, protected or restored [57];
- II. *educational paths and support for blind and visually impaired people within museums*: the opportunity offered by replicas is to make a tactile experience possible, which is rarely allowed to the general public for conservation and preservation reasons. Many museum institutions have chosen to make use of replicas, designed to enrich the

museum experience of visually impaired people [58]. The creation of replicas gives to these people a useful tool for mentally visualising works of art, because, by touching the replicas, they can perceive the surface conformation of the work, possibility that is often precluded in the case of original works [4,19,55]. Touch, in fact, is the sense that underpins learning, providing, together with the other senses, a multi-sensory experience that can promote knowledge [57,59];

III. customised packaging for safe transport of works of art: an important aspect that should not be underestimated is that one linked to the storage, exhibition and transport of particularly fragile artefacts [57,60]. The errors that can be made, for example, in measuring the size of the object, in the production of the packaging or in the tests to verify its effectiveness, are eliminated by a computerised process that, starting from a 3D digital model, produces a customised packaging. When it comes to the creation of specially designed artwork locations in museums, 3D printing is particularly effective and versatile;

IV. acquisition of artefacts: 3D digital models, which can be obtained by manual modelling using CAD software or by laser-scanning, are important not only for digitising heritage and enriching digital archives but also as a support for studying the artefact itself. Indeed, these technologies let interacting directly with the high-resolution 3D model and, simultaneously, to consult the documents associated with it [3];

V. support for restoration: another less common application, but equally important, is the use of digital fabrication technologies to aid the restoration. Many sculptures and objects of art have come down to us with numerous missing parts; gaps that can make the work difficult to be interpreted by the viewer can be replaced by artificial copies to fully explain to the public what the original structure looked like [57,61]. Also in this case 3D printing can intervene brilliantly, allowing to recreate the missing parts, even with particularly complex geometries. In this way, the visitor can see the work of art as a whole [61].

1.5 Plasma technology

To better understand how plasma can improve the surface characteristics of a material, it is first necessary to understand what it is. The following paragraphs define the characteristics and properties of the different types of plasma, as well as the different sources and instruments available on the market.

Plasma is a partially ionised gas containing an equal number of positive and negative charges. It is composed of electrons, ions and neutral particles that are in a fundamental or excited state. From a macroscopic point of view, plasma is electrically neutral but, because it contains free charge carriers, it is electrically conductive. As such, plasma is considered to be the *fourth state of matter* and is therefore distinct from the solid, liquid and aeriform states [63]. As the temperature of the system increases, molecules increase their kinetic energy. In much the same way as the transition from the liquid to the gaseous state is due to an increase in temperature, the transition from the aeriform to the plasma state occurs when the temperature of the gas is raised to around 10,000°C. Under these conditions, some of the atoms in the gas begin to split into positive ions and electrons, a process that enables the gas to pass into the plasma state. Therefore, the states of matter progress in this sequence: solid, liquid, aeriform and, finally, plasma.

A plasma is produced by applying energy to a gas in order to rearrange the electronic structure of species (atoms and molecules) and produce excited species and ions. This energy may be thermal or carried by an electric current or even electromagnetic radiation [64].

In atmospheric plasmas produced by electrical energy, the electric field transmits energy to the gas of electrons (which are the most mobile charged species), this electronic energy is then transmitted to the neutral species by collisions. The latter follows probabilistic rules and can be divided into:

- *elastic collisions*: these do not change the internal energy of the neutral species, but slightly raise their kinetic energy;
- *anelastic collisions*: when the energy is sufficiently high, the collisions change the electronic structure of the neutral species, creating excited species or even ions.

Most excited species have a very short lifetime and return to the fundamental state by emitting photons. In Figure 2, several different types of plasma can be identified if electron temperature (y-axis) and electron density (x-axis) are related.

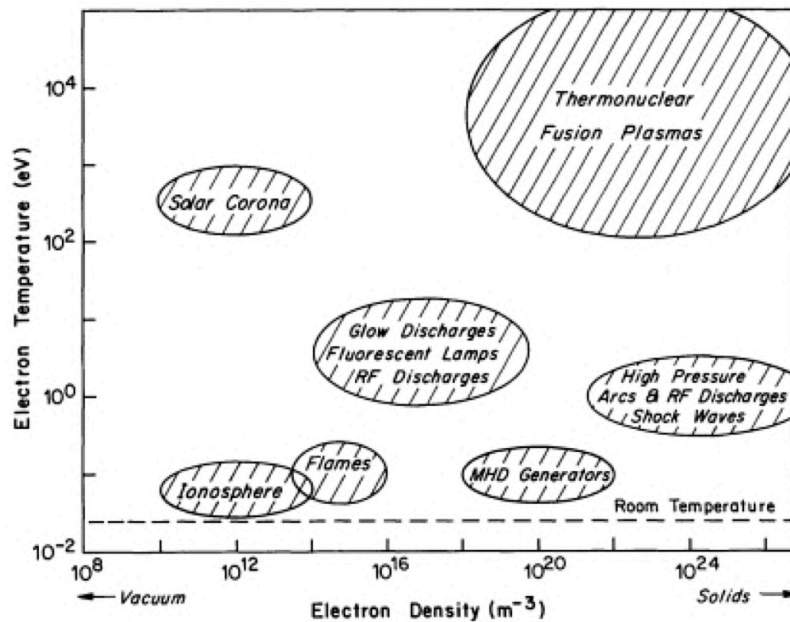


Figure 2. Classification of plasmas [61].

Plasmas, in turn, can be divided into two different categories depending on whether the heavy species (ions and neutrals) and electrons are in thermodynamic equilibrium, i.e. the equilibrium among temperatures of the particles of the plasma itself [65,66].

The categories are:

- *Local Thermodynamic Equilibrium plasmas* (LTE) or ‘hot plasma’;
- *non-Local Thermodynamic Equilibrium plasmas* (non-LTE) or ‘cold plasma’.

In non-LTE plasmas, the temperature of the electrons (T_e) remains considerably higher than that of the heavy species (T_h , around 300 K), ensuring a non-equilibrium state. If the temperature of the heavy species rises, the temperature difference between T_e and T_h decreases, bringing the plasma into a state of equilibrium and thus achieving LTE [67,68].

Table 2 shows some of the main differences between the two types of plasma.

Table 2. Difference between the two-plasma classification [66].

	LTE or ‘hot plasmas’	non-LTE or ‘cold plasmas’
Properties	$T_e = T_h$	$T_e \gg T_h$
	Large electron density: 10^{21} - $10^{26} m^{-3}$	Lower electron density: $< 10^{19} m^{-3}$
	Anelastic collisions between electrons and heavy particles create the reactive species	Anelastic collisions between electrons and heavy particles induce plasma chemistry.
	Elastic collisions heat the heavy particles (electronic energy is therefore consumed).	Heavy particles are slightly heated by a small amount of elastic collisions (this is the explanation for why the energy of electrons remains so high)

In cold plasmas, moreover, most of the heat is transmitted by the neutral gas fraction.

Electrons, on the other hand, carry only a small fraction of the heat despite their high temperature. This means that both electrons and positive ions in cold plasma can trigger a series of chemical reactions that would only occur at temperatures equivalent to those of the electrons, without risking altering the temperature of the materials to be processed [69,70]. This important property gives rise to a series of different applications, all specifically related to surface treatment [71].

In fact, the use of cold plasma at atmospheric pressure generally concerns the deposition of thin metal layers, the hardening of tools, the pre-treatment of surfaces to improve the adhesion of glues and dyes, the disinfection of containers, and the treatment of various instruments - especially for medical purposes - to eliminate bacterial and fungal agents [72]. It is essential to specify, however, that each application requires a particular combination of electron temperature, ionised fraction and gas. Consequently, specific plasma sources must be designed and studied for different purposes.

1.6 Atmospheric plasma sources

Sources of atmospheric pressure plasmas can be distinguished according to their mode of excitation, in three main groups:

- **direct current (DC) and low frequency pulsed DC discharges:** the source consists of a negative cathode and a positive anode separated by a space into which the gas flows. A DC voltage is then applied to the two electrodes so that some of the atoms and molecules present in the gas are ionised. The current that is generated must be continuous throughout the length of the discharge. The most commonly used sources belonging to this category are the plasma arc, corona discharge plasma and dielectric barrier discharge plasma [73].

Torches using arc plasma (Figure 3) always consist of three elements: cathode, gas injection system and nozzle, to direct the plasma. The latter, which is positively polarised, acts as the anode. The arc is ignited between the cathode and the anode and ionises the gas. The temperature of the plasma core can vary between 5000 and 15000 K, allowing this type of torch to be used in applications where high temperatures are required [74,76].

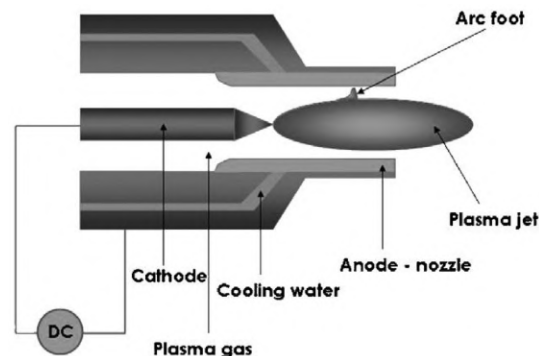


Figure 3. The basic structure of the plasma arc torch [76].

In comparison, corona discharge (Figure 4) which is a non-LTE type, the density achieved inside the plasma is lower than in the arc plasma. The device consists of a wire-shaped cathode, an anode made of the treated material and a pulsed direct current generator. The plasma creates a crown of light around the wire, which is why the discharge is called 'corona'. The positive ions are accelerated towards the wire, emitting secondary electrons that are accelerated towards the plasma: this high-energy front of moving electrons followed by a tail of lower-energy electrons is called 'streamer'.

Anelastic collisions between high-energy electrons and heavy particles lead to the formation of reactive chemical species [75,76].

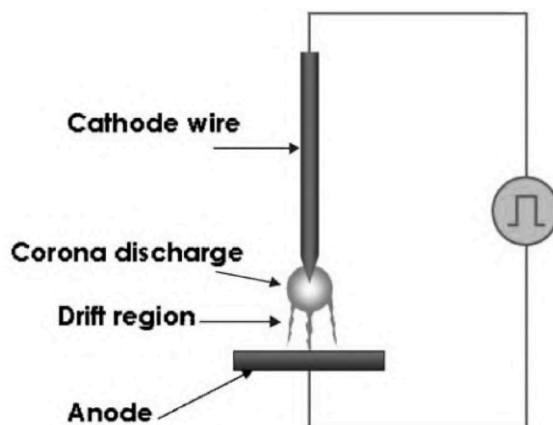


Figure 4. The fundamental structure of corona discharge device [76].

However, since the volume of the plasma is very small, in the case of surface treatments, the main drawback of the corona discharge is the small amount of material that can be treated. To overcome this problem, the cathode wire can be replaced by a planar electrode, arranged parallel to the surface to be treated; in this way it is possible to generate streamers perpendicular to the material. This, however, can lead to an irregular treatment of the surface, because the streamers tend to form at predefined points in the material, i.e. where the charges are most concentrated. Dielectric barrier discharge (DBD) can solve this problem. The instrument (Figure 5) consists of two parallel metal electrodes, at least one of which is covered with a dielectric material, thus incapable of conducting an electric current. Gas flows through the millimetric-thick cavity, which ensures the formation of a stable plasma. Depending on the composition of the working gas, the voltage and the frequency of excitation, the discharge can be either a glow or composed of streamers that develop on the surface of the dielectric material, thanks to the accumulation of electrons on its surface [75,76,77].

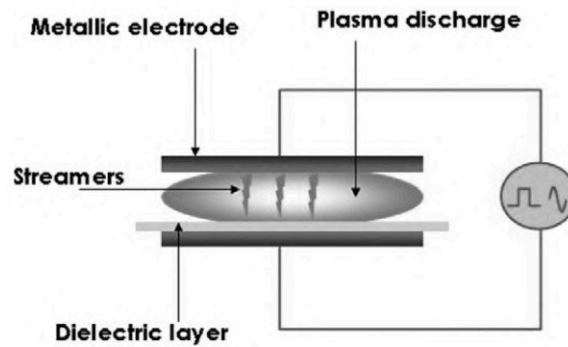


Figure 5. The essential structure of a dielectric barrier discharge [76].

- **radio-frequency wave discharges:** sources fed by radio-frequency discharges can have high power, where the impedance of the coupling is inductive, or low power, where the impedance is capacitive; depending on the type, a plasma with different properties and, therefore, different applications will be obtained. For high-power inductive discharges, an *Inductively Coupled Plasma* (ICP) torch is used (Figure 6), capable of exploiting the energy provided by the electric current created by electromagnetic induction. Their structure is quite simple: the plasma is started and maintained by a coil powered by radio frequency. The electric current circulating through the coil induces a magnetic field near the plasma area. The resulting circular electric field accelerates the electrons and keeps the discharge burning. The frequency of the current is at least 1 MHz so that the electrons follow the electric field and cannot reach the walls of the torch. The absence of contact means that there is no contamination of the plasma and the torch walls, which allows the use of different types of gas [69,76,78].

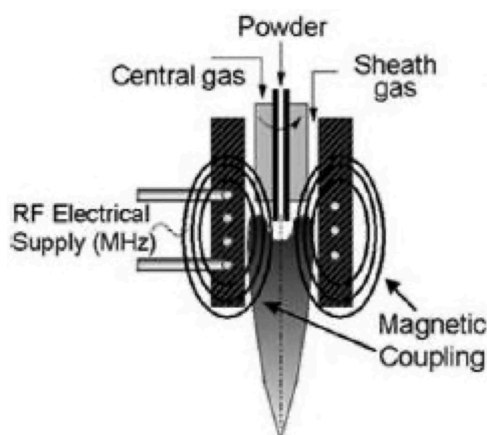


Figure 6. The basic structure of an ICP torch [76].

With low-power capacitive discharges, a minimum potential difference, known as the ‘threshold voltage’ or ‘discharge potential’, must be applied to cause a discharge in a gas flowing between two electrodes. This minimum potential depends on the pressure of the gas and the distance between the electrodes. *Atmospheric Pressure Plasma Jet* torch (APPJ) is used for this type of discharge; it consists of two concentric electrodes through which the gas to be ionised flows (Figure 7). The central electrode has a potential of approximately 100÷150 V at radio frequency [76,79,80].

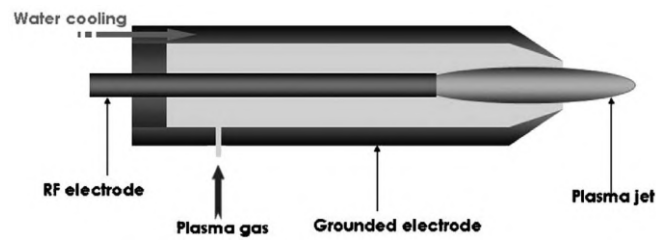


Figure 7. The fundamental structure of an APPJ torch [76].

One device which is structurally similar to the APPJ is the *hollow cathode torch* (Figure 8). In this case, the central radio-frequency electrode consists of a hollow needle, through which a gas flows, inserted in a quartz tube inside which flows an additional gas that acts as a coating for the primary jet, avoiding contamination by potential pollutants. Plasma is generated inside the hollow electrode and is then pushed outward by the gas flow [76,81].

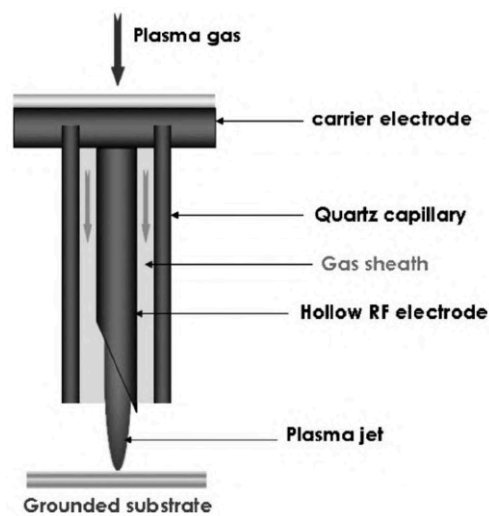


Figure 8. The essential structure of an hollow cathode torch [76].

Similar to APPJ and DBD are *cold plasma torches*, which operate at radio frequency. These devices consist of a stainless-steel electrode and a quartz tube placed between the cathode and the anode, which ensures a stable plasma. This flows in the space between the cathode and the dielectric tube [69].

- ***microwave-induced discharges***: the most widely used microwave systems share a common feature with those presented so far (except for ICP flashlights), namely the absence of electrodes in their structure. These systems, in fact, rely on the ability of microwaves to transmit energy to plasma electrons. The high oscillation frequency that characterizes these waves acts only on the electronic part of the gas, increasing the energy to the point of inducing ionization. The partially ionized gas becomes plasma and favours the propagation of microwaves [82]. The sources with microwave-induced discharges include the so-called ‘*plasma torch in free expansion*’ and, according to the structure, can be distinguished in metallic and semi-metallic. The former includes the *Axial Injection Torch* (AIT), visible in Figure 9, in which gas flows into the innermost duct of the coaxial line and exits through a nozzle [76,84]. Microwaves are generated by a magnetron and reach the gas through rectangular waveguides. The discharge is caused at the top of the nozzle [76].

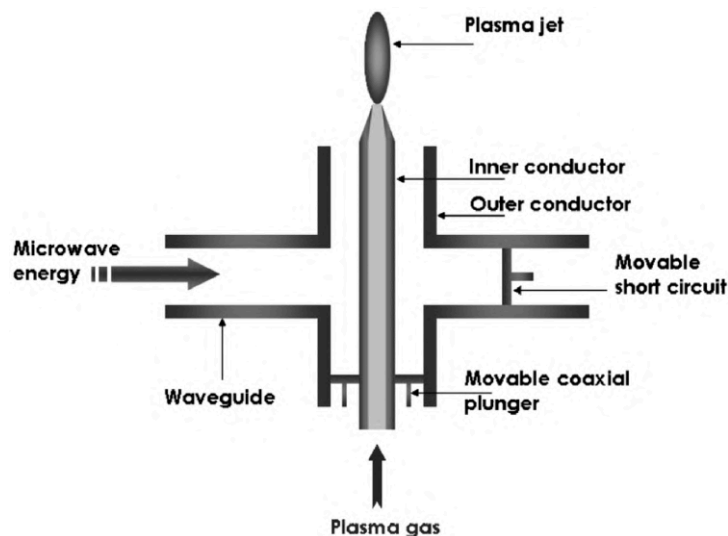


Figure 9. The basic structure of a TIA [76].

Plasma torch in free expansion with semi-metallic structure includes, instead, *Microwave Plasma Torch* (MPT). It is very similar to that of metal flashlights, the main difference lies in

the method of propagation of microwaves: in this case, the gas flows inside a quartz tube (transparent to microwaves) and the plasma is triggered in the area of intersection of the tube with the rectangular waveguide (Figure 10), then it is pushed by the gas outside the tube [76,84].

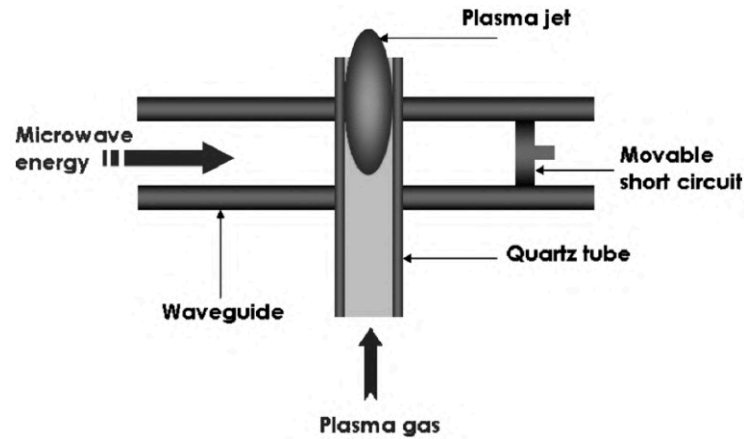


Figure 10. The fundamental structure of a MPT [76].

1.7 Atmospheric pressure cold plasma technology and 3D integration in Cultural Heritage

Since the early 1970s, industrial technologies based on the use of cold plasma have become increasingly popular. What has enabled its widespread use, especially in the microelectronics and optics industries, is the demonstrated effectiveness and its surprising versatility in surface processes. Depending on the field of use, cold plasma can be used both for the deposition of organic and inorganic films and for modifying the surface properties (from a few nanometers to a few microns) of various materials, preserving their original structural properties, such as mechanical strength, flexibility, hardness, extensibility, dielectric properties, etc.

Therefore, various plasma processes are generally used to obtain specific properties from the materials - such as hydrophobicity, hydrophilicity, oleophobicity, adhesion, barrier effect to gases and UV radiation, surface roughness and acid-base properties - thanks to [85]:

- *deposition of thin films*: either organic (siloxane precursors) or inorganic (oxides of various metals and semiconductors);
- *surface grafting*: functional groups are deposited on the material increasing its particular properties and making it more reactive;
- *ablation*: selective removal of organic or inorganic layers from the surface of the material, such as corrosion traces or biological films;

- *activation and/or cross-linking of substrates*: to make them reactive to specific environments.

Cold plasma technology at atmospheric pressure has innovative applications in the Cultural Heritage field:

- it allows making superficial modifications to the material to be treated allowing to implement its physical and chemical characteristics (conductivity, resistance to atmospheric agents, hardness, adhesiveness, biological compatibility, transparency) by acting only on the outermost part of the surface. The films that can be deposited by plasma-assisted techniques can be thin (from less than one μm to tens of microns). The surface modification is permanent, with excellent results in terms of stability and aesthetical aspect [82];
- it does not require the use of solvents which are harmful to the environment and sometimes to the user, thus bringing undoubted advantages in both economic and environmental terms [86];
- it does not require any contact with the surface of the artefact, a possibility often precluded in the case of seriously deteriorated works [87];
- it allows the complete removal of organic protective coatings and promotes the depolymerisation of aged and cross-linked polymers. It does not adversely affect the inorganic substrate where there is a need to remove traces of deterioration of an organic nature [87,88];
- it effectively removes corrosion marks on silver, various alloys, brass and iron artefacts [87,89];
- on materials, such as wood and paper, it can provide water repellent and antibacterial properties, reducing the possible degradation by chemical agents, such as acids and atmospheric particles, and biological agents, such as mould and bacteria [89];
- it is also particularly effective in increasing the adhesion capacity between polymer layers when passed during the 3D printing process. NadirTech has carried out interesting studies to verify the effectiveness of this treatment [90]. These have involved the deposition of a silazane nano-film which, during the initial tests, has

proved particularly effective in increasing the adhesion capacity between layers. In the context of this thesis, tetraethyl orthosilicate (TEOS), with the formula $\text{Si}(\text{OC}_2\text{H}_5)_4$, a siloxane material particularly used in the conservation field, was applied on the polymeric material. This amorphous silica was chosen for its consolidating properties and good chemical compatibility. In addition, due to the presence of short paraffinic chains between the alkoxy groups, it is able to produce silicate polymers which should better resist to tensile stresses.

To confirm that plasma treatment is effective in improving adhesion between 3D printed polymer layers, it is interesting to report on tests carried out by the company Nadir [91].

The samples, which are thinner but still square in shape, are four in number, two of which were plasma treated during printing. The treatment parameters used are as follows:

- Plasma power: 30 W
- Precursor vapours: HMDSN at 0.5 l/min
- Printing speed: 30-50 mm/sec

Two samples (1T and 1NT) were immersed for 240 hours in acetone (Fig. 11), the other two (1T and 1NT) were immersed in formic acid for the same time (Fig. 12).

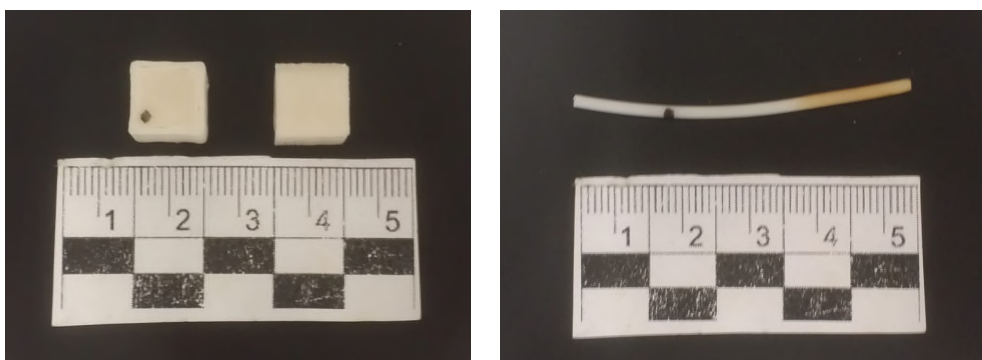


Figure 11. Acetone resistance test: on the left the treated sample and on the right the untreated one, both seen from the side.

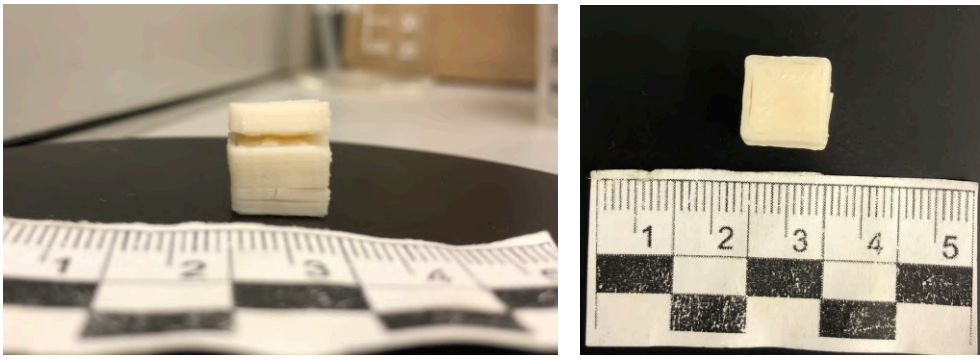


Figure 12. Formic acid resistance test: on the left the treated sample and on the right the untreated one, both seen from the side.

The effectiveness of the plasma treatment against degradation processes by acid hydrolysis is evident. The acids, both of organic nature, caused, in the untreated samples, a clear exfoliation along preferential planes consisting of the 3D printed polymer layers.

In the case of the plasma-treated samples, where there was the deposition of a silicate coating, the attack by the acids did not compromise the ability of the layers to adhere to each other, proving that the treatment works and is maintained even under the most extreme storage conditions.

1.8 Life Cycle Assessment

One of the objectives of this thesis, in addition to assessing the effectiveness of plasma treatment on a polymeric material ideally intended for the creation of art objects for inclusive museum routes, also in an outdoor location, is to evaluate the environmental impact of these innovative technologies and materials. The Life Cycle Assessment (LCA) is a useful investigation method to quantitatively determine the emissions that are released into the environment after the manufacture of a specific product. In the following paragraphs, therefore, a description of the steps of an LCA study is given. LCA, as defined by the UNI EN ISO 14044 standard, is a methodology used to assess the direct and indirect environmental impacts of a product or a service throughout its life cycle, i.e. starting from the extraction of raw materials, to the manufacturing of the product, to its use, until the end of its life. This system can quantify the environmental footprint generated by a service or product using numerical information [92].

LCA, according to ISO 14040 and ISO 14044, is divided into four phases [92,93,94]:

1. *Clear definition of purpose*: in this phase, the goals and objectives of the study must be defined. It is a very important step since it defines the quality of the work that will be carried out, determining the data, the parameters, the level of detail and the possible final interpretations. Therefore, after having made clear what the objectives are, some elements need to be defined the:
 - *functional unit*: it is the reference against which all input and output data of the system under review, as well as the results, are normalized. Thus the functional unit must represent a quantifiable and objectively verifiable performance of the system under consideration;
 - *system boundaries* determine the unit processes to be included in LCA. The choice of boundary must be consistent with the aim of the study, and the criteria used to establish it must be identified and justified. Boundaries allow for the creation of a flowchart, which is useful for sorting and collating all the various information in the case to be considered. During the LCA, it is also important to clarify what is considered and what is discarded as input/ output, justifying these choices [95-96].
2. *Drawing up the inventory* (Life Cycle Inventory - LCI): it is the most delicate and challenging phase of an LCA study. Here, the input and output flows in the life cycle of the system are defined and quantified and a model is built to represent them as truthfully as possible. All phases of the life cycle and their relationships are visualised in a flow chart, thus determining all inputs and outputs and thus the data to be collected [94]. All values are expressed in physical units, units of mass and energy, and normalised according to the functional unit. Once collected, all data must be categorised (raw materials, energy, transport, etc) and stored in an inventory table, which is the fundamental base for the next stage of impact assessment [95].
3. *Assessment of impacts* (Life Cycle Impact Assessment - LCIA): the purpose of this phase is to highlight the extent of environmental changes generated as a result of the environmental emissions and resource consumption caused by the production activity under consideration. It consists of attributing consumption and emissions to specific

impact categories, linked to known environmental effects, and quantifying the extent of the contribution.

According to ISO 14040 and ISO 14044 the LCIA involves the following steps [96]:

- *Choice of impact categories and classification*: ‘impact categories’ are used to define effects on environment and humans, whereas the term ‘classification’ is used to label inputs and outputs associated with one or more impact categories [97];
 - *Characterisation*: systems are modelled based on characterisation factors for each substance. These factors are multiplied by the flows present, thus identifying the possible environmental impact. This results in a limited number of inventory items represent the ‘eco-profile’, reported graphically as histograms;
 - *Standardization*: to compare possible impacts or products, the potential impact is related to a reference unit within the same area;
 - *Attribution of weights to emphasise the most relevant impacts*: the effects, multiplied by their respective weights, provide ‘eco-indicators’ that quantify the environmental performance of the system.
4. *Interpretation of results* (Life Cycle Interpretation - LCI): the work carried out in the previous phases leads to the formulation of conclusions, based on the results obtained, and recommendations, concerning the objective and purpose for which the life cycle analysis has been carried out [92,93].

Chapter 2

2.1 Materials

One of the polymer materials most used for the three-dimensional reproduction is PLA [2,3,9,11,20]. For this reason, within this study, a PLA-based filament was chosen: in particular, the product is commercially known as ‘neutral-opaline’ and produced by *Plantura Biopolymer*, a company belonging to the *Benvic Group*.

In this chapter, the creation, treatment and division of the samples, as well as the standards to which they refer, are reported. In addition, from a theoretical point of view, the analyses to be carried out on the samples are described, chosen to determine the chemical-mechanical properties of the filament under examination, whether treated with a plasma source and subjected to different degradation conditions. The aim is to verify the effectiveness of the plasma treatment and its ability to implement surface properties of the material, making it less susceptible to outdoor environmental conditions.

The technical data relating to the filament considered for the study are reported in Table 3.

Table 3. Technical data PLA filament [98].

Physical properties	
Density	1,3 g/cm ³
Mechanical properties	
Stress at break	36 MPa
Elongation at break	> 6%
Elastic modulus in traction	3200 MPa

2.1.1 Samples

The printing of the samples was carried out at the *FabLab of Venice* whose spaces are located in the *Scientific and Technological Hub* in Mestre.

Two types of specimens were printed, with a cube and a ‘dog-bone’ shape, and then equally divided into plasma-treated and non-treated. To treat specimens simultaneously to the printing

process, the atmospheric plasma torch was fixed on the nozzle arm thanks to a clamp in turn printed (§ 2.1.2).

A Delta Wasp 3MT Industrial 4.0 FDM 3D printer was used, setting parameters as follow:

- moulding speed: 40 mm/min;
- filling: 80% for the dog-bones and 100% for the cubes;
- nozzle temperature: 210°C.

So two cube-shaped (1x1 cm) and 30 dog-bone shaped (35x6x1) mm, according to ISO 527-2 2012, 5B) specimens were realised.

The number and the shape of test specimens was chosen based on the analyses that we decided to carry out to answer the research question that this thesis investigates: evaluating the chemical and mechanical properties of a 3D printed object that underwent plasma treatment at atmospheric pressure and establishing its suitability for outdoor use and the creation of inclusive museum paths. The shape of the dog-bone samples (Figure 13) was chosen to allow dynamometric tests to be carried out, in order to verify the mechanical strength of the polymer under tensile stress.

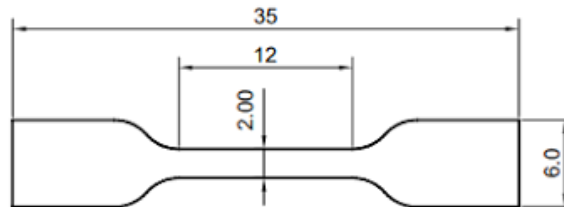


Figure 13. Graphical representation of dog-bone specimens, according to ISO 527-2 2012, 5B (dimensions in mm).

The cubes (1x1 cm), one of which was plasma treated, were made to test the resistance of the filament, both treated and untreated, to acids. The test, however, placed the filament in an extreme condition to which, normally, irrespective of relative humidity levels, temperature and pollutants, the material would never be subjected.

From now on, treated specimens will be indicated with 'T' and untreated ones with 'NT'.

Of all the specimens, considering both treated and untreated ones:

- 20 dog bones (10 T and 10 NT) were used for the different artificial ageing tests; then, after ageing, they were used (together with 10 others dog-bones (5T and 5NT) without any ageing) for dynamometric tests;
- 2 cubes (1 T and 1 NT) were used to test the polymer resistance to particularly aggressive acids;
- thermogravimetry (TG) and differential scanning calorimetry (DSC) analysis on the filament before and after annealing and on one treated and one untreated dog-bone samples after 2000 hours of ageing.

Spectroscopic and colorimetric data were also acquired on these samples at different ageing steps.

2.1.2 Plasma torch

The plasma torch used to treat PLA samples, the *Stylus Plasma Noble* (Figure 14), was developed by *Nadir Srl*. It is an innovative device, consisting of a DBD plasma jet, which allows the ionisation of a gas (in this case argon) by applying a high voltage near the channel in which the gas flows [99].

The device consists of two electrodes: the innermost permits the precursor to enter in the form of aerosol or gas; the outermost controls the atmosphere outside the torch to allow the generation of a stable plasma (usually with the aid of air or nitrogen). The gas chosen for the analysis is argon, as it enables us to work with a plasma characterised by a low temperature ($T < 50^{\circ}\text{C}$) and, moreover, avoids thermal thermisation caused by dissociation/recombination reactions or molecular vibrational motion. Given the low temperatures of the plasma, this device can be used for the surface treatment of heat-sensitive materials [100,101].

During the plasma treatment, a thin film of nano-structured material was deposited on the samples, layer by layer, modifying the characteristics of the surface, with the aim of implementing the wettability and adhesiveness characteristics between the layers and thus making it less susceptible to possible outdoor storage conditions. In this case, TEOS (tetraethyl orthosilicate) was tested, which has chemical formula $\text{Si}(\text{OC}_2\text{H}_5)_4$ was used.

Table 4 shows the technical characteristics of the Noble Plasma Stylus.



Figure 14. Plasma torch installed on the printhead.

Table 4. Technical specifications of plasma torch [99].

Mechanical dimensions	
<i>Control unit</i>	3 U dimension rack, trolley or benchtop
<i>Plasma jet</i>	20 cm long, 250 g
<i>Connection cables</i>	2 m
Supply	
<i>Power</i>	30÷100 W, 220 V
<i>Gas 1</i>	Ar 5÷10 slm
<i>Gas 2</i>	Carrier for chemical precursor vapour or reactive gas (0.2÷5 slm)
<i>Gas 3</i>	Cooling/shell (Air or N ₂ 10÷20 slm)
Treatment	
<i>Spot size</i>	1 cm ²
<i>Surface activation rate</i>	1-10 cm ² /s
<i>Deposition rate (cm²)</i>	10 nm/s
<i>Pulsing system</i>	T _{on} (30÷10.000 μs) T _{off} (50÷10.000 μs)
Options	
Interchangeable heads for different spots size: 5 - 10 or 50 nm ²	
Aerosol precursor feeding systems	
Table top robot with controlled atmosphere	

2.2 Methods of investigation

The analytical techniques used for characterising the polymeric material are described in the following paragraphs. These techniques were also used to follow the different steps of accelerated ageing in order to assess the stability of the filament under different storage conditions. The analyses thus also offer a direct comparison, before and after ageing, between treated and untreated samples at atmospheric pressure plasma.

2.2.1 Attenuated Total Reflectance - Fourier Transform - Infrared Spectroscopy (ATR-FTIR)

Fourier Transform Infrared Spectroscopy is an analytical technique used to study the structure and composition of a sample. In the present research work, it was used to chemically characterise the filament under analysis, to observe any differences in plasma-treated and non-plasma-treated samples, and to determine any structural and chemical changes during the various stages of artificial ageing.

IR spectroscopy is a vibrational spectroscopy, in which the radiation used is infrared, so that part of the electromagnetic spectrum between visible and microwave regions ($20\div 14000\text{ cm}^{-1}$), although the region of most interest in the cultural heritage field is limited to the mid-IR region ($400\div 4000\text{ cm}^{-1}$). An IR spectrum is obtained by irradiating the sample with an IR beam of a rather wide range and, for each wavelength, it is observed whether and where radiation is absorbed by the material [102,103].

To determine the molecular species present in the samples, this analytical technique was used in ATR (*Attenuated Total Reflectance*) mode, according to which the sample is placed on a support consisting of a crystal with a high refractive index, such as Germanium or diamond [104,105].

The instrument used was the Thermo Nicolet FTIR NEXUS 750, equipped with a Smart Endurance ATR accessory with a diamond tip and a survey area of $0,75\text{ mm}^2$. The FTIR-ATR spectra were recorded through 64 scans, considering a spectral range between 4000 and 400 cm^{-1} and a resolution of $\pm 4\text{ cm}^{-1}$. The spectra, once acquired, were processed with OMNIC

6.0a software, which allowed baseline and noise correction, as well as peak display. During the acquisition of the spectra, due to the high humidity in the room, the range between 2000 and 1800 cm^{-1} showed a strong absorption, which was removed to allow a better visualisation of the spectra.

The material under analysis is a filament of PLA, a polymer given by a lactide ring opening reaction or lactic acid esterification reaction, leading to C=O, C-O-C and C-H groups (saturated aliphatic hydrocarbons) in the main chain (Figure 15) [106,107].

In Table 5 the absorptions that should therefore be found in the FTIR spectra of polylactic acid.

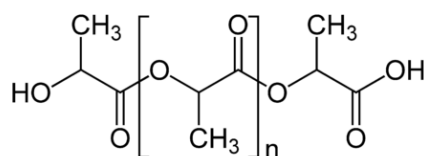


Figure 15. Structural formula of PLA [106].

Table 5. Assignments of FTIR absorption bands of PLA (the identification was based on the analysis of the literature data) [108,109].

Frequencies cm^{-1}	Association
$\approx 3000-2800$	C-H symmetrical and asymmetrical stretching of methyl groups
≈ 1750	Stretching C=O
$\approx 1455-1360$	CH stretching of methyl groups
≈ 1300	COC stretching
≈ 1270	COC stretching
≈ 1210	COC+CH ₃ group, COC stretching
≈ 1180	C-O- bond stretching vibration in -CH-O- group
≈ 1130	Stretching CH ₃ Or 1/3 characteristic peaks related to -C-O- stretching of the -O-C=O group
≈ 1080	Stretching CH ₃ C-O-C stretching Or 1/3 characteristic peaks related to -C-O- stretching of the -O-C=O group
≈ 1045	Stretching CH ₃ Or 1/3 characteristic peaks related to -C-O- stretching of the -O-C=O group
≈ 955	CH ₃ and CC rocking
≈ 890	C-COO stretching
≈ 870	C-COO stretching (association with amorphous phase)
≈ 755	CO bending (association with crystalline phase)
≈ 700	CO bending

In the case of samples that have undergone plasma treatment with the deposition of a silicate coating, in the present case study tetraethyl orthosilicate (TEOS), characteristic peaks are expected (Table 6).

Table 6. Assignments of FTIR absorption bands of TEOS (the identification was based on the analysis of the literature data) [110].

Frequencies cm⁻¹	Association
≈ 3678	Stretching vibrations of OH
≈ 2990	Stretching vibrations of CH
≈ 2145	Stretching of CO
≈ 1776	Stretching C=O
≈ 1747	Stretching C=O
≈ 1115	Stretching of CO
≈ 1070	Stretching of CO
≈ 800	Bending vibrations of the Si-O-Si

Furthermore, considering that this is a presumably additivated polymer, given the slightly opaque colour, in accordance with the literature data, we would expect to find additive-related absorptions. In the field of the polymer industry, one of the most widely used fillers is talc, because it makes it possible to reduce production costs and improves the equilibrium between stiffness and strength. Talc also acts as a nucleating agent, promoting an increase of the number of spherulites and reducing the size of the spherulite during the process [111]. Talc is a clay mineral, a magnesium phyllosilicate, with the formula $Mg_3Si_4O_{10}(OH)_2$. The characteristic peaks of talc can be seen in Table 7.

Table 7. Assignments of FTIR absorption bands of talc (the identification was based on the analysis of the literature data) [112].

Frequencies cm^{-1}	Association
≈ 3680	Stretching vibrations of the Mg_3OH
≈ 1020	In-plane Si-O stretching vibrations
≈ 670	Bending vibrations of the Si-O-Si
≈ 656	Si-O stretching vibrations
≈ 540	Perpendicular vibrations of Mg-O bond
≈ 500	Perpendicular vibrations of Mg-O bond
≈ 460	Translational vibrations of the OH groups
≈ 450	Bending vibrations of the Si-O-Si

When a thermoplastic material is subjected to ageing processes, it undergoes degradation processes, the type and extent of which vary according to the ageing process. In the case of the dog-bone samples, these were subjected to UV ageing, during which photolytic degradation of the polymer occurs, leading to a gradual loss of the physical and mechanical properties of the material and involving the formation of hydroperoxides with a consequent increase in carboxylic acids and diketone end groups, as well as carbonyl and vinyl groups. These products take part in the cleavage of the chain.

In the ATR-FTIR spectra of a PLA sample, UV-aged, according to the data in the literature, the characteristic absorption bands of the polymer should become more intense with time.

The intensity of the carbonyl peak at about 1750 cm^{-1} , in particular, should increase with time and a small shoulder at higher wavenumbers (at about 1845 cm^{-1}) should appear, which could be assigned to the anhydride functions [113,114]. The weak peaks at about 920 , 956 and 1654 cm^{-1} , given by the unsaturation vinyl groups, could intensify, and a small shoulder at 1684 cm^{-1} corresponding to α,β -unsaturated ketones could also appear. In addition, a small absorption band should form at 3500 cm^{-1} due to free hydroxyl groups [115]. According to the literature, UV ageing may lead to an increase in the peaks at 1380 and 1115 cm^{-1} due to symmetrical C-H bending vibrations in the methyl groups. Small changes in peak intensity at 850 cm^{-1} are also expected due to out-of-plane bending vibrations of the same group [116].

One parameter for quantifying the degree of degradation of a material undergoing ageing processes is the carbonyl index: a dimensionless value given by the ratio between the area of the carbonyl peak at 1750 cm^{-1} and the area of the peak at 2990 cm^{-1} , given by the stretching vibrations of CH_3 [117].

As regards, on the other hand, the ageing of PLA in the presence of high levels of relative humidity, the process of hydrolysis takes place, which not only leads to a reduction in the molecular weight of the material, but is also considered the first step in biodegradation, as it creates the metabolites necessary for microbial degradation. One of the major limitations associated with PLA, especially for durable applications, is its sensitivity to water: although it absorbs only small amounts of water ($<1.1\text{wt}\%$ at 25°C), those that manage to penetrate the polymer matrix convert the long polymer chain into low molecular weight, water-soluble oligomers. These degradation products have more hydroxyl and carboxyl groups than the unaged polymer, which increases the affinity of the polymer for water. These processes irreversibly compromise the performance of the material [118,119].

According to the information in the literature, there should be significant differences in the spectra of the polymer aged at high relative humidity compared to those of the unaged polymer. First and foremost, there is the decrease of the peak at 1750 cm^{-1} , given by the $\text{C}=\text{O}$ bond, as a result of the cleavage of the COO bond [119]. For the same reason there should also be a decrease of the peaks at 1384 and 1359 cm^{-1} , associated with the symmetrical bending vibrations of the CH_3 group, of the absorptions at $1180\div 1020\text{ cm}^{-1}$, due to the stretching vibrations of the $\text{C}-\text{O}-\text{C}$ bond of the esters and at 870 cm^{-1} , due to the $\text{O}-\text{CH}-\text{CH}_3$ absorption or a change in the mass of the crystalline fraction, since this band is generally attributed to the amorphous phase of the PLA.

Furthermore, in the present case study some samples were subjected to acid resistance tests, during which there should be decomposition of the polymeric material by acid hydrolysis.

According to the literature, this process leads to random breakage of the polymer chain and also to end-of-chain breakage, the latter occurring more quickly. This process leads to the formation of low molecular weight degradation products such as lactate and lactic acid, which in turn forms lactic acid oligomers. These oligomers then cause cleavage of the ester bonds, promoting degradation of the polymer matrix [120,121]. From the spectra, therefore, a

decrease in the peaks assigned to the esters and, at the same time, an increase in the absorptions given by the carbonyl group present in the degradation products at approximately 1746, 755 and 701 cm^{-1} should be observed [121].

2.2.2 Raman Spectroscopy

Raman spectroscopy can provide important information about the molecular composition, bonds, chemical environment, phase and crystal structure of the samples under investigation.

It is, therefore, suitable for the analysis of materials in multiple forms: gases, liquids and amorphous or crystalline solids [122]. This is an analytical technique widely used in the field of cultural heritage, especially for the study of substances with a crystalline nature, pigments and dyes, both organic and inorganic, as well as to determine the presence of degradation products on the surface of the material [123]. In the present case study, it was used to confirm the information obtained with infrared spectroscopy about the chemical composition of the filament and to identify any variations between plasma-treated and non-plasma-treated samples before and during ageing.

For our purposes, a BRAVO portable Raman spectrometer from the Bruker company was used which allows spectra to be acquired at different energies using laser diodes. It also has a good spectral precision thanks to the integrated neon lamp. The spectra were acquired considering the region between 3200 cm^{-1} and 400 cm^{-1} . These were then processed with OPUS and OMNIC 6.0a software.

Characteristic peaks related to the polymer matrix, silicate precursor (TEOS) and talc are shown in Table 8, 9 and 10, respectively.

Table 8. Assignments of Raman absorption bands of PLA (the identification was based on the analysis of the literature data) [121,122].

Raman intensity cm⁻¹	Association
≈ 3000	CH ₃ asymmetric stretching
≈ 2945	CH ₃ symmetric stretching
≈ 2889-2878	CH ₃ symmetric stretching
≈ 1773-1769	C=O stretching/ CH stretching
≈ 1456-1454	CH ₃ symmetric deformation
≈ 1388	CH ₃ symmetric stretching
≈ 1298	CH or COC vibrations
≈ 1128	CH ₃ rocking vibration
≈ 1046-1042	C-CH ₃ stretching
≈ 873	C-COO
≈ 742	C=O
≈ 408-399	C-COO

Table 9. Assignments of Raman absorption bands of TEOS (the identification was based on the analysis of the literature data) [123].

Raman intensity cm⁻¹	Association
≈ 1049	Si-O-Si stretching vibrations
≈ 980	Si-O-C stretching vibrations
≈ 880	C-O-C stretching vibrations
≈ 675	SiO ₄ stretching vibrations
≈ 484	Si-O-Si bending vibrations
≈ 435	Si-O-Si bending vibrations

Table 10. Assignments of Raman absorption bands of talc (the identification was based on the analysis of the literature data) [112].

Raman intensity cm⁻¹	Association
≈ 1035	SiO ₄ stretching vibrations
≈ 675	SiO ₄ stretching vibrations

In the identification of plastic materials, however, especially when subjected to ageing processes, the analysis by means of Raman spectroscopy presents some limitations compared to IR spectroscopy [124]. In comparing to Raman spectra, FT-IR spectra can easily highlight the presence of oxidative functional groups, such as hydroxyl and carbonyl groups, which cannot be observed in Raman spectra [125]. If a plastic material has therefore been subjected to chemical degradation processes in the environment, the degradation products can be easily identified by analysis of FT-IR spectra, but not by Raman spectra [125].

2.2.3 Thermogravimetric analysis (TG) and differential scanning calorimetry (DSC)

In a thermogravimetric analysis the mass of a sample located in a controlled atmosphere is measured as a function of temperature or time. A plot of the percentage of mass lost or gained as a function of time is called a 'thermogram' [126]. Thermogravimetry thus makes possible to study all those processes that occur with a variation in mass, such as decomposition, sublimation and vaporisation [110], into a range temperature that goes from 25 to 1500°C.

It allows also to analyse the composition of polymer that present some of inert fillers into the matrix. The sample weight is monitored using a thermobalance, which consists of a sensitive analytical balance; the analysis is carried out by heating the sample within a controlled furnace where a proper gas is purged, ensuring inert or reactive atmosphere conditions. The sample is placed in a crucible, commercially available in different shapes, sizes and materials. The crucible must be chosen so that no chemical reaction occurs between it and the sample. Usually, crucibles are made of platinum, aluminium, quartz, corundum or alumina. Many variables influence the analysis, some of these are heating rate, heat of reaction, furnace atmosphere and amount and characteristics of the sample.

From the thermogravimetric curve it is possible to determine the temperature at which the degradation of the material begins, defined as $T_{\text{onset-i}}$, the temperature of maximum degradation rate, or T_{max} , and the temperature at which the degradation ends, also known as $T_{\text{onset-f}}$.

In the specific case of polymeric materials, it is a technique that allows the thermo-oxidative stability of the material to be verified, as well as its stability in corrosive or reactive

atmospheres. It does not, however, provide information on any chemical or structural changes that do not cause a change in the mass of the material.

Differential scanning calorimetry (DSC) is a thermal method in which the difference between the heat fluxes in the test substance and a reference is measured while both are subjected to a thermal controlled program [101].

When a compound phase change occurs, energy is always absorbed or emitted in an amount proportional to the mass of the sample under examination. The energetic variation occurs most often as an exothermic or endothermic effect. It is important to note that the temperature at which the change occurs is constant and characteristic for each substance.

The specific task of the DSC technique is to evaluate characteristic temperatures of a material (such as the glass transition temperature, the melting temperature and the cold crystallization one) and quantify, when possible, the heat involved in the transformations [3]. This is done by comparing the sample under examination with an inert reference: the system provides the sample, during the transformation, with the amount of energy required to keep it at the same temperature as the reference. Any thermal modification of the system causes an imbalance, which is immediately corrected to re-establish thermal equality with the reference.

The electrical energy required to re-establish equilibrium is a direct measure of the energy developed or absorbed during the process. The amount of heat is measured as a function of temperature.

Many variables influence the performance of a DSC thermogram, some of these are the heating rate, the gas atmosphere, the amount and the chemical-physical characteristics of the sample [101]. During the analysis was calculated the degree of crystallinity of the samples, according to the formula (1):

$$\chi_c = 100x \frac{\Delta H_m - \Delta H_c}{\Delta H_0} \quad (1)$$

where ΔH_m is the enthalpy of fusion (J/g), ΔH_c is the enthalpy of crystallization (J/g) and ΔH_0 is the heat of fusion of the 100% crystalline polymer (J/g), which for PLA is 93.1 J/g.

In the present research work, TG was used coupled with DSC, in order to relate the mass loss of the material to variations of the heat flow and physical transitions of it. The instrument used is the Netzsch Termische Analyse TASC 414/3 Controller - model STA 409 cell. The

crucible where the sample was placed was made of platinum and the reference used was alumina, as it does not suffer chemical and phase changes at the set temperature range from 30°C to 700°C (heating rate 10°C min⁻¹); analyses were performed in an inert atmosphere under a nitrogen flux of 80 ml min⁻¹. In the case of the TG curves, the temperature range considered in the development of the considerations is 30 to 700°C, while for the DSC curves, the temperature range of 30 to 400°C was taken into account, within which the exothermic and endothermic characteristic peaks of the polymer are located.

TG-DSC curves were performed on the filament, on treated and untreated specimens, before and during the ageing processes, and on a portion of the filament that was stored for seven days in an oven at a temperature (around 80°C) that does not melt the material, but allows the molecules to rearrange themselves in space in order to acquire greater mobility.

2.2.4 Colorimetric measurements

Colourimetry is a non-invasive analytical technique that allows to directly measure and define the colour of a surface without altering it and without taking samples. It is a widely used technique in the field of cultural heritage, especially because of the possibility of performing *in situ* analyses.

Considering that there are different factors that can distort colour perception, like the subjective ability of each individual to perceive colour, the substrate characteristics of the material and the illumination, a method to describe colour objectively has been developed: the *CIE Lab System 1976* [126]. It defines the color thanks to three parameters, a*, b* and L*, where:

- a* represents green if the value is negative and red if positive;
- b* represents blue if the value is negative and yellow if positive;
- L* represents brightness. It can have values ranging from 0 (minimum brightness), i.e. black, to 100 (maximum brightness) equal to pure white.

When more than one measurement is taken on the same sample, these parameters can be used to determine the colorimetric variation, ΔE_{ab}^* . The equation (2) is the following:

$$\Delta E_{ab}^* = \sqrt{(\Delta L^*)^2 + (\Delta a^*)^2 + (\Delta b^*)^2} \quad (2)$$

The values obtained lie on a scale that goes from 0, where no colour difference is perceived, to values greater than 3, where a colour change starts to be perceived by the observer.

For ΔE_{ab}^* values around 1, the colour change can be usually considered negligible [128].

In the field of Cultural Heritage, colourimetric analysis are a detection method of indubitable usefulness not only to check colour coordinates and determine any colour variation over time, but also to monitor restoration operations and to verify the effectiveness of a treatment [129].

Colorimetric analysis are a detection method of indubitable usefulness not only to check colour coordinates and determine any colour variation over time, but also to monitor restoration operations and to verify the effectiveness of a treatment or a material [130].

For the elaboration of this study, the acquisition of colorimetric parameters was aimed to evaluate the entity of chromatic variations, such as yellowing or discoloration, induced by artificial ageing. This measurements were performed not only before subjecting the samples (both plasma and non- plasma treated) to the accelerated ageing tests, but also after 500, 1000, 1500 and 2000 hours from the start of ageing. For each sample, the values of L^* , a^* and b^* were acquired. Using these values, it was possible to calculate ΔE_{ab}^* and thus determine the amount of colour change. The yellowing index (Y) was also calculated.

For the data acquisition, a portable UV-vis spectrophotometer, model CM 2600d/2500d Konica- Minolta, with 8° angle, standard illuminant D65 (colour temperature 6500 K) and 83mm diameter observation spot was used. This device also permits to measure all reflected light (SCI, specular component included), or to exclude the specularly reflected portion and measure only the light diffused in the other directions of space (SCE, specular component excluded).

2.2.5 Accelerated ageing

The need to assess how the a material may behave when subjected to certain environmental conditions for a certain period of time is one of the most important issues in the field of Cultural Heritage and materials science. A material, especially if innovative and not yet consolidated, presents many unknowns, mainly related to the knowledge of the material itself

and how it can interact with the external environment and, eventually, with the materials it is placed in contact with that made up the work [131].

There are a wide variety of factors - such as oxygen, natural light, atmospheric conditions, pollution and micro-organisms - that can chemically and mechanically modify a product. For plastics, in particular, the degradation mechanism is specific to each type of polymer and even for the same polymer, there are differences due to the nature of the raw material, the molecular weight, the synthesis process, the type of procedure undergone and post-production treatments.

For this reason, it is important to subject materials to accelerated ageing processes in order to predict its their behaviour and assess in advance their effectiveness, harmlessness and durability. Precise simulation, however, is impossible; these tests must be considered 'relative', as they only give an idea of how a material may behave when subjected to hypothetical storage working conditions [132]. In reality, degradation factors may be different and with different magnitude, and they act in a synergic way. To partly overcome this problem, some standard exposure procedures have been developed in order to provide an acceptable reproducibility of the results. There are chambers and tools, commonly used in the field of Cultural Heritage - like thermoventilated ovens operating in air, under vacuum and with gas streams and Xenon or UV lamp ageing chamber - to subject materials to accelerated ageing cycles compared to natural exposure; tools that allow the control of the most important variables, such as the emission spectrum of the lamps, the emitted power, temperature, humidity and so on [133].

For our purposes, it was decided to subject the samples to two different types of treatment, one under an incandescent lamp to simulate photodegradation and a mild thermal ageing, and one in a desiccator with an over-saturated solution of potassium iodide to maintain constant relative humidity levels at around 70%. In the latter case, the samples, 5T and 5NT, were kept in a desiccator for approximately 2000 hours. For UV ageing, 10 dog-bone specimens, 5T and 5NT, were tied to a fine mesh net to facilitate movement and placed in a fume hood under an incandescent lamp, also in this case for 2000 hours. In addition, the net was rotated about 180° degrees every 125 hours to allow an homogeneous irradiation.

During several stages of ageing, the irradiance levels of the lamp were measured using a luximeter (Lux Meter model LX1010BS). Table 11 shows the average values of the irradiance data.

Table 11. Luminous flux between the lamp and the net. Values are given in lux (lx).

	11	12	13	14	15	16
E	5090	8963	21700	36267	19000	9100
F	4943	8667	21667	35700	18900	8780
G	4160	6827	12000	14533	10433	6517

During various stages of ageing, both in UV and relative humidity, the Raman and FTIR spectra of the samples were acquired, as well as colorimetric data, in order to determine the changes in the composition and structure of the polymer material compared to its initial state and to verify the effectiveness of the plasma treatment.

2.2.6 Acid attack resistance tests

When a polymeric material is brought into contact with acids for which the material does not have good chemical stability, swelling and softening of the polymer occurs, with the inevitable loss of its mechanical properties and functionality.

The purpose of these tests is to evaluate the resistance of the material when placed, over a certain period of time, in direct contact with acids, whether organic or inorganic, so that useful information can be drawn about its resistance of the material to an aggressive environment.

However, in the case of polymers, the effect of inorganic chemical agents is different from that of organic ones. In the first case, neither water nor inorganic substances dissolved in it, such as acids, alkalis or salts, can significantly affect thermoplastics, if the concentration is low. The exceptions are polyethylene (PE) and polypropylene (PP), which, on the contrary, are particularly sensitive to concentrated inorganic substances. In the case of organic chemicals, however, they may lead to the a partial dissolution of the polymer (as in the case of polyvinyl-chloride in methyl-chloride) and to the subsequent swelling. For mixtures of different chemical agents, unfortunately, it is not possible to predict whether the thermoplastic will be attacked or not. A polymer may in fact be stable when in contact with a particular acid, but

subjected to chemical degradation when immersed in a mixture of the same acid and another substance [133].

For our purposes, a piece of the filament under analysis (approximately 2 centimeter), directly taken from the bobbin, and two 3D printed cubes (1T and 1NT) have been immersed in nitric acid (HNO₃) at pH 2, diluted to 70%, for about 2200 hours; at the end of which, due to the high resistance of the material to an inorganic acid, it was decided to place only the cubes in glacial acetic acid (CH₃COOH). Data from the data sheets of the two products are given in Tables 12 and 13, respectively. According to this, organic acids, in our case acetic acid, should be more aggressive towards PLA because they are more chemically related.

In order to verify the effectiveness of the plasma treatment, it was decided to immerse the two cubes, one plasma-treated and the other not, in acetic acid, leaving them in the test tubes for about 840 hours. To verify the effects produced by the acid, ATR-FTIR spectra were acquired for both cubes.

Table 12. Product Specification of Nitric Acid - ACS reagent, 70% [134].

TEST	Specification
Appearance (Clarity)	Clear
Appearance (Color)	Colorless
Appearance (Form)	Liquid
MW	63.01 g/mol
Density	1.413 g
Color Test	≤ 10 APHA
Arsenic (As)	≤ 0.01 ppm
Chloride (CL)	≤ 0.5 ppm
Iron (Fe)	≤ 0.2 ppm
Heavy Metals (as Pb)	≤ 0.2 ppm
Sulfate	≤ 1 ppm

Table 13. Product Specification of Glacial Acetic Acid [135].

TEST	Specification
Vapor density	2.07 (vs air)
Content	≥ 99% (acidimetric)
Form	Liquid
pH	2.5 (20°C, 50 g/L in H ₂ O)
Density	1.049 g/mL at 25°C

2.2.7 Dynamometric tests

Important in the characterisation of materials is the definition of their properties – that are divided into physical, chemical, mechanical, technological and magnetic - which provide information on the attitude of these materials to be transformed or to resist to the external stresses.

Mechanical properties, in particular, indicate the ability of a material to resist the outer forces that tend to deform it.

The mechanical behaviour of a material may depend on a number on many factors, such as:

- nature of the material;
- stresses to which it has been and will be subjected;
- mode of processing;
- geometry;
- environmental storage conditions.

One of the most interesting tests in the evaluation of the characteristics of polymeric materials is the ‘tensile test’. This finds procedural indications in ISO 527-1 (*Plastics - Determination of tensile properties: General principles*) [136], ISO 5893 (*Rubber and plastics test equipment - Tensile, flexural and compression types (constant rate of traverse) - Specification*) [137] and ASTM D 638 (*Standard test methods for tensile properties of plastics*) [138].

In the tensile test, the test specimen is stretched along its major longitudinal axis at constant speed until it breaks or until the *unit load* (load) or *deformation* (elongation) has reached a

predetermined value. The load carried by the test specimen and the elongation are measured throughout the test. In this way, the behaviour of the specimens in tensile mode is investigated and the tensile resistance, tensile elastic modulus and other aspects of the unit load/deformation relationship are determined [139].

The instrument consists of two horizontal crossbars, one fixed and the other mobile, to which the ends of a sample of the material are anchored, so that the longitudinal axis coincides with the tensile direction of the testing machine. The distance between the two grips is indicated by h . Then, the mobile crossbar is progressively moved away from the fixed one at a constant speed and, as a result, the specimen is stretched until it breaks. The force acting on the test specimen through a load cell is continuously graphically recorded with the corresponding elongation.

Therefore, the characteristic values of a tensile test are determined both on the new product and after defined conditioning and ageing periods [140].

For our purposes, thirty dog-bone samples were subjected to the dynamometric test: 10 (5T and 5NT) before ageing, 10 (5T and 5NT) after 2000 hours of UV ageing and another 10 (5T and 5NT) after approximately 2000 hours of ageing in relative humidity.

This analysis involved the use of an extensometer model MTS Insight System Corporation 50 kN Extended Length, with a cell type 569332-01, equipped with steady band clamps MTS Advantage Wedge Action.

Chapter 3

The analyses reported in this chapter were carried out with the aim of chemically characterising the polymer and determining possible physical-chemical variations induced by accelerated ageing steps. Dynamometric tests were carried out, on the other hand, to verify the mechanical resistance of the specimens, both plasma treated (T) and non-treated (NT), after ageing; so as to assess the effectiveness of the plasma treatment at atmospheric pressure on the polymeric material.

3.1 Filament and samples characterization

The samples created using the FDM additive manufacturing technique, as discussed in the previous chapter, were 32 (30 dog-bones and 2 cubes), 16 of which (15 dog-bones and one cube) underwent to plasma treatment during the printing process.

Ten of the dog-bones samples were placed for approximately 2000 hours into a desiccator with an over-saturated potassium iodide solution to maintain a stable relative humidity level of approximately 70%. Others ten samples, 5T and 5NT, were placed for 2000 hours under an incandescent lamp to simulate photochemical ageing and mild thermal ageing.

A small portion of the filament was placed in an oven for seven days at a temperature of 80°C to perform thermal analysis tests. In addition, Raman and ATR-FTIR spectra were acquired on the filament before and after storage in the oven. Acid resistance tests were carried out on two cube-shaped samples, one T and one NT. Raman and ATR-FTIR spectra were also acquired in the case of the two cubes.

In the following paragraphs, according to the different analytical techniques, such as Raman and ATR-FTIR spectroscopies, TG-DSC and colorimetry, data obtained from samples without any ageing, whether plasma-treated or not, will be presented. In the section on accelerated ageing, on the other hand, data obtained from the various investigation techniques performed on the samples every 500 hours of their ageing will be discussed.

- ATR-FTIR Spectroscopy

The ATR-FTIR spectra presented below (Figures 15 and 16) was acquired on the filament directly taken from the spool and the annihilated filament, respectively.

The spectra of the PLA filament clearly showed the characteristic absorption peaks of PLA at 2995, 2944 and 2848 cm^{-1} , due to the C-H asymmetric stretching vibration of methyl and methylene groups, and at 1747 cm^{-1} , for the carbonyl group [108,109]. It also showed the presence of bands at 1041, 1454, 1382 and 1360 cm^{-1} for C-H stretching in the CH_3 group. Peaks at 1303, 1267, 1206, 1181 and 1082 cm^{-1} indicate the stretching of the C-O-C groups, while the one at 1128 cm^{-1} represents the stretching vibration of the C-O-O.

The peak at 667 cm^{-1} can easily be attributed to the bending vibrations of the Si-O-Si bridge of talc, with chemical formula $3\text{MgO}\cdot 4\text{SiO}_2\cdot \text{H}_2\text{O}$. The same is true for the peak at 1018 cm^{-1} , assigned to the in-plane Si-O stretching vibration. The peaks at 534 and 501 cm^{-1} represent the perpendicular vibrations of the Mg-O bond, the one at 463 cm^{-1} the translational vibrations of the OH groups and the one at 449 cm^{-1} indicates the bending vibrations of the Si-O-Si bond [110,112]. According to literature data, there should also be a slight absorption peak around 3680 cm^{-1} assigned to the stretching of the Mg_3OH unit [112], hidden in this case by humidity absorption at high wavenumbers.

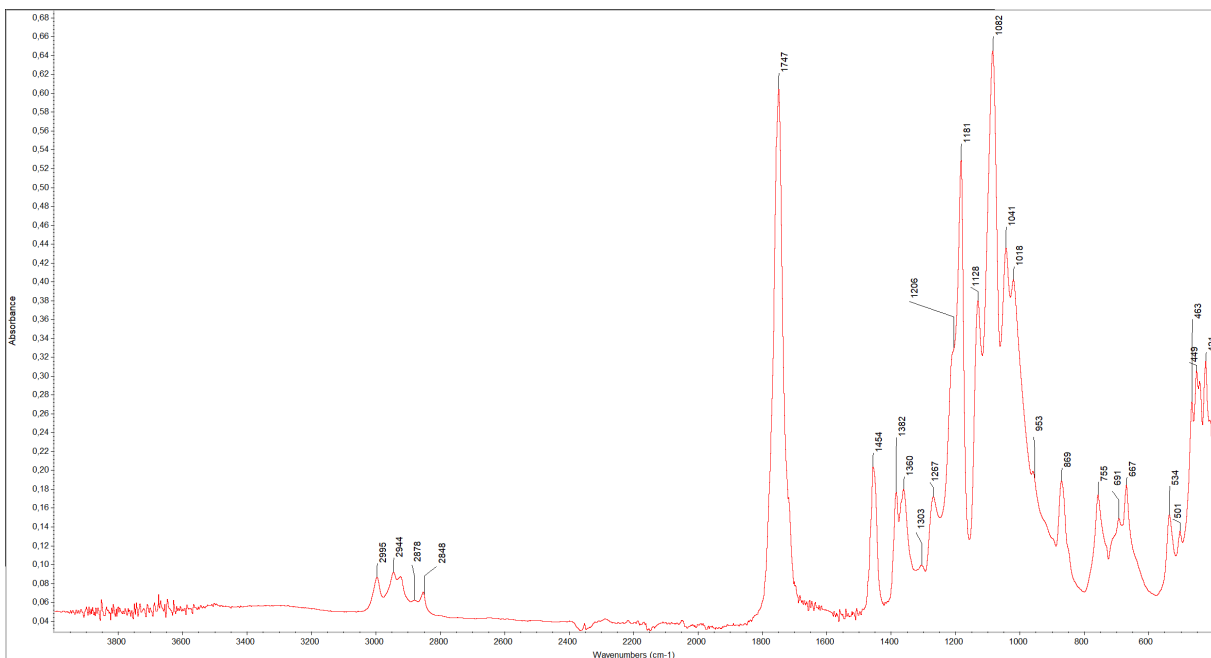


Figure 15. ATR-FTIR spectrum of the spool material.

When comparing the spectrum of the annealed filament with that of the filament directly extracted from the bobbin, some differences are observed: the annealed spectrum shows an increase in the peaks at 1454 and 1393 cm^{-1} . There is also an increase in the intensity of the peaks at 1206 and 1181 cm^{-1} . The former is due to the chain vibrations of alkyl-ketones in the PLA crystal structure and the latter to the stretching vibrations of the COC bonds.

In addition, a new 920 cm^{-1} peak was formed which, together with the peaks listed above, indicates that the polymeric material underwent minimal crystallisation during the annealing process [141-145]. The absorptions in the spectral range from 1129-400 cm^{-1} show a higher intensity than the peaks in the same area of the non-annealed filament; however, this variation is probably due to the baseline. Even in the case of the annihilated filament, the peak at 3680 cm^{-1} , assigned to stretching, is not visible as it is covered by carbon dioxide absorption.

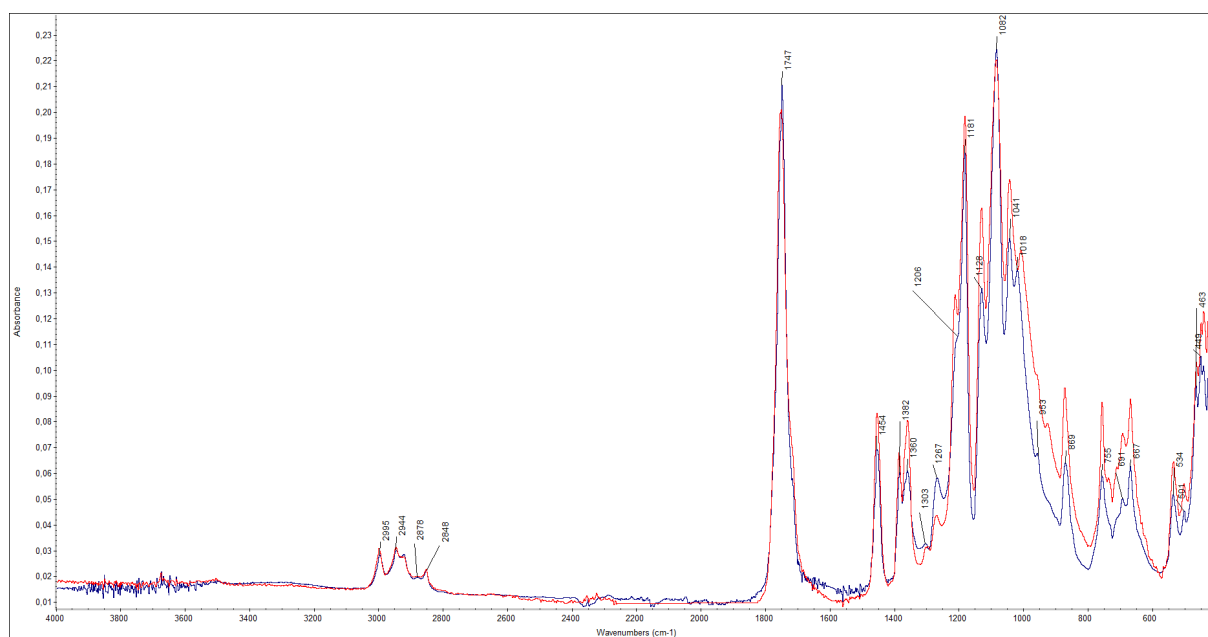


Figure 16. ATR-FTIR spectrum of the annealed filament (red) and of the filament directly extracted from the bobbin (blue).

The IR spectrum of treated and untreated 3D printed samples was also acquired (Figure 17). According to the literature, atmospheric plasma treatment with argon should lead to a slight increase in the intensities of the peaks related to the C-O, COOH and C=O groups, for the deposition of species that contain oxygen, and, at the same time, a decrease in the peaks related to the C-H and C-C bonds [146,147,148,149]. In this case, however, none of these was

detected; slight differences in absorption intensities were observed, but ascribable to the baseline effect, especially from 1000 to 450 cm^{-1} .

Furthermore, in the plasma treated sample, there was also the deposition of a silicate-based precursor, in this case TEOS. In the spectra, however, the absorption peaks associated to the deposition of silica-based nano films are not visible (Table 6). It is worth to remember that the thickness of the coating is approximately 200 nm, too thin to be detected with this technique, because the IR beam can penetrate only few microns. In addition, the TEOS-related peaks fall at approximately the same frequencies as the absorptions associated with the additive which, like the precursor, is silicate-based.

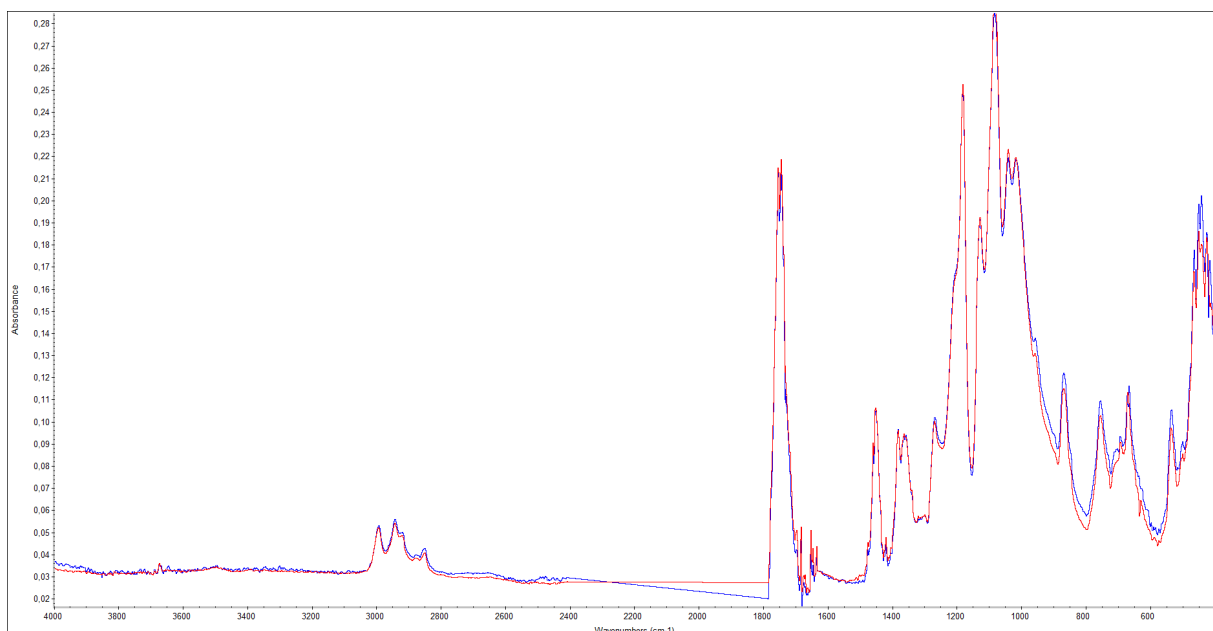


Figure 17. ATR-FTIR spectrum of two 3D printed dog-bones, one treated (red) and one non-treated (blue) before ageing.

- Raman Spectroscopy

Raman spectroscopy is a molecular spectroscopic technique useful to obtain information about the composition of the material. At the beginning of this research work, before subjecting the samples to accelerated ageing, Raman spectra were acquired on the filament directly taken from the spool (Figure 18) and on two dog bones, one untreated and one treated with plasma source (Figure 19), in order to obtain further information about the chemical composition of the material.

For the spool filament spectra, the absorption stronger absorption at 1770 cm^{-1} is due to the presence of C=O bonds, and the medium absorption at about 872 cm^{-1} , as well as the very weak peak at approximately 410 cm^{-1} , is due to the stretching of the ester bond, COO. The low absorption peak at 1044 cm^{-1} is due to the symmetrical stretching vibrations of the C-CH₃ bond. The weak peak at 1128 cm^{-1} , the medium peak at about 1452 cm^{-1} and the very strong peak at 3000 cm^{-1} are given by the asymmetric stretching of the methyl group. The peak at 1129 cm^{-1} indicates methyl group rocking vibrations. The low intensity peak at 1385 cm^{-1} , the very strong peak at 2947 cm^{-1} and the medium peak at about 2880 cm^{-1} , on the other hand, indicate symmetrical stretching for the same group.

The weak absorption at approximately 1295 cm^{-1} is given by the vibrations of the CH or the C-O-C bonds [150,151]. The peak at 1613 cm^{-1} is assigned to the conjugate stretching vibrations of the C=C bond.

The weak absorption at 675 cm^{-1} can be assigned, instead, to the stretching vibrations of SiO₄, absorption typical of talc. It also has a peak at 1050 cm^{-1} , which can be associated with stretching of the Si-O bond, but may also depend on the stretching of the C-CH₃ bond from the PLA matrix.

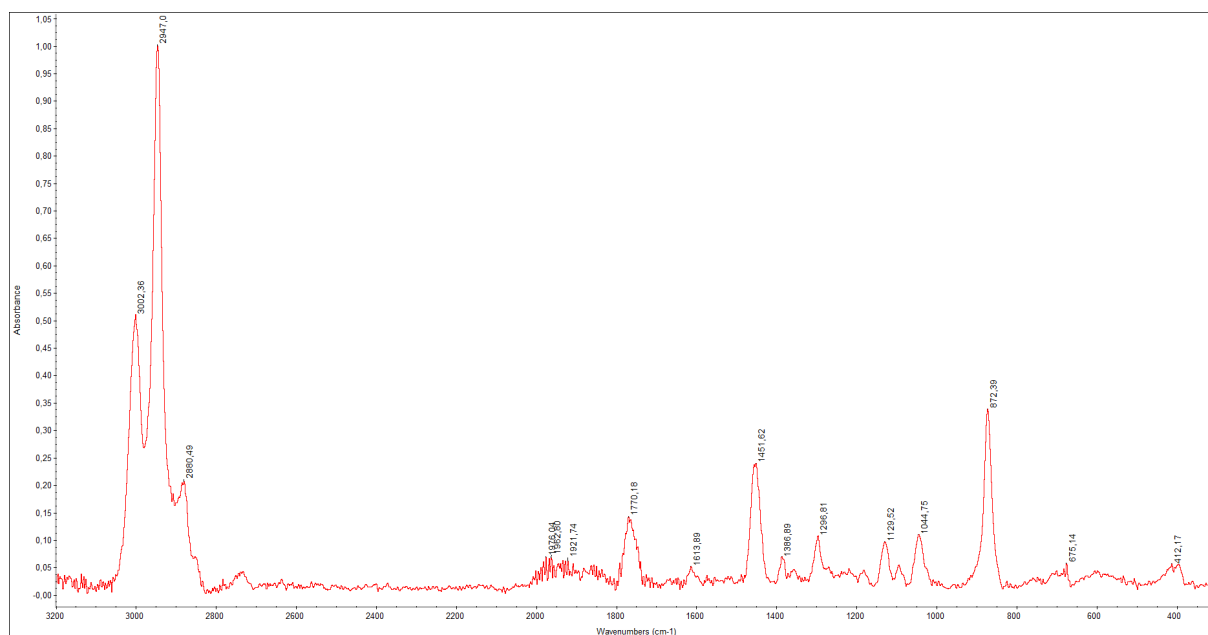


Figure 18. Raman spectrum of the spool filament.

Between the spectra of the printed samples, despite the fact that one is not plasma-treated and the other is, no significant differences are visible, neither in terms of shift and change of the intensity of the bands, nor in terms of creation of new peaks.

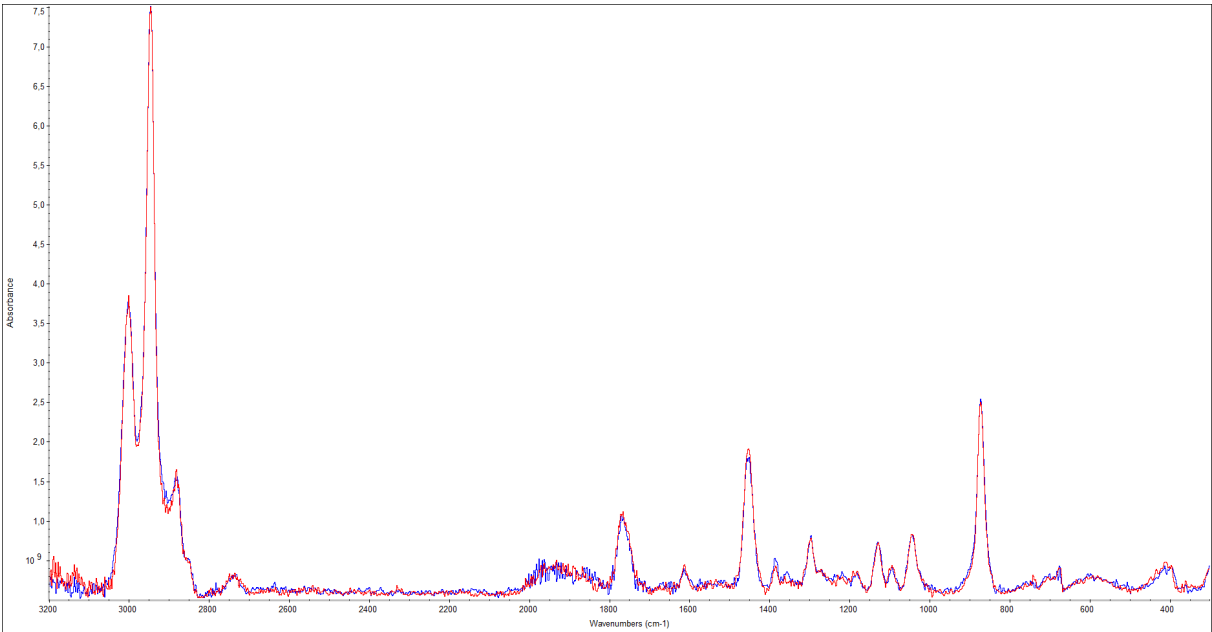


Figure 19. Raman spectrum of two 3D printed dog-bones, one treated (red) and one untreated (blue), without ageing.

- TG-DSC

The characterisation of the filament was continued by subjecting it to thermogravimetric and calorimetric analysis. Figure 20 shows the thermogravimetric and calorimeter curves of the filament.

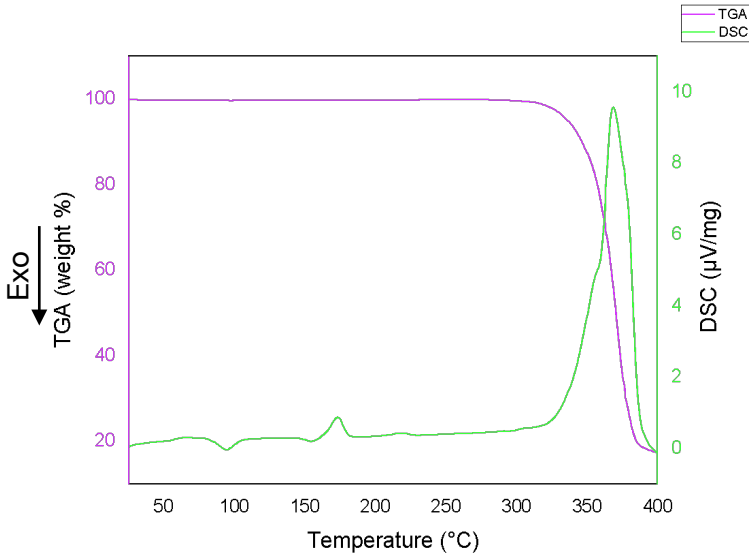


Figure 20. TG-DSC curve of spool filament before ageing.

The thermal degradation of PLA (purple curve) took place in a single weight loss step. From 30 up to about 310°C, the polymer is stable, so the TG curve does not show changes in the slope, symptomatic of an initial loss of weight from the sample, but proceeds linearly. From 310 to 390°C the polymer degradation takes place; 370°C is the temperature of maximum decomposition rate (T_{max}). From 390 (identified as the final onset temperature, $T_{onset-f}$) the thermal analysis curve slows down to complete the decomposition of the polymer matrix in order to reach a constant mass. The residue that remains at the end of a TGA experiment corresponds to the inorganic material added to the polymer matrix [138], and was equal to 12%.

As far as the calorimetric curve is concerned (green line), the typical trend of a semi-crystalline thermoplastic material should show three characteristics [148]. From left to right the DSC curve displays: heat flow at the glass transition temperature (T_g), an exothermic reaction associated with cold crystallisation (T_{cc}) and an endothermic reaction related to the melting temperature (T_m).

The T_g of the PLA under examination seems to be around 65°C, in accordance with the literature data [148,150,152,153,154]. The T_{cc} temperature falls at 91°C, at around 174°C an isotherm peak indicates the T_m , also in this case in agreement with the literature data [149,151,155,156,157]. A very intense peak between 330 and 390°C falls within the temperature range where the maximum degradation of the polymer occurs, indicating the pyrolytic nature of the degradation process.

In the case of the filament under analysis, however, in addition to the glass transition, cold crystallization and melting temperatures, there are other two peaks: an exothermic after the cold crystallization temperature, located at about 150°C, and an endothermic after the melting one, approximately at 220 °C. The distance between the crystallization peak and the exothermic one is the same of the distance between the melting peak and the second endothermic one, which suggests that this is not an instrumental trick.

Figure 21 shows an enlargement, in the temperature range between 30 and 280 °C, of the filament before ageing.

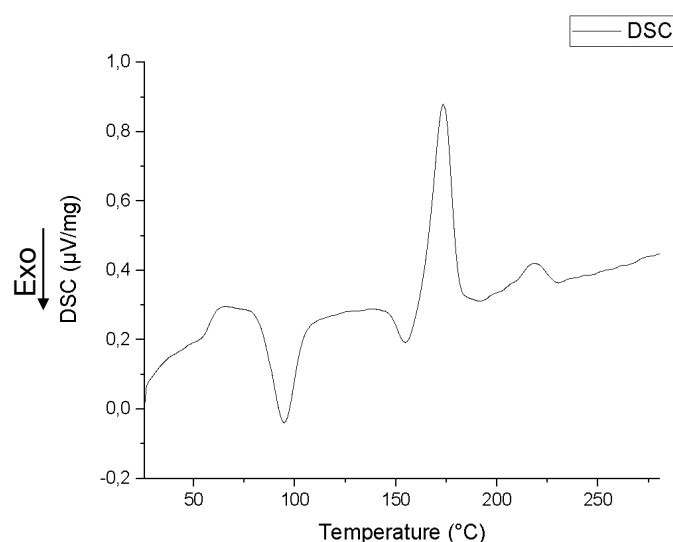


Figure 21. Detail of the DSC curve of the filament before ageing into the temperature range between ~ 30 to 280°C .

The presence of these peaks seems to be due by the insertion, within the polymer matrix, of polylactide stereocomplexes (scPLA), prepared by blending solutions of poly (L-lactide) (PLLA) and poly (D-lactide) (PDLA) [158,159]. The one at 150°C is associated to a second cold crystallisation peak (T_{cc2}) while the second at 220°C to a second melting temperature peak (T_{m2}). Stereocomplex crystallites from the homo-polymer mixture of D-lactide and L-lactide have a higher crystallisation and melting point (around 150 and 220°C) than PLLA homo-crystallites. Enthalpy and temperature data are summarised in Table 13.

Table 13. Enthalpy and temperatures from DSC curve of PLA filament.

Sample	Atmosphere	T_{cc1} ($^{\circ}\text{C}$)	ΔH_{cc1} (J/g)	T_{cc2} ($^{\circ}\text{C}$)	ΔH_{cc2} (J/g)	T_{m1} ($^{\circ}\text{C}$)	ΔH_{m1} (J/g)	T_{m2} ($^{\circ}\text{C}$)	ΔH_{m2} (J/g)	χ_1 (%)	χ_2 (%)
Filament	Air	95	-18,24	154	-7,15	174	28,23	217	6,451	10,73	0,75
Annealed filament	Air	-	-	156	-7,25	175	25,73	221	3,726	-	-3,78

The absence of the first cold crystallisation temperature is due to the fact that, during annealing, the crystallisation process has not been perfectly completed. Factor given by the slow kinetics of the PLA polymer matrix [160].

The TG-DSC curves of treated and non-treated dog-bone samples were made in air and in an inert atmosphere. The curves, performed in the presence of nitrogen, of treated and non-treated samples before ageing are shown below (Figure 22).

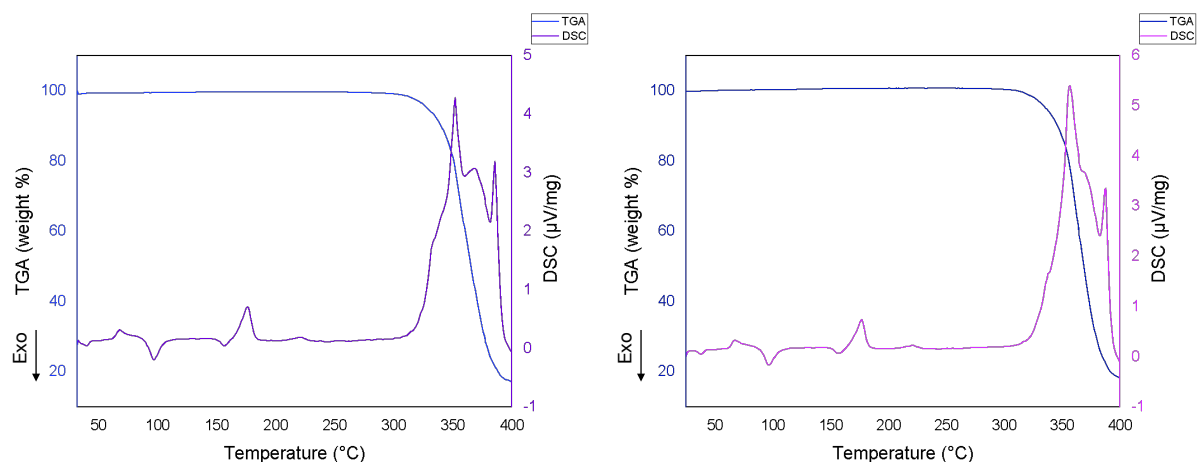


Figure 22. TG-DSC curve in nitrogen of the treated (left) and non-treated samples (right) before ageing.

The TG curves of all the samples appear similar to each other, however, when compared to the TG curve of the filament, they show a lower degradation $T_{i-onset}$ (approximately 310°C); this occurs both for samples heated in air and in nitrogen. This is an aspect that could be due to the 3D printing process, in which the polymer was heated to a temperature of 210°C, whereby structural changes took place, in which molecular chains were able to rearrange themselves, giving to the polymer material different physical properties.

The exothermic peak of the DSC curves show a three-step degradation. For the non-treated sample the peaks fall at 351, 368 and 385 °C and, for the treated one, they are more or less the same. In addition, the DSC curves of all samples showed the same exothermic and endothermic peaks of the filament before ageing (Figure 23).

Table 14. Enthalpy results and temperatures obtained from DSC curve of treated and non-treated samples before ageing.

Sample	Atmosphere	T_g (°C)	T_{cc1} (°C)	ΔH_{cc1} (J/g)	T_{cc2} (°C)	ΔH_{cc2} (J/g)	T_{m1} (°C)	ΔH_{m1} (J/g)	T_{m2} (°C)	ΔH_{m2} (J/g)	χ_1 (%)	χ_2 (%)
NT	Air	61	95	-21,90	154	-4,77	174	38,67	218	4,13	18,01	9,56
T	Air	62	96	-17,59	153	-5,79	175	37,69	221	3,33	21,59	22,46
NT	N	61	96	-18,55	154	-4,75	176	37,99	221	3,95	20,88	24,17
T	N	61	95	-20,51	152	-5,12	177	38,79	220	4,37	19,63	9,80

The degree of crystallinity in air of non-plasma treated samples is lower compared to treated samples when heated in air than in nitrogen.

The exothermic crystallisation peaks are absent in the filament stored in the oven (Figure 23), which means that the crystallisation process was completed during annealing [160].

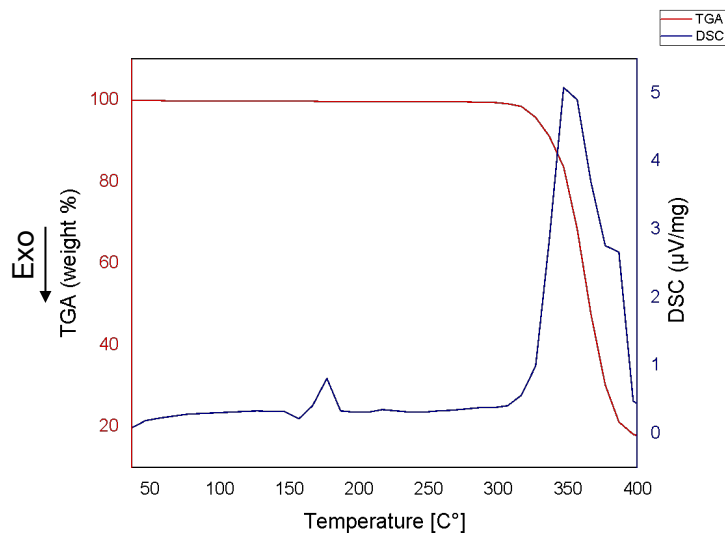


Figure 23. TG-DSC curve of spool filament before ageing.

- Colorimetric measurement

Colorimetric analysis was performed on plasma-treated and non-plasma-treated samples, before the ageing tests. For these samples, therefore, an average of the values of L^* , a^* and b^* , which will be used to determine the colour variation (ΔE) after 500, 1000 and 1500 hours, are reported (Table 15).

Table 15. Colorimetric parameters of reference samples.

Sample	L^*	SD L^*	a^*	SD a^*	b^*	SD b^*	ΔE
NT_rif	80,19	0,12	-0,15	0,01	11,19	0,04	-
T_rif	82,49		-0,36		9,38		2,9

The samples show similar colorimetric values. The brightness parameter, whose values can range from 0 to 100, is particularly high (~ 80) both for the treated and non-treated samples. The negative sign in front of a^* places the value in the green range, even if only in small

quantities. On the other hand, the value of b^* , accompanied by a positive algebraic sign, represents yellow. The samples, in fact, are opalescent and tend to yellow.

The reflectance spectra for the treated and non-treated samples before ageing were acquired (Figures 24).

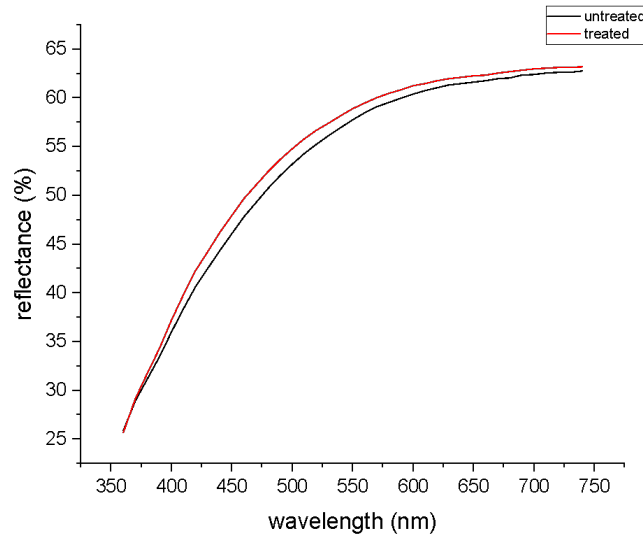


Figure 24. Reflectance curves of a non-treated (black curve) and treated sample (red curve).

The spectra appear very similar, both in fact show an initial rise in the curve followed by an approximately linear trend, typical of white pigments, the only slight difference being the scale of the ordinates: the plasma-treated sample has a higher reflectance than the untreated one. The plasma treatment, therefore, seems to modify the aesthetic properties of the 3D printed PLA, albeit in an infinitesimal and therefore negligible way.

- Dynamometric tests

The dynamometric tests, before being performed on the aged specimens, were performed on the plasma-treated and non-treated samples without ageing.

For each group of specimens, the average of the modulus, peak load, peak stress and strain at break values (Tables 16 and 17), the load-extension curve (Figures 25 and 26) and a photo with the specimens after the tensile test (Figure 27) are reported.

Table 16. Average values of dynamometric tests on six non-treated samples before ageing.

Results	Average values	SD
Modulus	463,715 MPa	22,141
Peak load	56,80 N	6,12
Peak stress	4,6 MPa	0,5
Strain at break	1,346%	0,238

Table 17. Average values of dynamometric tests on five treated samples before ageing.

Results	Average values	SD
Modulus	445,454 MPa	40,916
Peak load	52,879 N	4,761
Peak stress	4,4 MPa	0,4
Strain at break	1,229%	0,361

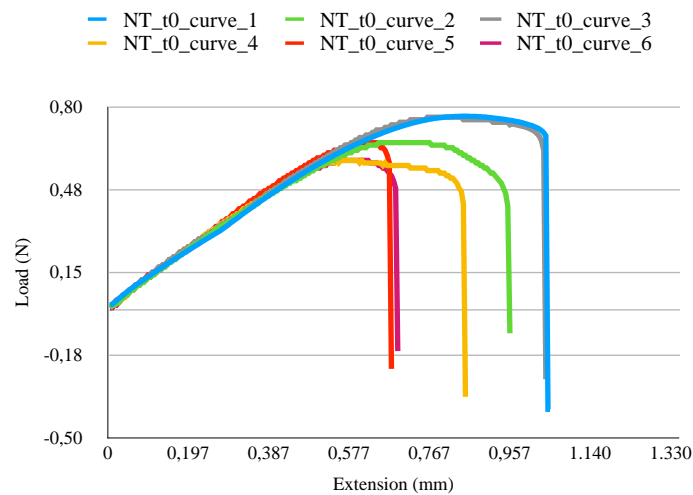


Figure 25. Load-extension curves of six non-treated samples before ageing.

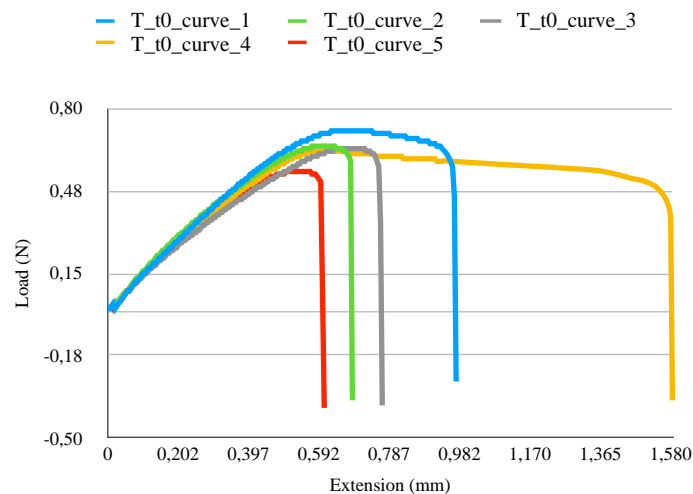


Figure 26. Load-extension curves of five treated sample before ageing.



Figure 27. Six non-treated samples (left) and five treated sample (right) after tensile tests.

According to literature data, plasma treatment performed on dog-bone-shaped PLA samples promotes adhesion between the layers, thus improving the mechanical properties of the material [157].

Comparing the results obtained, however, the average values of the untreated samples, with the exception of the strain at break, are higher than those of the treated ones. The plasma treatment, therefore, does not seem to have improved the mechanical properties of the material, making it apparently more brittle than the untreated polymer. However, for the treated specimens, whose mean values were calculated with four specimens, given the fifth outlier, the even more limited ability to elongate when subjected to tensile stress may not be due to the ineffectiveness of the treatment, but rather to the excessive deposition of silicate precursor, TEOS, during printing; in fact, it may have led to the creation of vitrified surfaces between the layers of moulded polymer. This must have given the treated specimens greater rigidity and therefore lower tensile strength. By observing the fracture points of the specimens, important information about the ductility and brittleness of the material can be obtained. A fracture is ductile when it occurs at about 45° with respect to the direction of stress; the material therefore has a plastic behaviour, according to which the crystals slide in oriented planes. A brittle fracture occurs perpendicularly to the direction of stress, because the crystals are not cohesive [157]. The untreated specimens show a tendentially brittle fracture, breaking in correspondence to the shrinkage of one of the two ends; on the contrary, the treated specimens seem to present a tendentially ductile fracture and to break preferentially in correspondence to the centre of the specimen.

3.2 Accelerated ageing

In this section, spectra acquired with the different investigation techniques, of plasma-treated and non-plasma-treated samples underwent to ageing processes, are reported. ATR-FTIR spectra were acquired after 80, 1500 and 2000 hours from the start of both ageing tests. Raman spectra were acquired after 80, 500, 1000, 1500 and 2000 hours. Colorimetric measurements were performed after 500, 1000 and 2000 hours.

- ATR-FTIR spectroscopy

Below are the spectra of the plasma-treated and no-plasma-treated samples at different UV ageing steps (Figures 27 and 28, respectively).

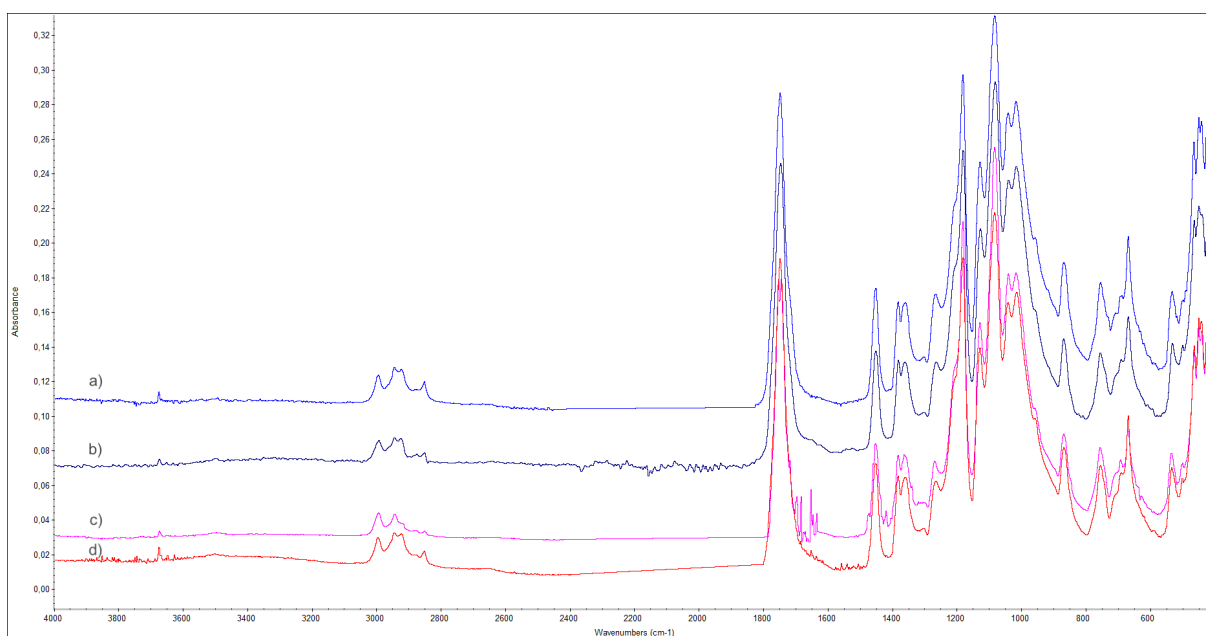


Figure 27. ATR-FTIR spectra of the printed non-plasma-treated sample at different UV ageing steps: a) 0 hours, b) 80 hours, c) 1500 hours and d) 2000 hours.

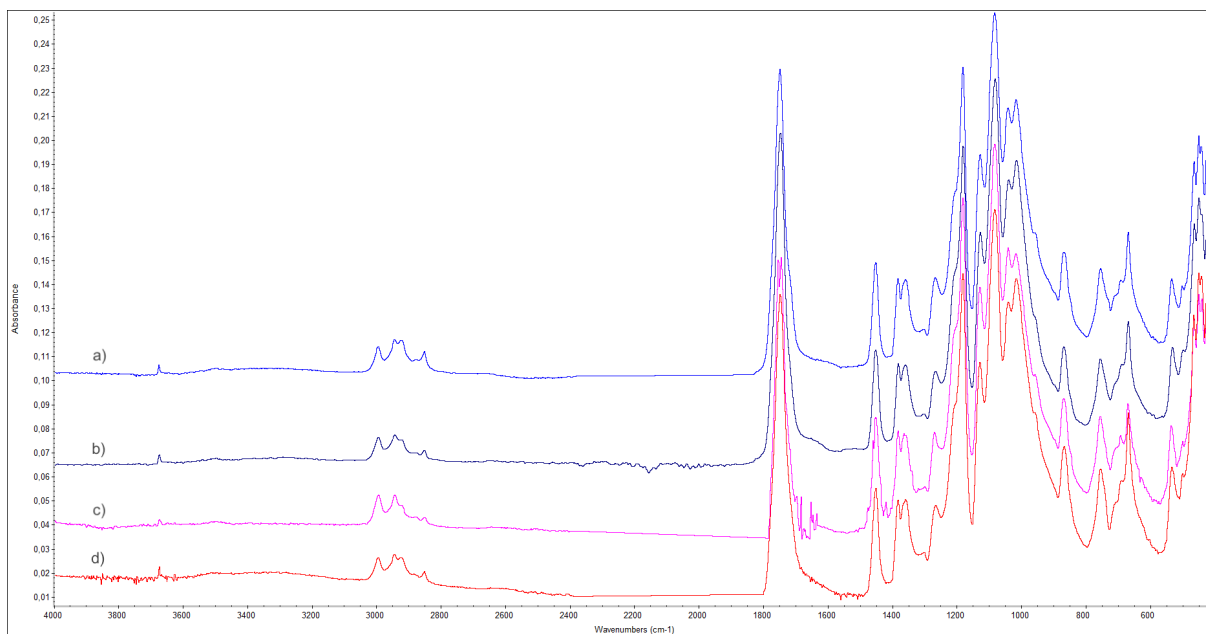


Figure 28. ATR-FTIR spectra of the printed plasma-treated sample at different UV ageing steps: a) 0 hours, b) 80 hours, c) 1500 hours and d) 2000 hours.

Comparing the spectra of the samples subjected to ageing with that of the sample in its initial state, some differences between the absorption intensities are visible. Indeed, the intensities of the peaks associated with the polymer matrix are slightly higher in the samples subjected to artificial ageing; aspect probably due to different baseline. The shoulder that should be observed at around 1845 cm^{-1} is not visible for the aged samples: in fact, it falls within the range that showed a strong absorption due to the humidity present in the environment at the time of data acquisition, which, to allow a better visualisation of the spectra, was removed.

The peaks at 920 , 956 and 1654 cm^{-1} , given by the unsaturation vinyl groups, intensified with ageing, as did the peaks at 1380 and 1115 cm^{-1} .

As with the non-plasma treated samples, the same changes due to photodegradation of the polymer matrix are observed in the plasma treated samples. As far as the talc-related peaks are concerned (Table 7, page 49), for both the treated and the untreated sample in the different ageing steps, they do not vary in intensity.

To determine the changes in the structure and composition of the polymer under analysis, the spectra of the non-treated and treated samples after 80, 1500 and 2000 hours of ageing in relative humidity are presented below (Figures 29 and 30, respectively).

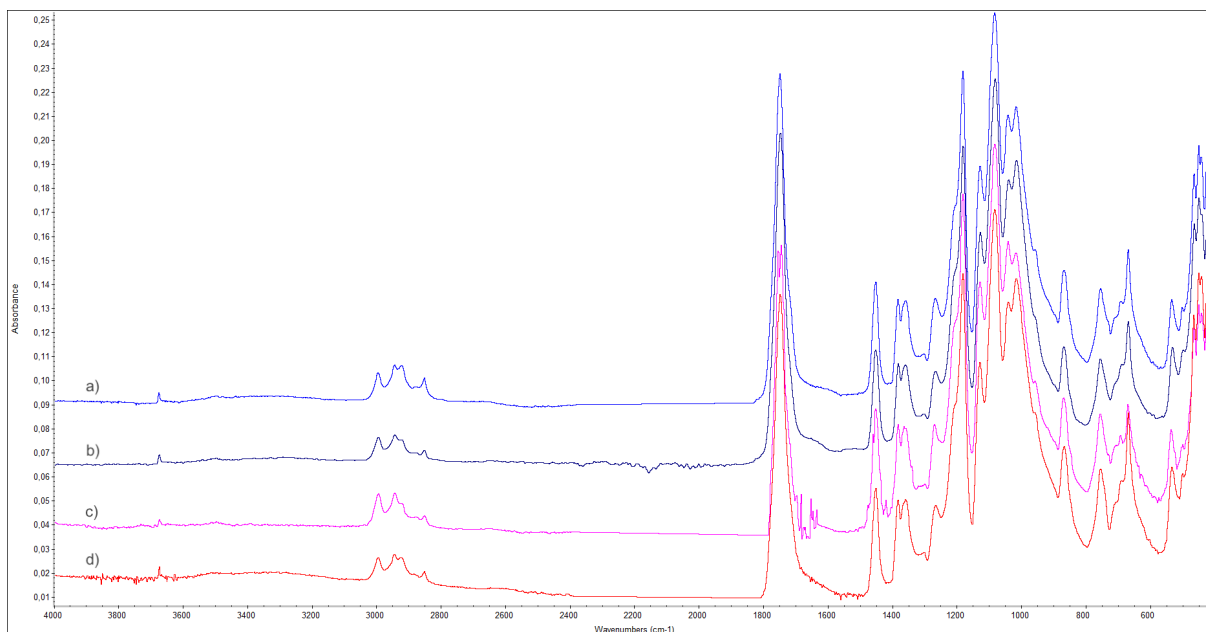


Figure 29. ATR-FTIR spectra of the printed non-plasma-treated sample at different RH ageing steps: a) 0 hours, b) 80 hours, c) 1500 hours and d) 2000 hours.

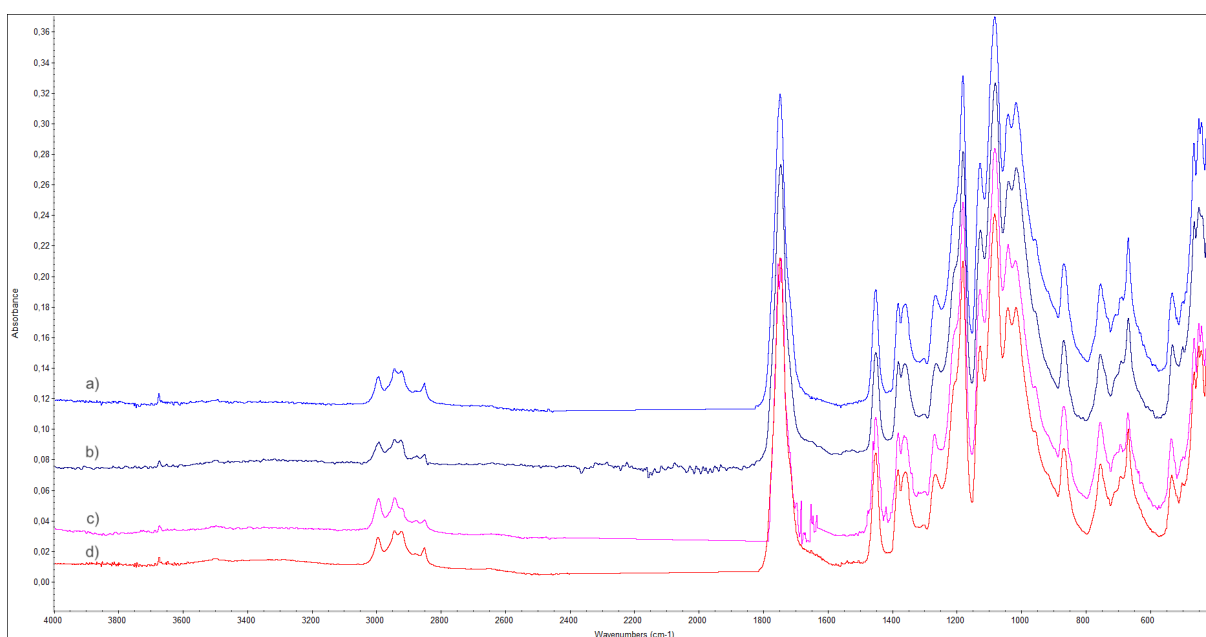


Figure 30. ATR-FT-IR spectra of the printed plasma-treated sample at different RH ageing steps: a) 0 hours, b) 80 hours, c) 1500 hours and d) 2000 hours.

In the case of the spectra of the non-treated samples obtained at different ageing stages, the peak at 1750 cm^{-1} , given by the carbonyl group, decreases for the cleavage of the COO bond. For the same reason there are the decrease also of the peaks at 1359 and 1384 cm^{-1} , for the bending vibrations of the CH_3 group, of the absorptions at $1180\text{-}1020\text{ cm}^{-1}$, for esters and at 870 cm^{-1} , due to the O-CH- CH_3 absorption.

As regards the spectra of the plasma-treated samples, there are no significant variations, either in terms of shift of the characteristic bands and in terms of the formation of new peaks, compared to the untreated ones. The variations in the intensities of the peaks associated with the species involved in the hydrolysis process are the same as for the untreated samples. In contrast to the ATR-FTIR spectra acquired on the filament and the annealed filament, the talc peak at high wavenumbers (3680 cm^{-1}), previously covered by absorptions from humidity, is now clearly visible in the spectra of the aged samples.

In addition to the dog-bone samples, infrared spectra were also acquired for the two cube-shaped 3D-printed samples, in order to investigate the material resistance to aggressive acid attack. In order to determine whether chemical changes occurred between the treated and untreated samples, before and after direct contact with acids (Figures 31 and 32).

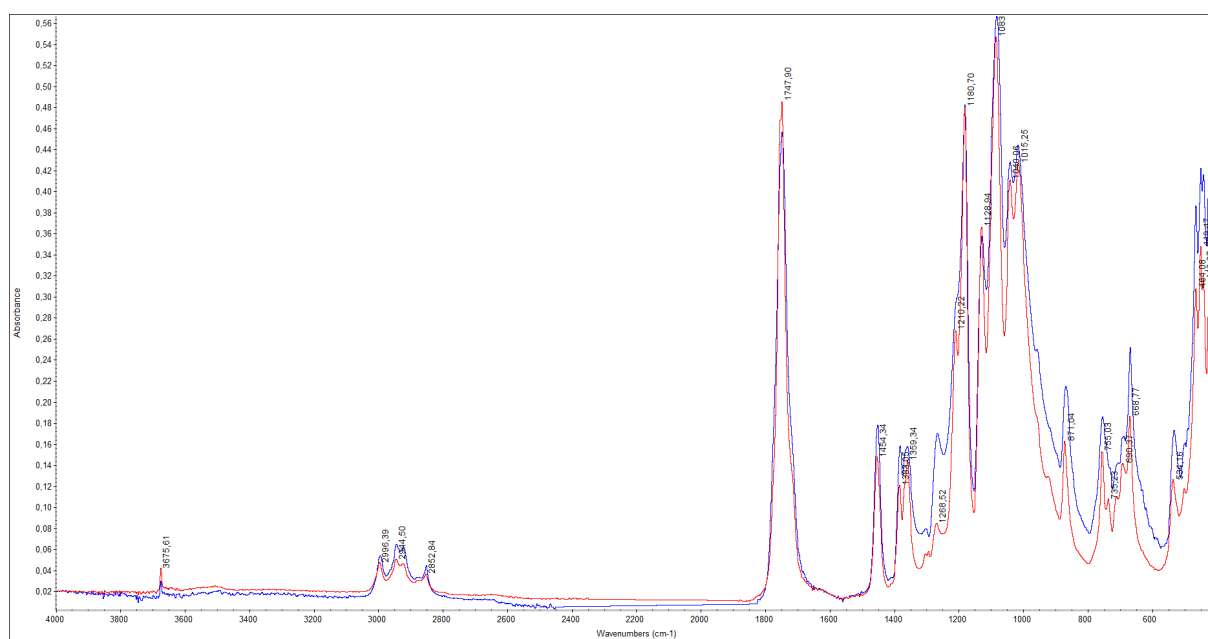


Figure 31. ATR-FTIR spectra of the printed non-plasma-treated cube before (blue line) and after (red line) acid resistance test.

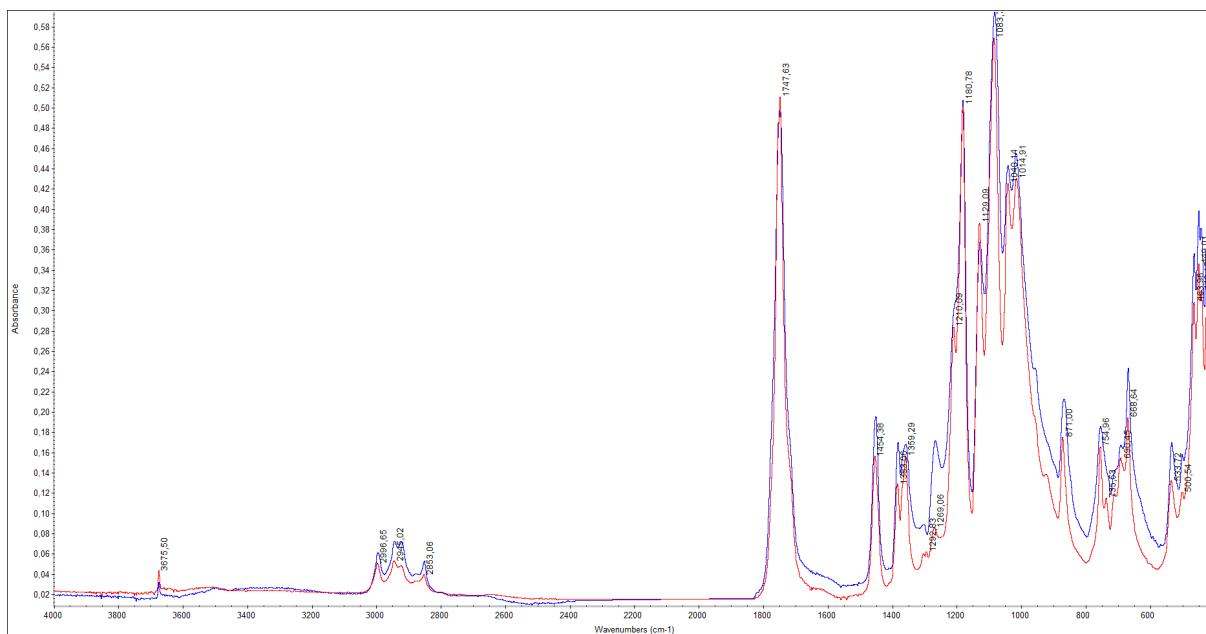


Figure 32. ATR-FT-IR spectra of the printed plasma-treated cube before (blue line) and after (red line) acid resistance test.

In the present case, the characteristic absorptions of the polymer matrix and talc are clearly visible, whose peaks are shown in Table 5 and 7 (page 49 and 51), respectively. In both cubes, the peak at about 1209 cm^{-1} , given by the stretching of the COC group, seems to increase following immersion in acid; on the contrary, the peaks from 1455 to 1368 cm^{-1} , associated with methyl stretching, decrease. The formation of a new small peak at 919 cm^{-1} , and a shoulder at about 735 cm^{-1} is also observed. In both, there is a decrease in the absorption band linked to the ester group at about 870 cm^{-1} , as well as a slight increase in the peak at 1745 cm^{-1} given by the C=O bond. From the spectra, therefore, a decrease in the peaks assigned to the esters and, at the same time, an increase in the absorptions given by the carbonyl group present in the degradation products at approximately 1746, 755 and 701 cm^{-1} is observed [166]. According to the literature, the acid hydrolysis of polylactic acid leads to random breakage of the polymer chain and also to end-of-chain breakage. This leads to the formation of degradation products such as lactate and lactic acid, which in turn forms lactic acid oligomers; the latter, in turn, promote the degradation of the degradation of the polymer matrix [120,121].

- Raman spectroscopy

Raman spectra were acquired on treated and untreated samples aged under UV light and relative humidity. Below are the spectra of the samples treated and non-treated at 0 and after different UV-ageing (Figures 32-33) and RH-ageing (Figures 34-35) steps.

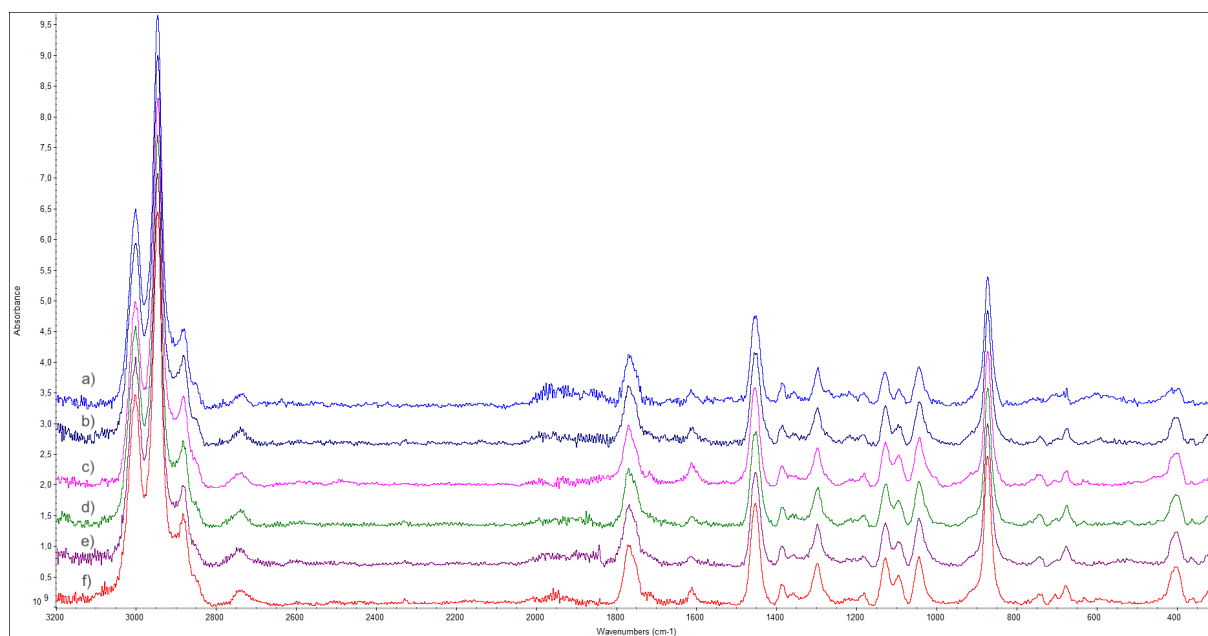


Figure 30. Raman spectra of non-treated UV-aged sample steps: a) 0 hours, b) 80 hours, c) 500, d) 1000, e) 1500 hours and f) 2000 hours.

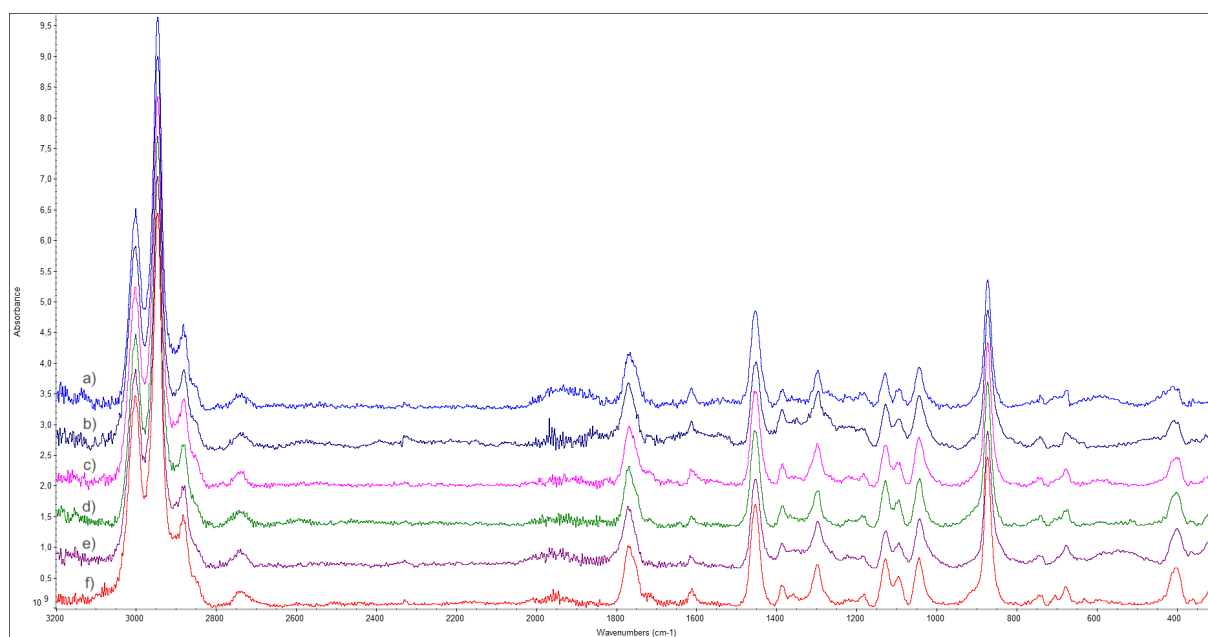


Figure 31. Raman spectra of plasma-treated UV-aged sample steps: a) 0 hours, b) 80 hours, c) 500, d) 1000, e) 1500 hours and f) 2000 hours.

The Raman spectra show that there are no significant variations between PLA samples, whether treated or untreated, subjected to UV ageing or relative humidity. There are, however, differences in the intensities of the characteristic peaks of the polymer matrix.

In the case of both the spectra of treated and untreated photo-aged samples, there is an increase in the intensity of the peak at 2740 cm^{-1} , due to the stretching of the methyl group, as well as the peak at 1090 cm^{-1} , related to the C-O-C group.

With regard to the stretching of the CH_3 group, the absorptions at 3000 and 2880 tend to decrease as age increases. The same applies to the peaks at 1450 and 740 cm^{-1} , given by the C=O group.

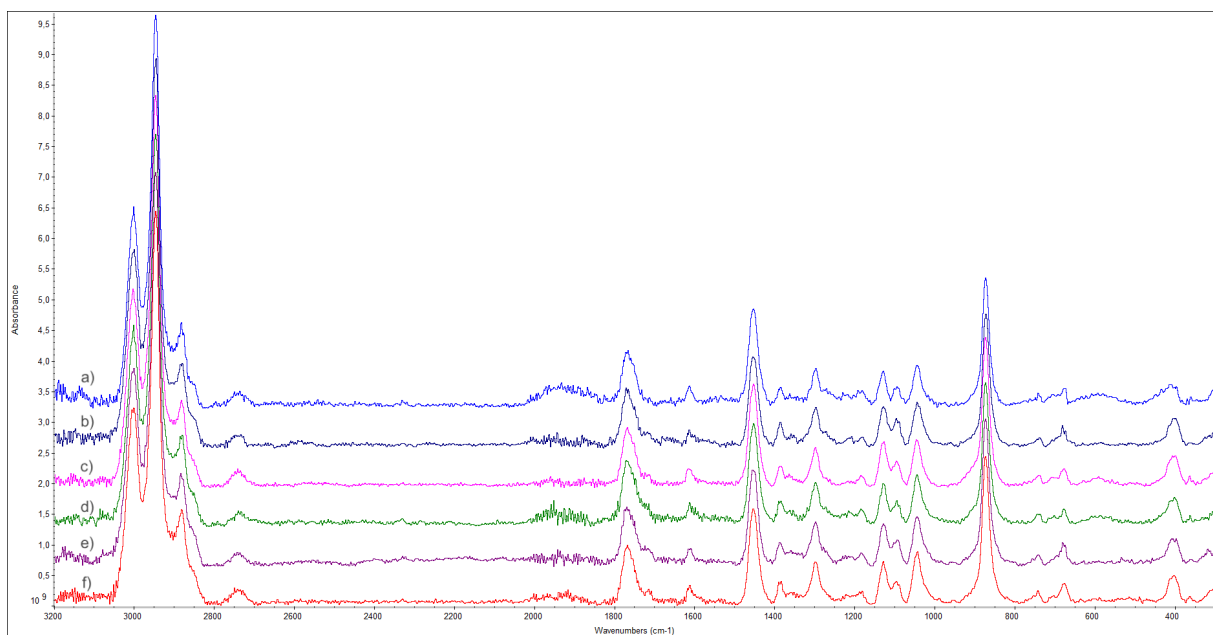


Figure 32. Raman spectra of non-treated and RH-aged sample steps: a) 0 hours, b) 80 hours, c) 500, d) 1000, e) 1500 hours and f) 2000 hours.

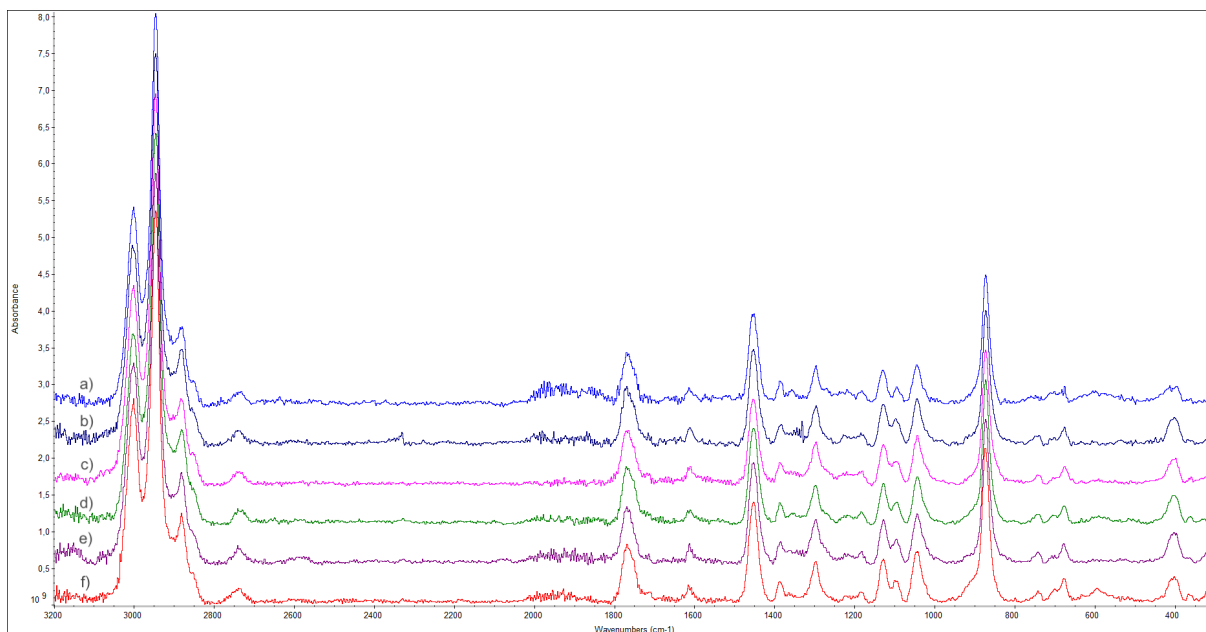


Figure 33. Raman spectra of plasma-treated RH-aged sample steps: a) 0 hours, b) 80 hours, c) 500, d) 1000, e) 1500 hours and f) 2000 hours.

When comparing the Raman spectra of the treated and untreated samples during ageing in relative humidity, no significant differences or the formation of new peaks are observed; the only variations are in the different intensities of the characteristic absorptions of the PLA before and during ageing. In fact, in all the samples subjected to ageing in relative humidity, the peaks at 3000, 2950, 2880, 1768, 1450, 860 and 670 cm^{-1} tend to increase as ageing continues.

Therefore, in the Raman spectra of aged samples no significant changes are visible, apart from small, and sometimes negligible, variations in the intensity of some peaks, with respect to those in the initial state.

- TG-DSC

The TG-DSC analyses were performed on the treated and untreated samples after 2000 hours of ageing in relative humidity and UV. As an exemplification, the TG-DSC curve of the untreated sample subjected to 2000 hours of ageing in relative humidity is shown below (Figure 34); it shows the highest enthalpy values (Table 18).

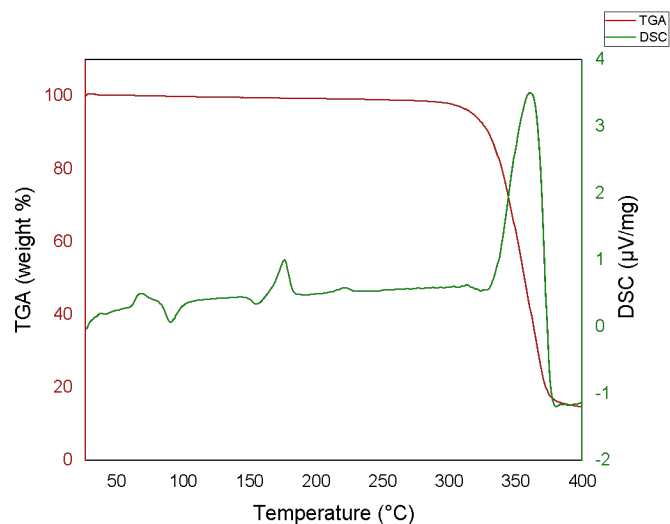


Figure 34. TG-DSC curve in air of a non-treated RH-ageing.

Table 18. Enthalpy results and temperatures obtained from DSC curve of treated and non-treated samples after ageing.

Sample	Atmosphere	T_g (°C)	T_{cc1} (°C)	ΔH_{cc1} (J/g)	T_{cc2} (°C)	ΔH_{cc2} (J/g)	T_{m1} (°C)	ΔH_{m1} (J/g)	T_{m2} (°C)	ΔH_{m2} (J/g)	χ_1 (%)	χ_2 (%)
NT_RH 2000	Air	61	95	-18,43	154	-5,20	174	38,03	218	4,11	60,64	10
NT_UV 2000	Air	62	96	-17,51	153	-3,54	175	37,89	221	4,02	59,60	8,21
T_UV 2000	Air	61	96	-15,92	154	-3,83	176	39,08	221	3,68	59,07	8,06
T_RH 2000	Air	61	95	-16,65	152	-5,08	177	37,94	220	3,56	58,63	9,28

- Colourimetric measurements

For convenience in interpreting and evaluating the data, for each type of sample, treated or untreated, in relative humidity or UV aged, the following are shown: a table with the values obtained from the colorimetric measurements in the different ageing phases (Tables 13-16), a graph with the trend of the colourimetric variation (Figures 35, 38, 41 and 44), a graph with the trend of the yellowing index (Figures 36, 39, 32 and 45) and a spectra with the reflectance curves (Figures 37, 40, 33 and 46).

For the plasma-untreated-UV-aged samples:

Table 19. Colourimetric data of the non-plasma-treated samples at 0, 500, 1000, 1500 and 2000 hours of UV-accelerated ageing.

NT_UV	L*	a*	b*	ΔE	Y
0h	80,19	-0,15	11,19	-	57,02
500h	83,43	-0,96	9,5	3,74	62,98
1000h	82,91	-0,87	9,6	3,23	61,99
1500h	81,72	-1,27	10,15	1,91	59,77
2000h	84,376	-1,106	9,5	3,77	64,824

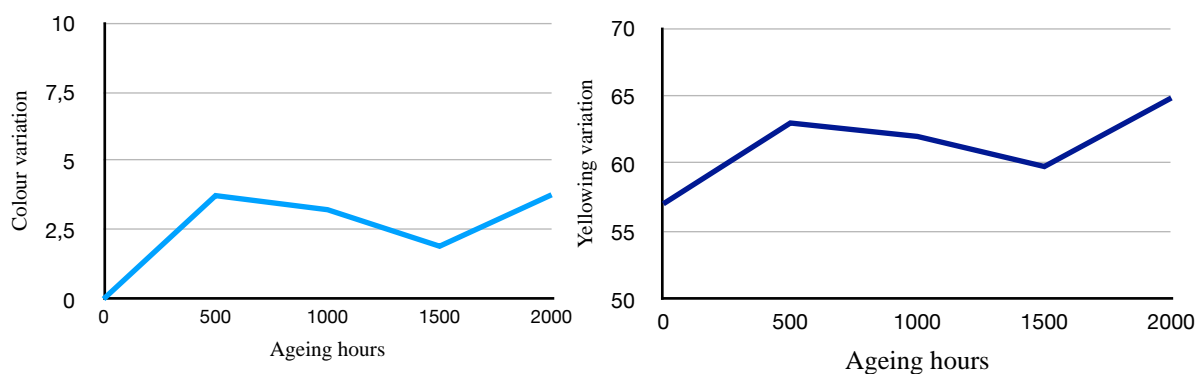


Figure 35. Color change (ΔE) and yellowing index (Y) of non-plasma-treated samples at 0, 500, 1000, 1500, and 2000 hours of UV-accelerated ageing.

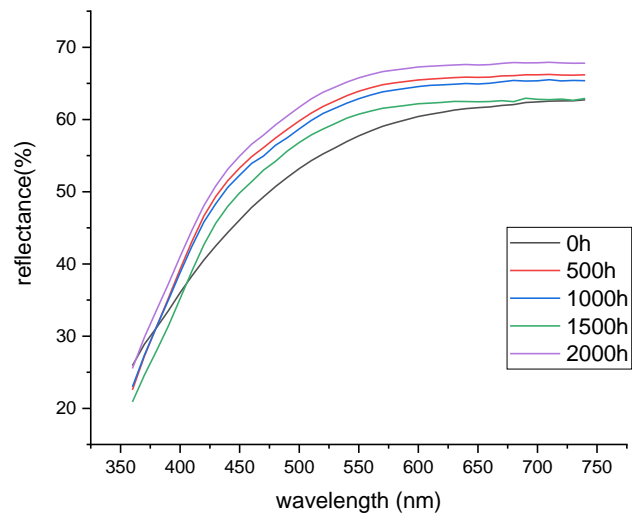


Figure 36. Reflectance spectra of non-plasma-treated samples at 0, 500, 1000, 1500, and 2000 hours of UV-accelerated ageing.

For the plasma-treated-UV-aged samples:

Table 20. Colourimetric data of the plasma-treated samples at 0, 500, 1000, 1500 and 2000 hours of UV-accelerated ageing.

T_UV	L*	a*	b*	ΔE	Y
0h	82,49	-0,36	9,38	-	61,2
500h	83,45	-1,21	12,46	3,33	63,02
1000h	82,23	-0,79	10,97	1,66	60,73
1500h	82,61	-1,42	11,08	2,08	61,44
2000h	83,766	-1,338	10,706	1,96	63,62

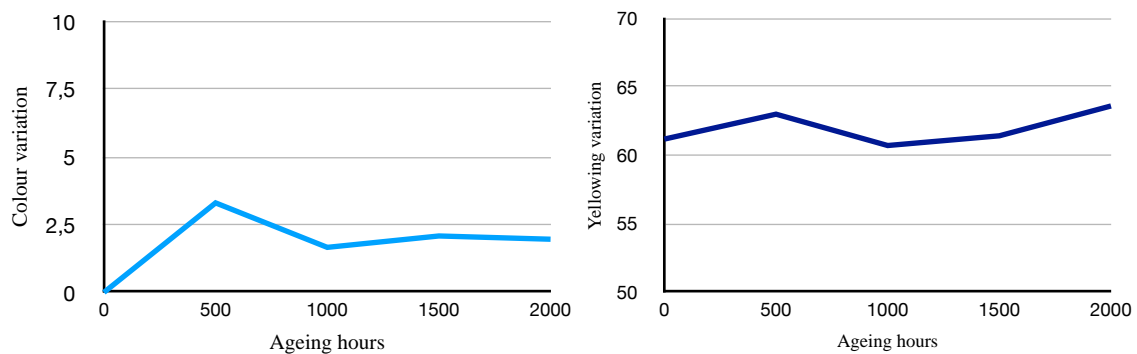


Figure 39. Color change (ΔE) and yellowing index (Y) of plasma-treated samples at 0, 500, 1000, 1500, and 2000 hours of UV-accelerated ageing.

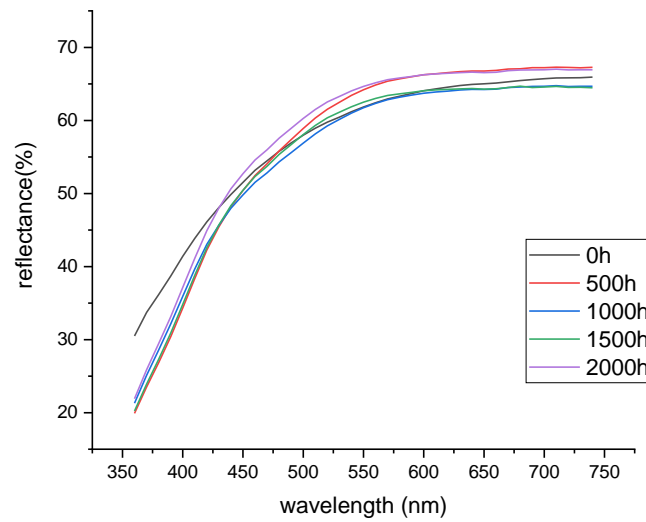


Figure 40. Reflectance spectra of plasma-treated samples at 0, 500, 1000, 1500, and 2000 hours of UV-accelerated ageing.

As regards the non-plasma-treated-RH-aged samples:

Table 21. Colourimetric data of the non-plasma-treated samples at 0, 500, 1000, 1500 and 2000 hours of RH-accelerated ageing.

NT_RH	L*	a*	b*	ΔE	Y
0h	80,19	-0,15	11,19	-	57,02
500h	82,65	-0,96	12,09	2,74	61,5
1000h	83,05	-1,7	17,35	6,96	62,25
1500h	80,9	-1,23	15,41	4,45	58,29
2000h	82,044	-1,248	16,56	6,74	60,43

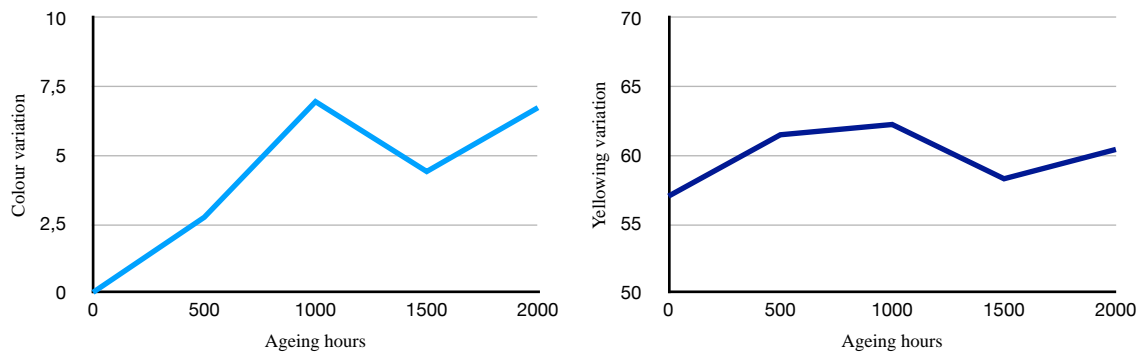


Figure 41. Color change (ΔE) and yellowing index (Y) of non-plasma-treated samples at 0, 500, 1000, 1500, and 2000 hours of RH-accelerated ageing.

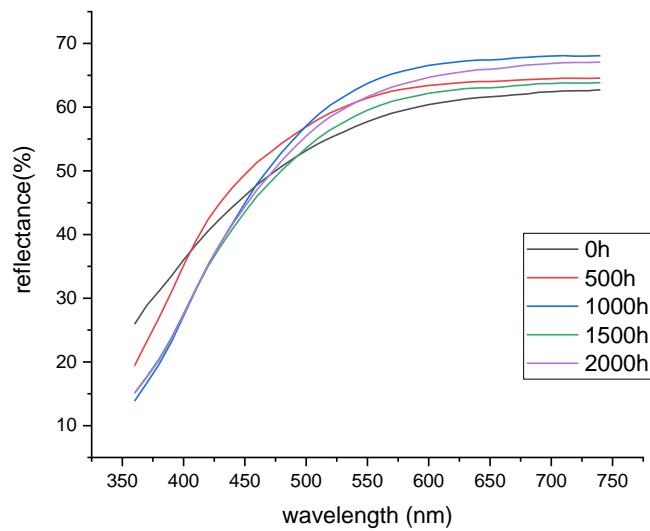


Figure 43. Reflectance spectra of non-plasma-treated samples at 0, 500, 1000, 1500, and 2000 hours of RH-accelerated ageing.

In the case of the plasma-treated-RH-aged samples:

Table 16. Colourimetric data of the plasma-treated samples at 0, 500, 1000, 1500 and 2000 hours of RH-accelerated ageing.

T_RH	L*	a*	b*	ΔE	Y
0h	82,49	-0,36	9,38	-	61,2
500h	82,11	-0,98	11,11	1,88	60,5
1000h	80	-0,81	18,04	9,02	66,68
1500h	81,66	-0,72	13,01	3,74	59,67
2000h	83,038	-0,814	12,784	2,53	60,28

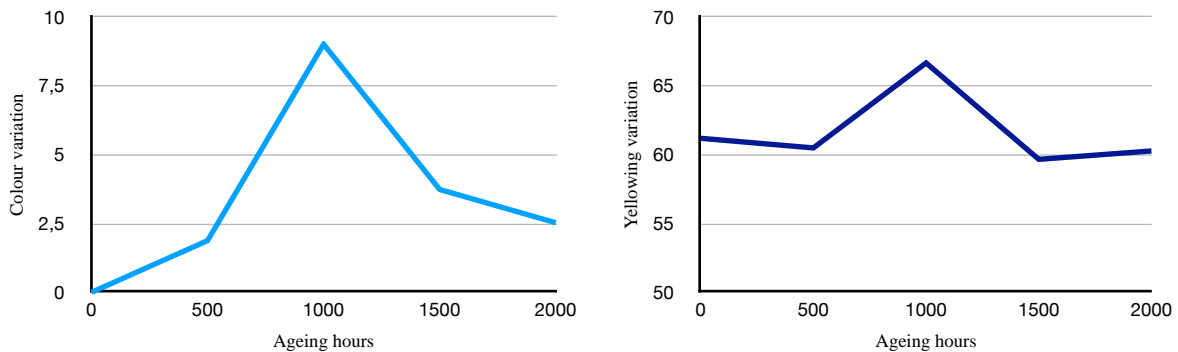


Figure 44. Color change (ΔE) yellowing index (Y) of plasma-treated samples at 0, 500, 1000, 1500, and 2000 hours of RH-accelerated ageing.

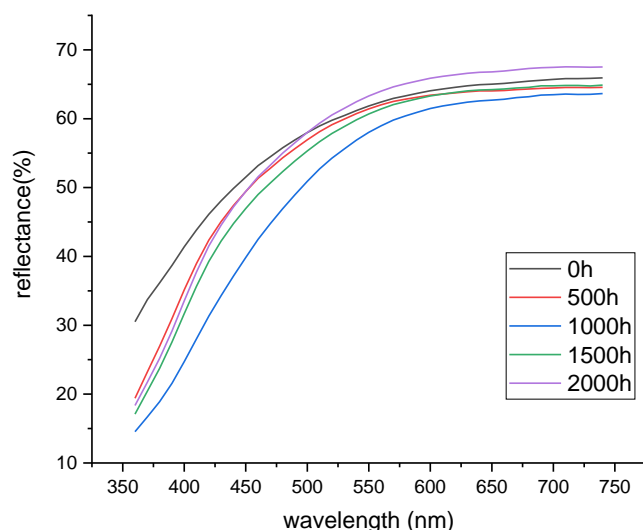


Figure 46. Reflectance spectra of plasma-treated samples at 0, 500, 1000, 1500, and 2000 hours of RH-accelerated ageing.

With regard to the plasma-treated and non-plasma-treated samples that were subjected to UV ageing, the final ΔE value after 2000 hours is slightly lower in the plasma-treated samples (1,96) than in the non-treated samples (3,77). Considering that a chromatic variation is often a symptom of chemical-physical transformations within the structure of the material, the fact that the treated samples present a negligible ΔE value would seem that the treatment partially avoided the chromatic variation of the material. The value that has had the greatest influence on the colour variation of the material is b^* , a parameter linked to yellowing.

This colour change is due to the incorporation, during accelerated ageing processes, of yellow chromophore species, which alter the aesthetics of the material. With regard to the reflectance spectra, they all show a similar trend, although they all present a slight absorption around the 450 nm, area of blue.

The samples that have been subjected to ageing in relative humidity, as in the case of the UV-aged samples, show a higher ΔE value for the untreated samples (6,74) than for the treated ones (2,53). Also in this case, the parameter that seems to have most influenced the variation is b^* . The oscillating trend of the ΔE value of the samples at the different ageing steps is one of the most relevant problems in the commercial polymer industry. In fact, this phenomenon is due to the synergic action of several factors, such as light, heat, humidity, extreme pH and

contaminants, which favour the coupling of radicals with the peroxide radicals formed by degradation.

The UV-aged samples, both plasma-treated and non-plasma-treated, have shown a rather pronounced colour change after the first 500 hours, then it has decreased between 1000 and 1500 hours and then increased slightly. This is due to the fact that, with UV degradation, cross-linking and cleavage processes take place on the polymer surface that form the yellow chromophore species responsible for the colour change and that favour an increase in the density of the polymer on the surface, but at the same time preventing subsequent penetration by light and oxygen into the structure [165,166]. This process, therefore, once completed, seems to decrease the rate of degradation of the material. However, as the irradiation time increases, the cross-linking breaks down and a sudden, and sometimes larger, increase in colour variation is observed [167]. The extent of photodegradation, however, is limited by the ability of the radiation to penetrate the interior of the material; this ability varies with radiation, exposure time and material.

Moisture also had a negative effect on the yellowing process of the samples aged in relative humidity; these show more marked colorimetric changes than UV-aged samples. The marked increase in the yellowing index observed between 500 and 1000 hours of ageing suggests that the humidity favoured the formation of yellow species.

3.1.6 Acid attack resistance tests

In order to obtain information about the effectiveness of the deposition treatment of the silicate coating, it was decided to place a small portion of the filament and the two 3D printed cubes, one treated and one untreated, in cuvettes containing nitric acid at pH 2. The samples were immersed for a total time of approximately 2200 hours, after which the samples were washed and visually examined (Figure 47).

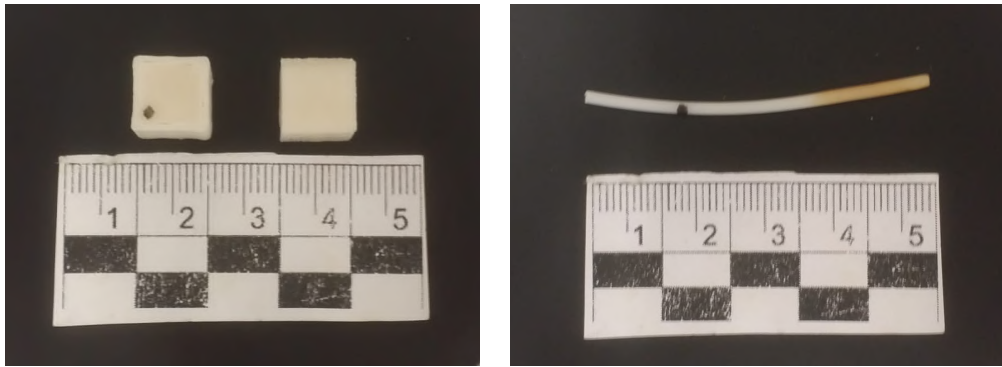


Figure 47. Nitric acid resistance test: on the left the two PLA cubes (treated on the right and untreated on the left) and on the right the filament after about 2200 hours of immersion.

In both cubes, therefore, there were no obvious signs of loss of adhesion between the layers of print: the acid did not cause swelling or softening of the polymeric material, nor was the formation of micro-fractures observed. Given in fact the inorganic nature of nitric acid, the polymer, which is of organic origin, showed excellent resistance to acid hydrolysis that, unlike basic and neutral ones, which involve random chain breakage, includes two mechanisms: random cleavage and end-of-chain cleavage, with the latter occurring more rapidly [167].

Since the aim of the test is to check the effectiveness of the plasma treatment, which should improve the adhesion between the various layers through the deposition of TEOS, and since the first acid test did not allow any conclusions to be drawn in this respect, it was decided to place the cubes in glacial acetic acid for approximately 350 hours (Figures 39 and 40).

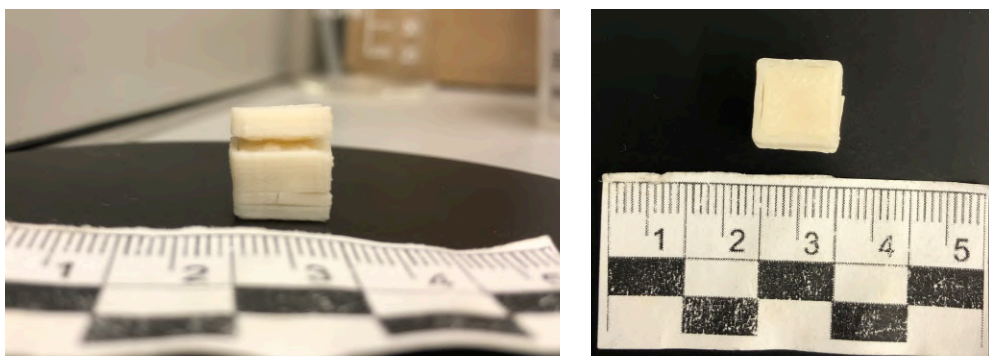


Figure 48. Glacial acetic acid resistance test, non-treated cube: on the left seen from the side and on the right seen from above.

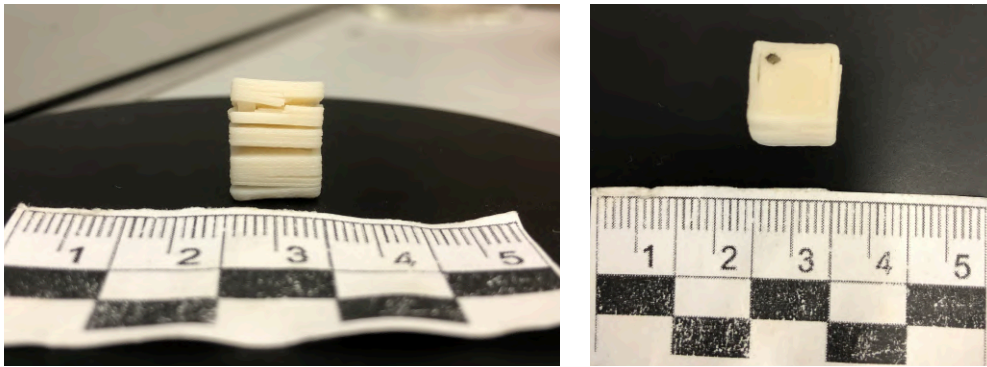


Figure 49. Glacial acetic acid resistance test, treated cube: on the left seen from the side and on the right seen from above.

At the end of the immersion, it is possible to notice the effects of the acid which, being of an organic nature, and therefore chemically similar to the polymeric matrix of the samples, has shown an aggressive behaviour towards the material itself.

This is because organic acids are able to interact with the molecular chains of the polymeric material, leading to the consequent swelling, softening, dissolution and breaking of its structure. The effects of acid hydrolytic degradation are, however, more pronounced in the plasma-treated cube than in the untreated cube. This might be due not to the treatment itself, but to the printing parameters and the amount of precursor deposited for each layer (excessive in relation to the extrusion speed of the polymer). This caused the silicate precursor develop a vitrification effect between the printing layers, which, instead of promoting adhesion between them, favoured their separation once in contact with the acid.

3.1.7 Dynamometric tests

Average values for untreated and RH-aged samples are shown below:

Table 19. Average dynamometric test values of five non-treated samples after 2000 hours of RH ageing.

Results	Average values
Modulus	533,599 MPa
Peak load	40,4 N
Peak stress	3,4 MPa
Strain at break	0,912%

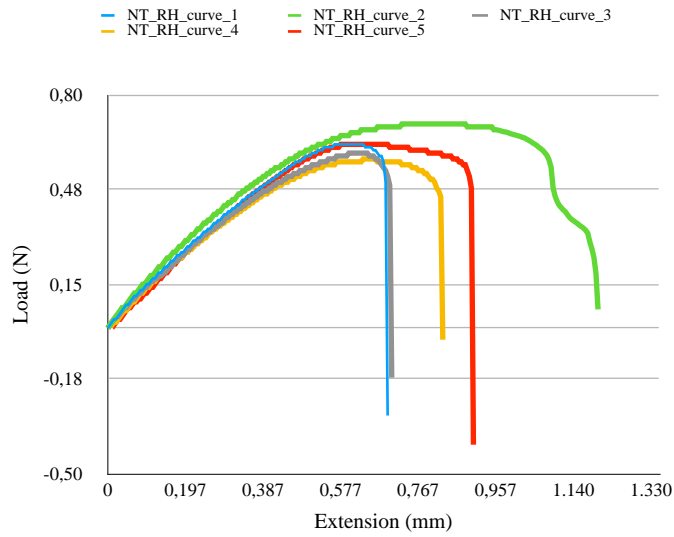


Figure 50. Load-extension curves of five non-treated samples RH-aged.



Figure 51. Untreated samples RH-aged after tensile test.

These results were obtained for the RH-aged plasma-treated samples:

Table 20. Average dynamometric test values on five treated samples after 2000 hours of RH ageing.

Results	Average values
Modulus	488,275 MPa
Peak load	47,346 N
Peak stress	3,94 MPa
Strain at break	1,278%

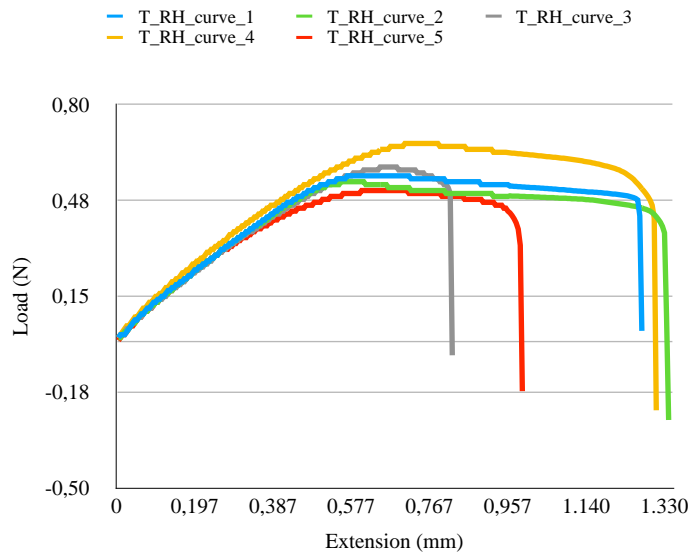


Figure 52. Load-extension curves of the treated samples RH-aged.

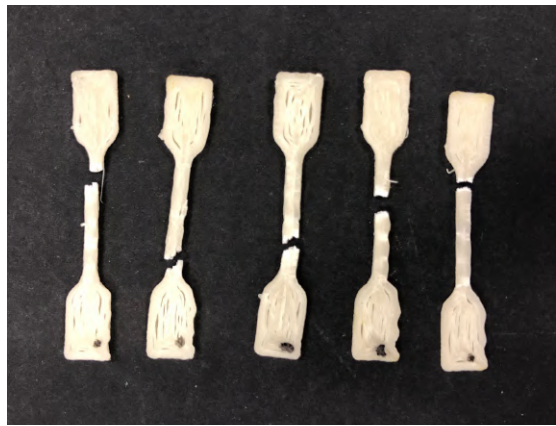


Figure 53. Treated samples RH-aged after tensile test.

For non-plasma-treated UV-aged samples:

Table 21. Averages dynamometric test values on five untreated samples after 2000 hours of RH ageing.

Results	Average values
Modulus	523,062 MPa
Peak load	45,2 N
Peak stress	3,6 MPa
Strain at break	0,938%

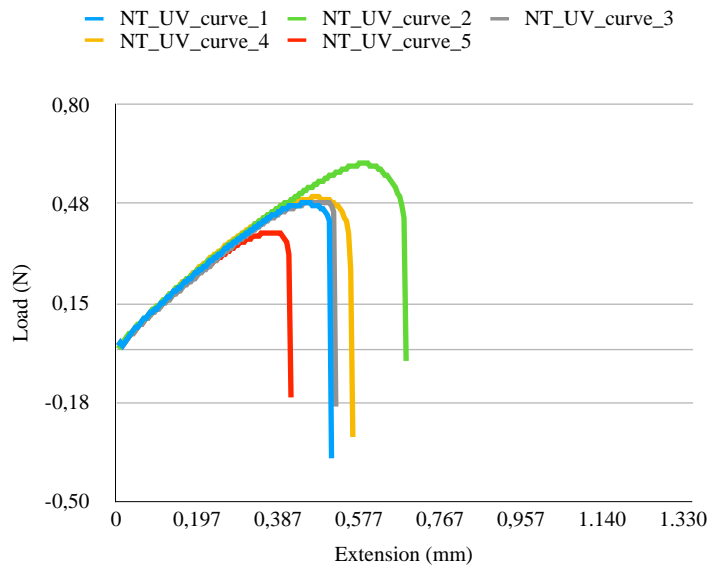


Figure 54. Load-extension curves of the untreated samples UV-aged.



Figure 55. Untreated samples UV-aged after tensile test.

In contrast, in UV-aged plasma-treated samples:

Table 22. Average dynamometric test values on four samples treated after 2000 hours of UV ageing.

Results	Average values
Modulus	533,751 MPa
Peak load	51,9 N
Peak stress	4,3 MPa
Strain at break	1,285%

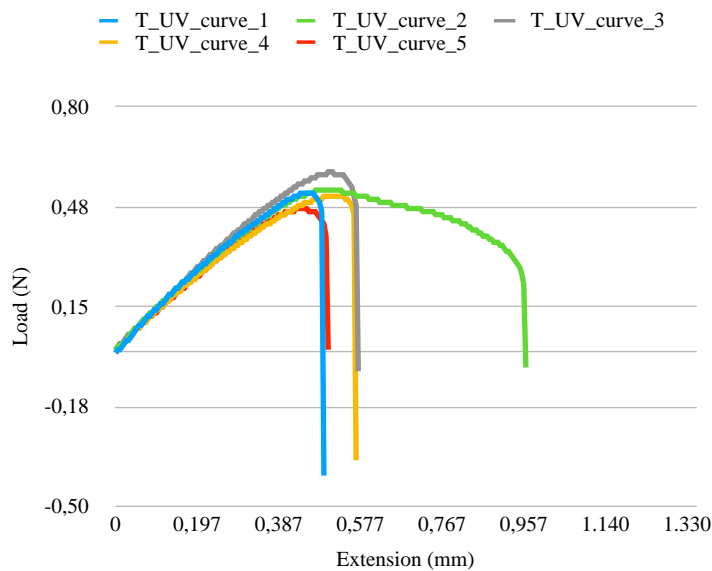


Figure 56. Load-extension curves of the treated samples UV-aged.



Figure 57. Treated samples UV-aged after tensile test.

Looking at the data from the tensile tests performed on the untreated and treated specimens, aged in UV or relative humidity, the average values of peak load, peak at stress and strain at break are always higher in the untreated specimens. In contrast, the averaged modulus of elasticity values are slightly higher in the treated specimens (1,285% for RH and 0,938% for UV) than in the untreated ones (1,27% for RH and 0,912% for UV).

Furthermore, as in the case of the samples in their initial state, the treated ones show a tendentially ductile fracture, with the fracture plane oriented at 45° with respect to the direction of stress. The untreated specimens, on the other hand, show a more brittle fracture, perpendicular to the direction of stress and more in correspondence to the shrinkage near one of the two edges, than the treated ones.

In general, the elastic modulus of specimens in their initial state exhibit higher stress-at-break values than specimens that have been subjected to UV and RH-ageing. This is because degradation processes generally lead to chain scission and embrittlement of the thermoplastic material, resulting in a decrease in elastic modulus and tensile strength, as well as lower ductility. The loss of ductility is manifested by a decrease in the strain-at-break values [156].

These values in the samples aged in relative humidity are higher than in the samples that have undergone photo-oxidation; this is probably because the water molecules that have been able to penetrate inside the polymer chains have given the material greater plasticity and therefore greater tensile strength.

As in the case of unaged specimens, therefore, specimens treated with a plasma source that included the deposition of a silicate coating tended to fracture earlier than those that had not undergone the treatment. However, this unexpected result might be due to the plasma treatment, but rather to the excessive precursor deposition that led to vitrification of the space between the printed polymer layers.

Chapter 4. Life Cycle Assessment

4.1 Comparison between two case study

This chapter focuses on the application of the Life Cycle Assessment methodology to two hypothetical cases of integrative restoration: the first, carried out with PLA additivated with talc and plasma treated during the 3D printing process; the second, with Araldite® and silicone rubber.

The aim is to quantify the environmental impact given by each case study and, according to the results obtained, to evaluate if the restoration intervention performed with innovative materials and techniques can be considered a valid alternative in terms of performance and durability to traditional ones. Before proceeding with the identification of the inputs and outputs for each case study, it is important to define the functional unit and the boundaries of the system.

4.1.1 Unit function of the system

The functional unit is the reference against which all input and output data are normalised.

For our purposes, in agreement with others in the literature, the functional unit chosen for both the case study is the volume unit 1 cm³, a cube-shaped sample, with a total mass of 1147.26 mg.

In the case of integrative restoration performed with innovative materials and methods, it was made with PLA using the FDM additive manufacturing technique; in the case of restoration using traditional techniques and materials, it was made from epoxy resin and a silicone rubber mould.

4.1.2 Boundaries of the system

The system boundaries define which life cycle phases and processes belong to the analysed system. For both integrative proposals, considering the aim of the analysis, it was considered

unnecessary to start from the extraction of raw materials in the environmental impact evaluation, especially considering the small amount of material required. Therefore, for the integrative proposal carried out with innovative materials and techniques, it was considered more coherent with the aim to focus on the impact given by the processes of manufacturing and chemical synthesis of the products as they reach the consumer, as well as their consequent use and disposal. As concerns the durability of the thermoplastic polymer and the epoxy resin, once the printing process or drying inside the mould has been completed, it is closely related to the environment in which the materials are placed. The advantages and disadvantages of using traditional materials for making positives and casts, such as epoxy resins and silicone rubbers, are almost already known: they are highly resistant to degradation factors, even if they tend to change colour in a short time, they are easy to use, have a low shrinkage index during drying, can be loaded with any material and allow the object to be faithfully reproduced [163]. It can therefore be assumed that an artistic integration made of Araldite® can last at least ten years, without showing significant signs of deterioration, when preserved in an outdoor environment under the direct action of the weather [162]. Doubts still exist, however, about the durability of thermoplastic polymers. In an indoor environment, they can have a considerable life span, since they are not subject to the same degradation factors that affect materials exposed to weathering [2]. At present, there are not many studies on the durability of thermoplastic polymers in an outdoor environment and most of them do not present encouraging results, especially for polymers obtained from biomass and subjected to direct weathering [164,165,166,167]. Moreover, the resistance of PLA can be favoured by a series of factors, like the presence or absence of additives within the polymer matrix, able, for example, to provide protection against photo-degradation, or the execution of treatments, like the deposition of a surface coating during the printing process, which can instead implement the chemical-mechanical properties of the material. According to the research carried out in this field, it has been seen that PLA, without any surface functionalisation treatment, placed under the direct action of the weather, shows the first signs of degradation after two years [3]. It is therefore reasonable to assume that the same PLA placed in the same conditions of preservation, but treated with a plasma source capable of depositing a surface coating, can have a life of at least five years.

To relate the two cases of integrative restoration, considering the different life expectancy of the materials, normalising boundaries of one year were taken into account.

In order to make the life cycle phases, processes and flows visually clearer, the boundaries are shown, both for the case of integration with traditional materials and techniques, and for the case with innovative ones (Figures 58 and 69, respectively).

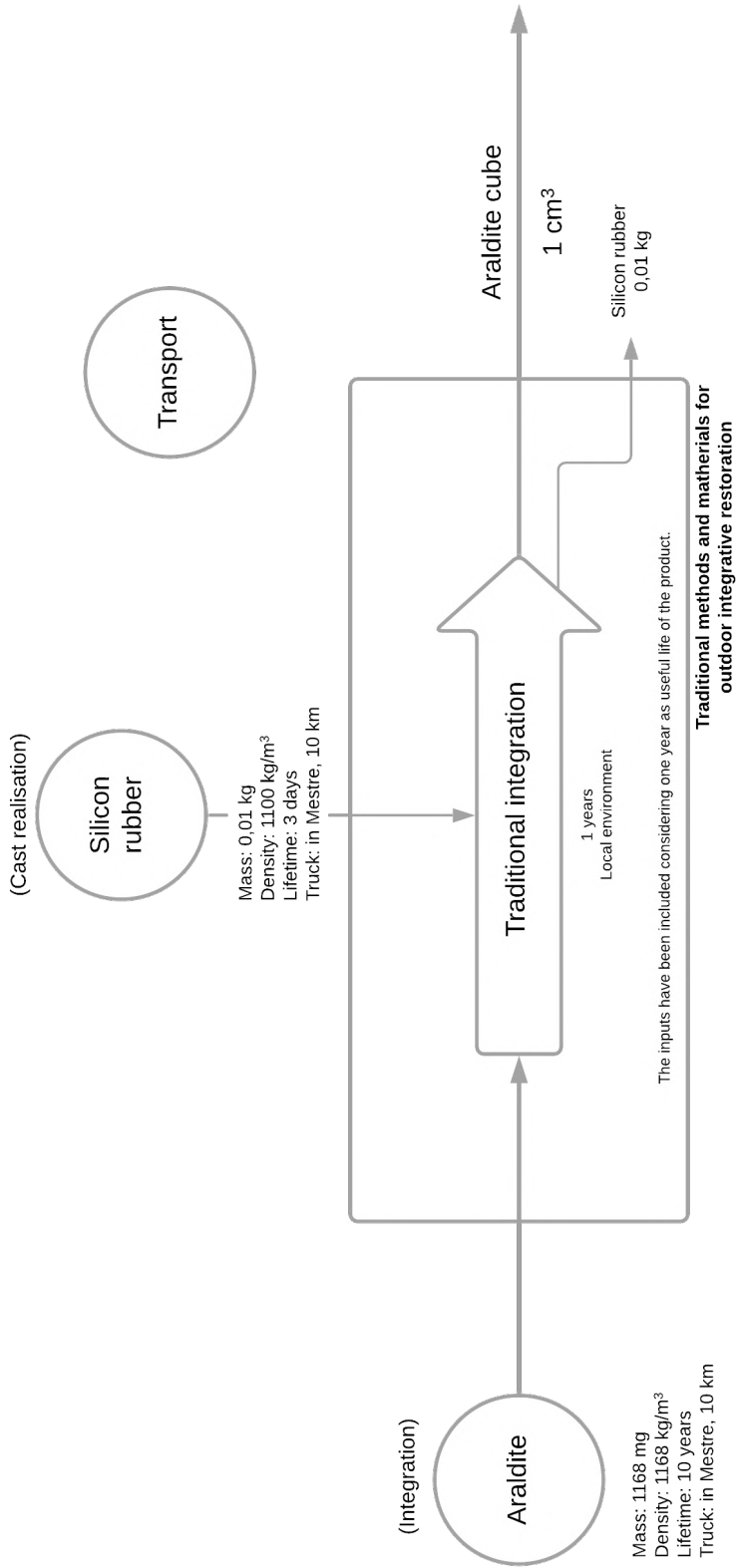


Figure 59. System boundaries case of restoration with traditional materials and techniques.

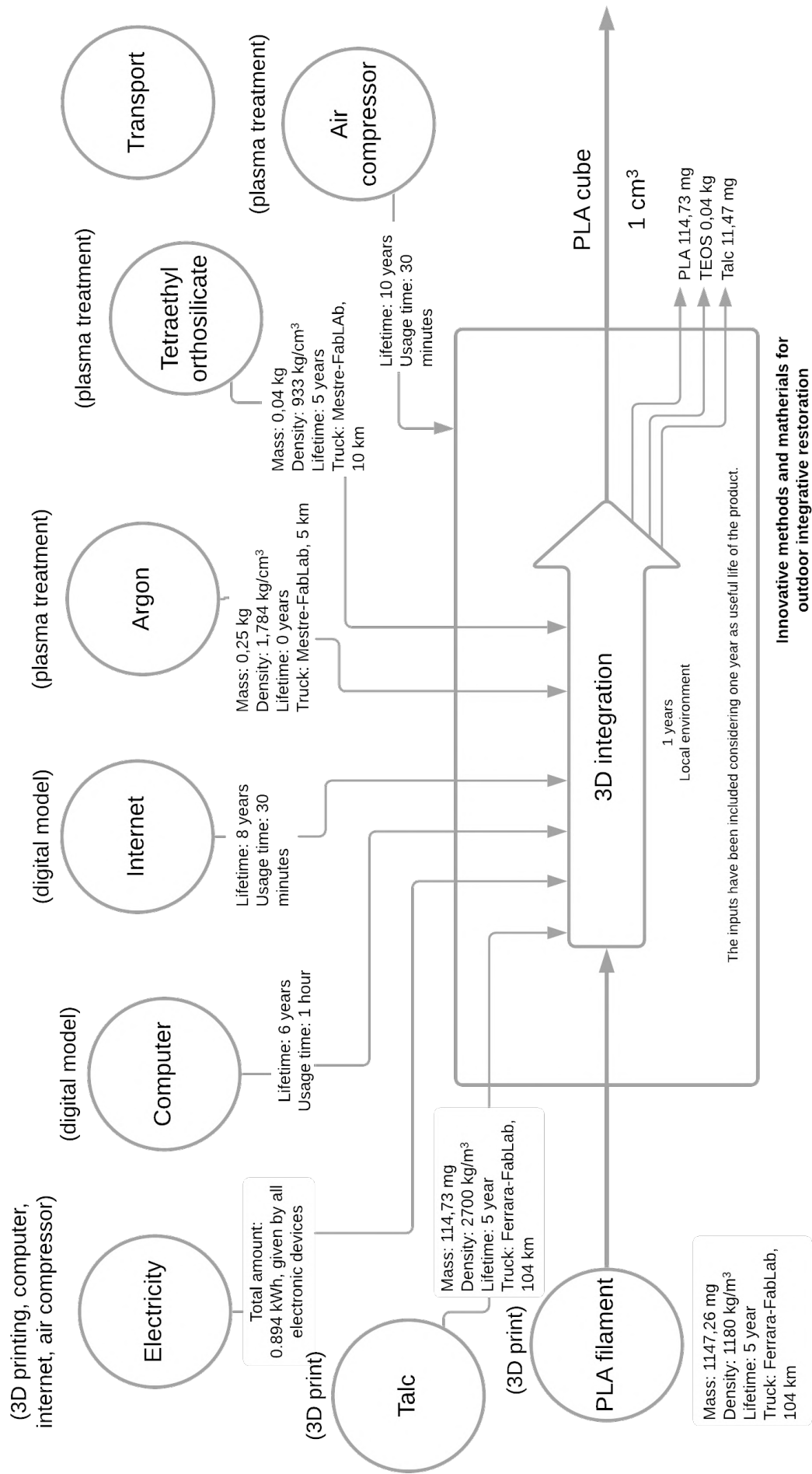


Figure 59. System boundaries case of restoration with innovative materials and techniques.

4.2 Life Cycle Inventory

At this stage, the materials used in both restoration cases must be correctly inventoried and the reasons for the choices made reported.

Congruently with the object and purpose of the analysis, input and output data were selected from the database ‘Ecoinvent 3 - allocation, cut off by classification’, which provides detailed process documentation for thousands of products, and ‘Methods’.

All quantities of materials entered in the inventory phase, for both case studies, were multiplied by their density and the functional unit they refer to, the result was then divided by their lifetime.

Tables 23 and 24 show the products and processes used in both supplementary proposals, and the entries under which they have been entered in SimaPro, so that they can be displayed more clearly.

Table 22. Inventory of products and processes of the traditional integration case, inserted in SimaPro thanks to the Ecoinvent database.

Phase	Materials	Inventory	Density (kg/m ³)	Quantity (g or p)	Energy (kWh)	Lifetime and/or usage time	Waste (g) and allocation	Transport (km)
Moulding	Araldite®	Bisphenol A, powder {RoW} production Cut-off, S	1168	0,584	-	10 year	-	-
		Epichlorohydrin {GLO} market for Cut-off, S		0,584	-	10 year	-	-
	Silicone rubber	Synthetic Rubber {RoW} production Cut-off, S	1100	10	-	3 days	-	-
		<i>Transport, freight, light commercial vehicle {Europe without Switzerland} market for transport Cut-off, S</i>	-	-	-	-	-	10
		<i>Municipal solid waste {IT}, treatment of incinerator Cut-off, S</i>	-	-	-	-	10 (100%)	-
End of life	Araldite®	Bisphenol A, powder {RoW} production Cut-off, S	-	-	-	-	0,584	-
		<i>Municipal solid waste {IT}, treatment of incinerator Cut-off, S</i>	-	-	-	-	-	-
		<i>Transport, freight, light commercial vehicle {Europe without Switzerland} market for transport Cut-off, S</i>	-	-	-	-	-	-
		Epichlorohydrin {GLO} market for Cut-off, S	-	-	-	-	0,584	-

		<i>Municipal solid waste {IT}, treatment of incinerator Cut-off, S</i>	-	-	-	-	-	-
		<i>Transport, freight, light commercial vehicle {Europe without Switzerland} market for transport Cut-off, S</i>	-	-	-	-	-	11

Table 23. Inventory of products and processes of the innovative integration case, inserted in SimaPro thanks to the Ecoinvent database.

Phase	Materials	Inventory	Density (kg/m ³)	Quantity (g or p)	Energy (kWh)	Lifetime and/or usage time	Waste (g) and allocation	Transport (km)
3D moulding	Computer	<i>Computer, desktop, without screen {GLO} production Cut-off, S</i>	-	1 p	0,2	6 year - for 60 minutes	-	-
	Desktop	<i>Display, liquid crystal, 17 inches {GLO} production Cut-off, S</i>	-	1 p	0,05	6 year - for 60 minutes	-	-
	Internet	<i>Router, internet {GLO} market for Cut-off, S</i>	-	1 p	0,006	8 years - for 90 minutes	-	-
3D printing	3D print	<i>Electricity, low voltage {IT} electricity voltage transformation from medium to low voltage Cut-off, S</i>	-	-	0,66	-	-	-
	PLA	<i>Poly lactide, granulate {GLO} production Cut-off, S</i>	1180	1,14	-	5 years	-	-
		<i>Transport, freight, light commercial vehicle {Europe without Switzerland} market for transport Cut-off, S</i>	-	-	-	-	-	104
		<i>Municipal solid waste {IT}, treatment of incinerator Cut-off, S</i>	-	-	-	-	0,103 (10%)	11
	Talc	<i>Clay {GLORoW} market for Cut-off, S</i>	2700	0,11	-	5 years	-	-
		<i>Transport, freight, light commercial vehicle {Europe without Switzerland} market for transport Cut-off, S</i>	-	-	-	-	-	104
<i>Municipal solid waste {IT}, treatment of incinerator Cut-off, S</i>		-	-	-	-	0,011 (10%)	-	
Plasma treatment	Air compressor	<i>Air compressor, screw-type compressor</i>	-	1 p	0,25	10 years - for 30 minutes	-	-
	TEOS	<i>Tetraethyl orthosilicate {GLO} production Cut-off, S</i>	933	20	-	5 years	-	-
		<i>Transport, freight, light commercial vehicle {Europe without Switzerland} market for transport Cut-off, S</i>	-	-	-	-	-	11
		<i>Municipal solid waste {IT}, treatment of incinerator Cut-off, S</i>	-	-	-	-	2 (10%)	-
	Argon plasma torch	<i>Argon, liquid {Row} production Cut-off, S</i>	1,784	250	0,06	-	-	-
<i>Transport, freight, light commercial vehicle {Europe without Switzerland} market for transport Cut-off, S</i>		-	-	-	-	-	5	
End of life	PLA	<i>Municipal solid waste {IT}, treatment of incinerator Cut-off, S</i>	-	1,03	-	-	1,03 (90%)	-

		<i>Transport, freight, light commercial vehicle {Europe without Switzerland} / market for transport / Cut-off, S</i>	-	-	-	-	-	11
	TEOS	<i>Municipal solid waste {IT}, treatment of incinerator / Cut-off, S</i>	-	-	-	-	18 (90%)	-
		<i>Transport, freight, light commercial vehicle {Europe without Switzerland} / market for transport / Cut-off, S</i>	-	-	-	-	-	11
	Talc	<i>Municipal solid waste {IT}, treatment of incinerator / Cut-off, S</i>	-	-	-	-	0,01 (90%)	-
		<i>Transport, freight, light commercial vehicle {Europe without Switzerland} / market for transport / Cut-off, S</i>	-	-	-	-	-	11

In the case of artistic integration with innovative materials and techniques, the products and processes used were selected on the basis of some considerations.

As regards the moulding phase, the energy was included under the item '*Electricity, low voltage {IT} / electricity voltage transformation from medium to low voltage / Cut-off, S*', with a total amount of 1,226 kWh. This amount was calculated, according to the energy consumption data present on the net. Given the considerable life expectancy of electronic devices, it was decided to proportionate the impact of producing the technological devices to the impact given by their effective use; so the time they were actually employed for this case study was divided by their average life-time.

The electronic devices are:

- a computer ('*Computer, desktop, without screen {GLO} / production / Cut-off, S*') and a monitor ('*Display, liquid crystal, 17 inches {GLO} / production / Cut-off, S*'), used during the digital modelling phase for a total of one hour. Both have an average life expectancy of about 6 years. Together they resulted in an electricity consumption of 0.25 kWh;
- an internet router for the creation of the digital CAD file ('*Router, internet {GLO} / market for / Cut-off, S*'), also used for data transmission to the 3D printer, consumed 0.006 kWh.

The lifetime is about 8 years.

For the 3D printing and plasma treatment, in accordance with the literature data on the printing process, it was found to be more consistent with the aim of this research to consider only the energy impact of the 3D manufacturing processes, rather than include the materials that make up the printer itself and assess the impact of their production or, alternatively, to look for a pre-existing process in the software that could be adapted [144].

So, the 3D printing and plasma treatment phases include the energy consumption of a 3D printer, always entered with the item *'Electricity, low voltage {IT}| electricity voltage transformation from medium to low voltage / Cut-off, S'*, was used for 30 minutes, with a total energy consumption of 0.66 kWh. A plasma treatment was also carried out during the printing process, using a torch to deposit an ionised argon beam on the surface. In this case too, the energy impact of half an hour use was considered, equal to 0,06 kWh. During the plasma treatment, the use of a compressor was foreseen (*'Air compressor, screw-type compressor'*), which total consumption energy for half hour of use is 0,25 kWh and a like expectancy of 10 years.

However, the integration process involved the 3D-printed production of a cube with a volume of 1 cm³ and a total mass of 1147.26 mg. Of this, around 90%, so 1032.54 mg, is made up of polylactic acid: a thermoplastic polymer, which was entered into the system under the heading *'Polylactide, granulate {GLO} | production / Cut-off, S'*. In addition to this quantity, a further small amount of PLA had to be used for the creation of the print base on which the object was then moulded, which, if compared to the size of the cube, has required an additional quantity of material presumably around 10% of its total mass, approximately 114.73 mg. Also in this case, however, 90% is polylactic acid, so 102.84 mg. Thus, the total amount of thermoplastic material inserted into the system is 1135.38 mg, including both the 1032.54 mg consisting of the cube and the 102.84 mg made up by the printing base.

As regards the polymer, the fact that it was inserted in the form of pellets and not as a filament was not considered crucial, since, given the quantity of PLA required for the analysis, the energy used for its extrusion process would have been negligible and would not have affected the final evaluation. With regard to the remaining 10% of the mass of the cube not inserted in the form of PLA, since the polymer studied in this thesis is added with an inorganic substance, more specifically talc, it was decided to insert 126.15 mg of *'Clay {RoW}| market for clay / Cut-off, S'*, including both the 114.26 mg of additive present in the cube and the 11,42 mg contained in the printing base of the cube itself. The talc, as well as the PLA, was transported from the manufacturing site in Ferrara to the FabLab in Venice, where the printing took place. This data has been entered as *'Transport, freight, light commercial vehicle {Europe without Switzerland} | market for transport / Cut-off, S'*, for a total of 104 km. Since

the printing base, 10% of PLA, was thrown away immediately after its creation and, since the plasma functionalisation process cannot be recycled, it was decided to enter '*Municipal solid waste {IT}, treatment of incinerator | Cut-off, S*', which involved a transport distance of 11 km to the nearest ecological disposal centre.

During the printing phase an argon-ionised plasma torch deposited, layer by layer, a siloxane precursor, tetraethyl silicate (TEOS), inserted with the input '*Tetraethyl orthosilicate {GLO} | production | Cut-off, S*' in an amount equal to 0.02 kg. It has an indicative lifetime of five years, the same as that considered for the portion of PLA used to produce the cube itself. This is because it is a material that, during plasma treatment, becomes part of the polymer matrix itself and, therefore, its lifetime is closely related to that of the polymer and vice versa. Argon, on the other hand, was added to the inventory, in a quantity of 0.25 kg, under the entry of '*Argon, liquid {Row} | production | Cut-off, S*'.

For the end-of-life phase the PLA cube, plasma-treated with TEOS deposition and used for hypothetical artistic integration, must be discarded. However, since it has undergone treatment not commonly involved in the 3D printing process, it was allocated in the undifferentiated waste and then incinerated. Therefore, the end-of-life disposal of the remaining 90% PLA that makes up the cube and was not discarded with the print base, the amount of TEOS used to create the coating between each cube's layer (18 g) and the additive (0,01 g) were destined for the incinerator (*Municipal Solid Waste {IT}, incinerator treatment | Cut-off, S*), with a transport distance of 11 km from the first waste disposal centre.

Concerning instead the case of artistic integration with traditional materials and techniques, the products and processes used were selected on the software according to some reasoning.

In this case, there is production of a cube in Araldite®, an epoxy resin widely used in the field of cultural heritage. The cube has a volume of 1 cm³ and a mass that was estimated to be, in accordance with the final volume and density of the material, 1168 mg.

Epoxy resin which, however, was not available in any of the processes in the selected databases. It was therefore decided to incorporate it, in a 1:1 ratio, in the form of Bisphenol A and Epichlorohydrin. Araldite® was then entered into the system with 584 mg of '*Bisphenol A, powder {RoW} | production | Cut-off, S*' and a further 584 mg of '*Epichlorohydrin {GLO} | market for | Cut-off, S*'. The 3D object was realised through the creation of a silicone rubber

mould, inserted under '*Synthetic Rubber {RoW}| production | Cut-off, S*' in an indicative quantity of 0.01 kg.

As regards the waste treatment, the waste that this process has ideally produced includes, immediately after the cube's production, the silicone rubber; in fact once the mould has been made and the Araldite® has solidified, it is discarded and disposed according to the '*Municipal Solid Waste {IT}, incinerator treatment | Cut-off, S*'. The end-of-life disposal of the cube was also considered, in the same way as for the cast. For this case study, moreover, it was not necessary to use any energy input and the transport, always included under the heading '*Transport, freight, light commercial vehicle {Europe without Switzerland}| market for transport | Cut-off, S*', involved both the Araldite® and the silicone rubber, starting at the Mestre Science Campus and ending at the waste disposal centre 11 km away.

4.3 Life Cycle Impact Assessment

In the Life Cycle Impact Assessment, the effects related to environmental impacts are quantitatively assessed using calculation tools. In the present research work, the IPCC 2013 GWP 100a and ReCiPe 2016 Midpoint (H) methods were used: the first one is based on the characterisation, in a 100-year horizon, of the different gaseous emissions according to their global warming potential; the second one, instead, allows to evaluate the impact that the products and processes used have on the environment according to different damage categories. The values obtained for each impact category in both cases of integrative restoration are correlated to calculate the percentage variation between them (Tables 24).

Below are the values obtained by the ReCiPe 2016 Midpoint (H) method.

Table 24. ReCiPe values obtained from each impact category of the two case studies, considering both the assembly and end-of-life phases, with calculation of the percentage change of both phases.

Impact category	Unit	Innovative restoration case		Traditional restoration case		Percentage variance	
		Assembly	End-of-life	Assembly	End-of-life	Assembly	End-of-life
-	-						
Global warming potential	kg CO ₂ eq	21,3	5,57	3,92E+03	913	2%	-9%
Stratospheric ozone depletion	kg CFC11 eq	1,24E-05	3,36E-06	0,00227	0,000384	9%	-32%
Ionizing radiation	kBq Co-60 eq	1,85	0,256	214	1,75	13%	-93%
Ozone formation, human health	kg NOx eq	0,0444	0,0245	9,42	0,395	49%	-89%
Fine particulate matter formation	kg PM2.5 eq	0,0362	0,00837	7,21	0,137	21%	-90%
Ozone formation, territorial ecosystems	kg NOx eq	0,047	0,0253	10,3	0,4	48%	-89%
Terrestrial acidification	kg SO ₂ eq	0,076	0,0188	15	0,258	23%	-91%
Freshwater eutrophication	kg P eq	0,0111	0,00119	1,18	0,0385	7%	-67%
Marine eutrophication	kg N eq	0,00119	8E-02	0,075	0,0395	-83%	1237%
Terrestrial ecotoxicity	kg 1,4-DCB	40,6	29,5	7E+03	392	64%	-87%
Freshwater ecotoxicity	kg 1,4-DCB	0,549	0,369	90,5	489	-74%	110%
Marine ecotoxicity	kg 1,4-DCB	0,768	0,519	128	639	-72%	107%
Human carcinogenic toxicity	kg 1,4-DCB	0,775	0,257	124	31,4	6%	-19%
Human non-carcinogenic toxicity	kg 1,4-DCB	15,5	11,3	2,71E+03	9,82E+03	-63%	86%
Land use	M2a crop eq	0,738	0,153	103	3,54	17%	-81%
Mineral resource scarcity	kg Cu eq	0,0425	0,0197	14,5	0,171	45%	-96%
Fossil resource scarcity	kg oil eq	8,15	1,84	2,38E+03	15,5	22%	-96%
Water consumption	m ³	1,88	0,0209	58,4	0,977	-1%	50%

In order to allow a better visualisation of the percentage changes obtained and to determine which impact categories show substantial differences between the first and second case of integrative restoration, histogram graphs are proposed (Figs. 61 and 62).

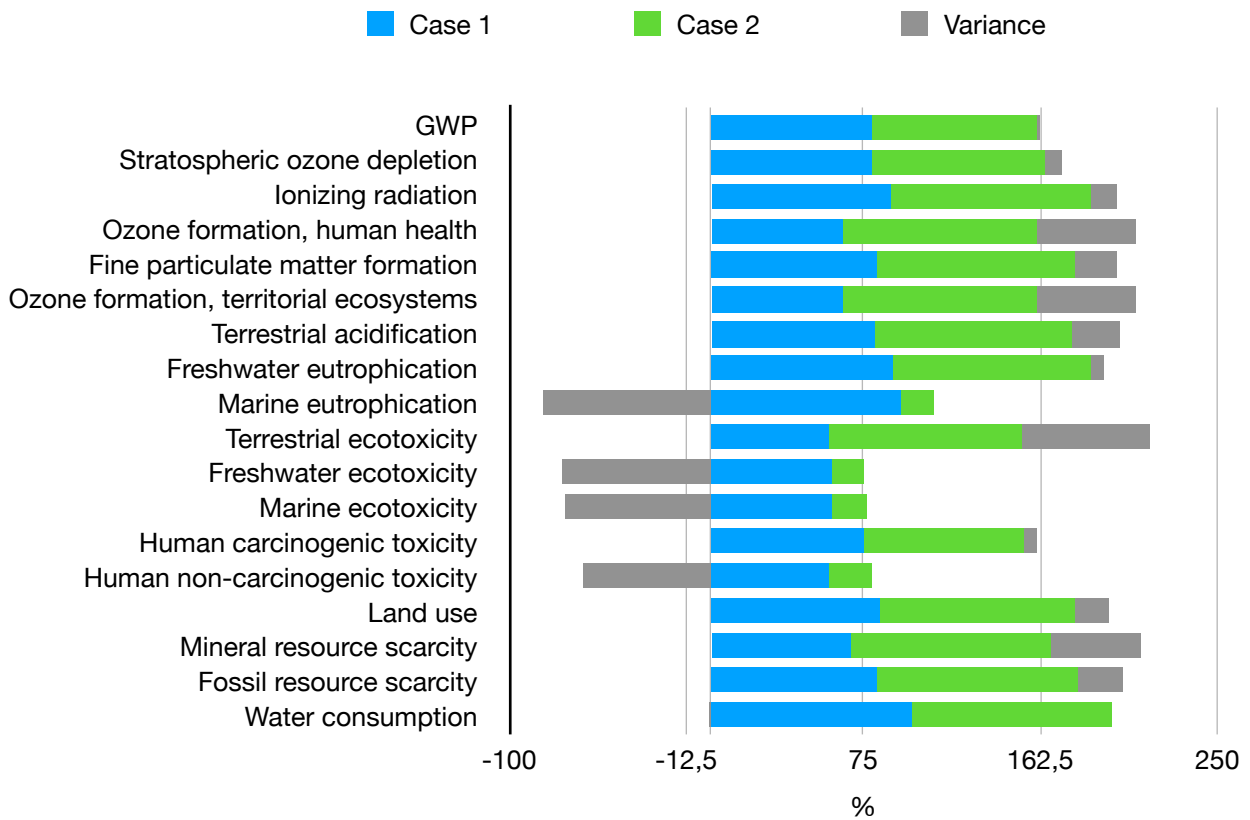


Figure 61. Histograms with variance % of the different impact categories on the assembly phase.

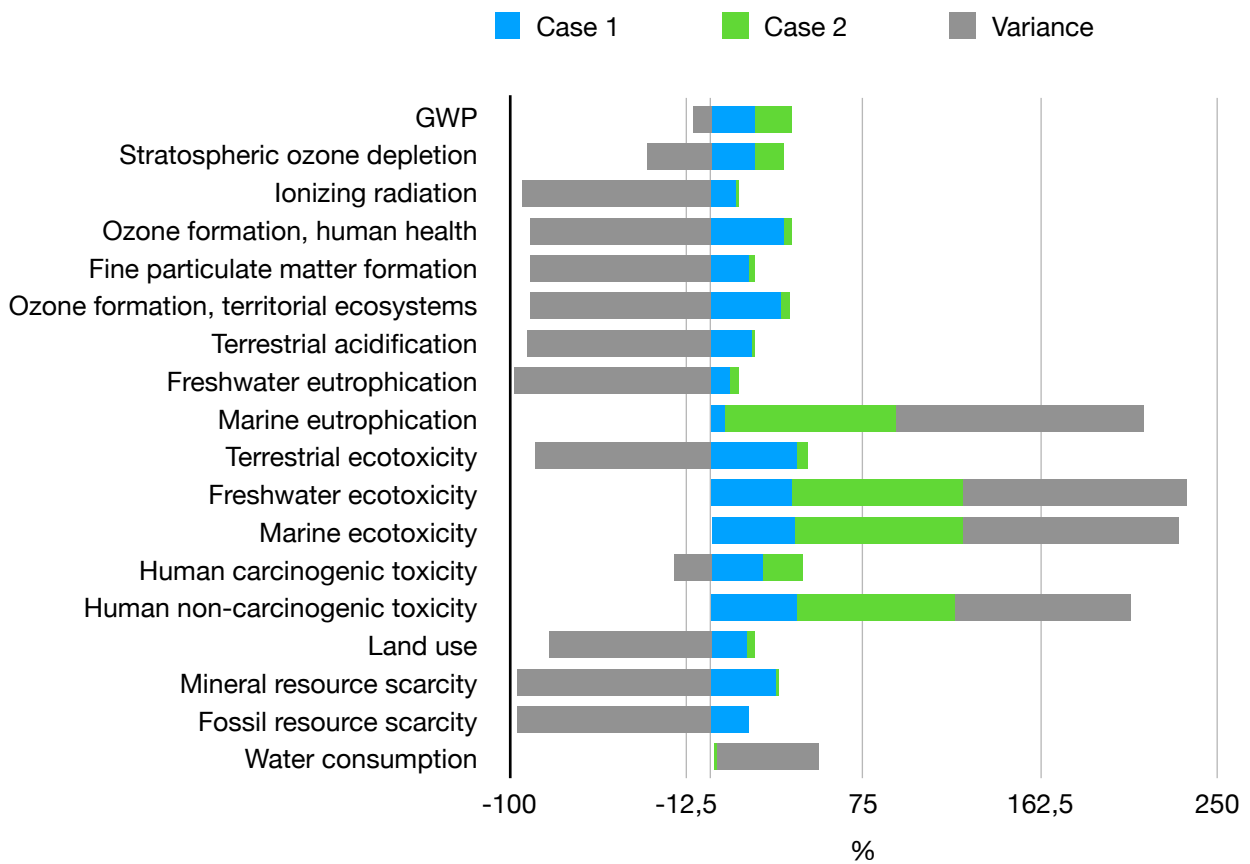
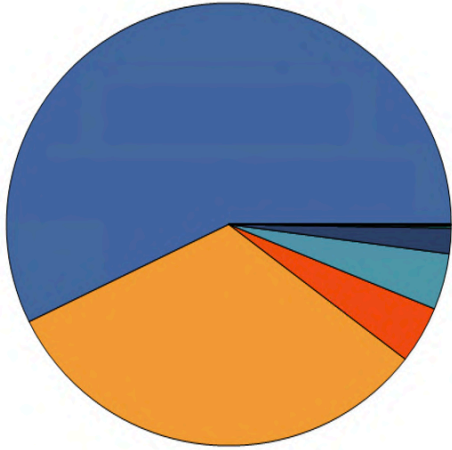
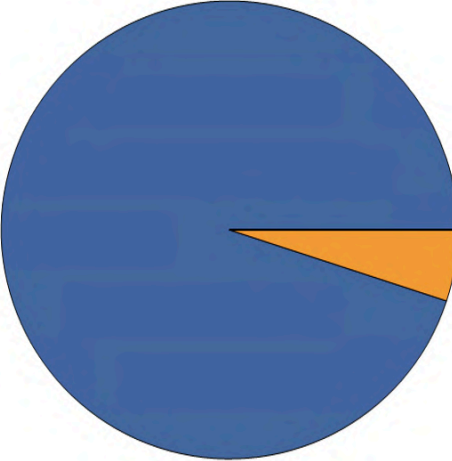


Figure 62. Histograms with variance % of the different impact categories on the end-of-life phase.

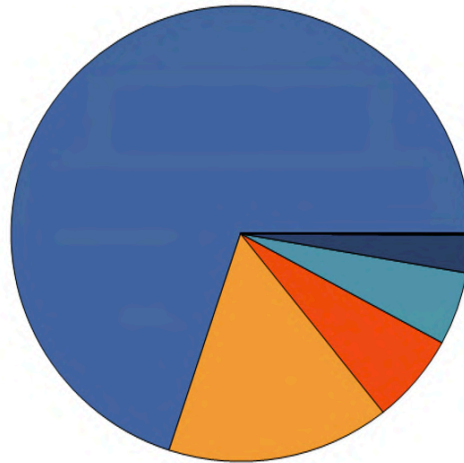
On the basis of the data obtained so far, it was decided to consider the impact given by the two case studies in the following impact categories: ‘ozone formation - human health’, ‘fine particulate matter formation’, ‘marine eutrophication’ and ‘human non-carcinogenic toxicity’. Below are pie charts, for both the cases, useful in determining which inputs mostly contributed to the specific impact category considered (Table 25).

Table 25. Selected impact categories and total influence of different inputs.

Ozone formation, human health	
Case 1	 <ul style="list-style-type: none"> ■ Tetraethyl orthosilicate (GLO) production Cut-off, S ■ Transport, freight, light commercial vehicle (Europe without Switzerland) processing Cut-off, S ■ Argon, liquid (RoW) production Cut-off, S ■ Polylactide, granulate (GLO) production Cut-off, S ■ Electricity, low voltage (IT) electricity voltage transformation from medium to low voltage Cut-off, S ■ Municipal solid waste (IT) treatment of, incineration Cut-off, S
Case 2	 <ul style="list-style-type: none"> ■ Synthetic rubber (RoW) production Cut-off, S ■ Municipal solid waste (IT) market for municipal solid waste Cut-off, S ■ Bisphenol A, powder (RoW) production Cut-off, S

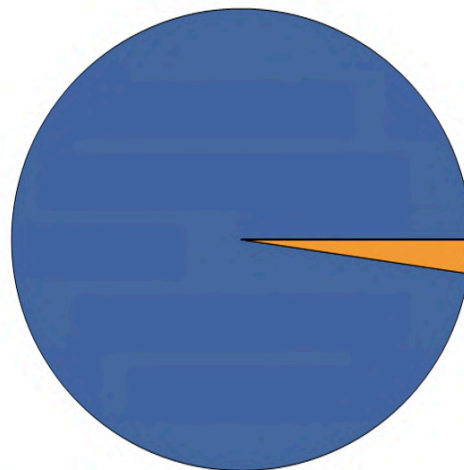
Fine particulate matter formation

Case 1



- Tetraethyl orthosilicate (GLO) | production | Cut-off, S
- Transport, freight, light commercial vehicle (Europe without Switzerland) | processing | Cut-off, S
- Argon, liquid (RoW) | production | Cut-off, S
- Polylactide, granulate (GLO) | production | Cut-off, S
- Electricity, low voltage (IT) | electricity voltage transformation from medium to low voltage | Cut-off, S
- Transport, freight, light commercial vehicle (Europe without Switzerland) | market for transport, freight, light commercial vehicle | Cut-off, S

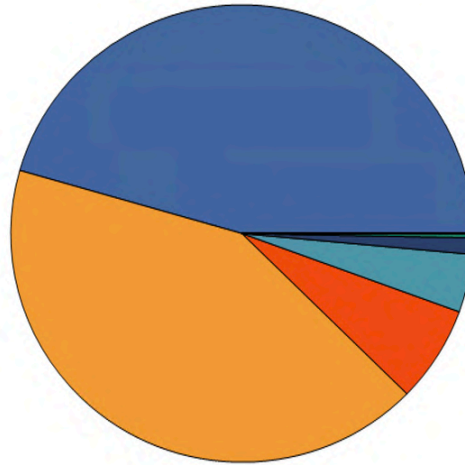
Case 2



- Synthetic rubber (RoW) | production | Cut-off, S
- Municipal solid waste (IT) | market for municipal solid waste | Cut-off, S
- Bisphenol A, powder (RoW) | production | Cut-off, S

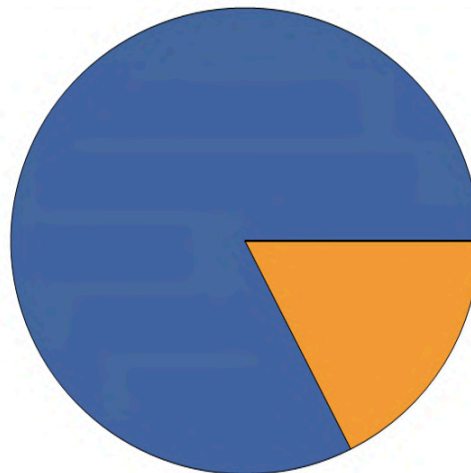
Marine eutrophication

Case 1

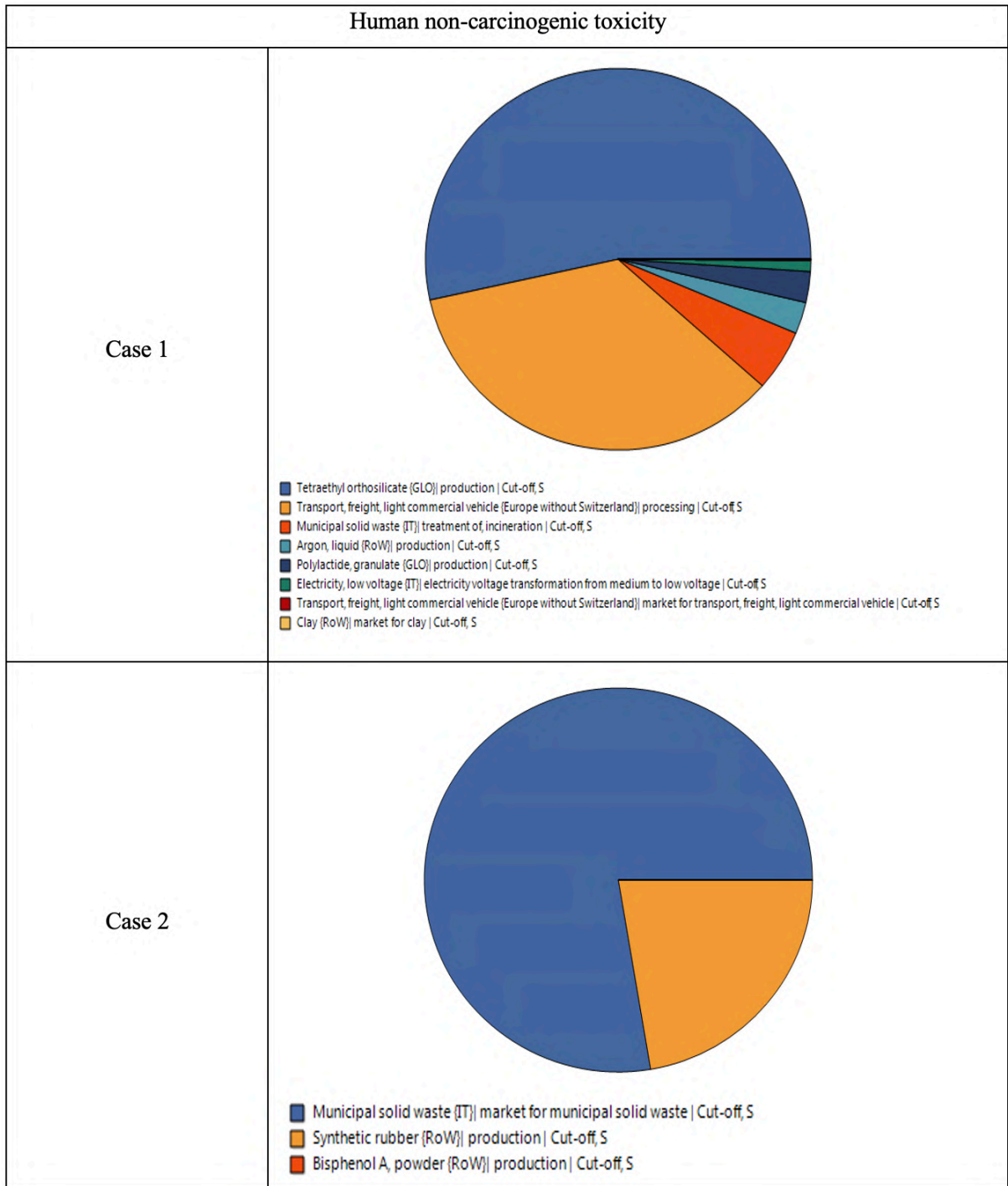


- Tetraethyl orthosilicate (GLO) production | Cut-off, S
- Polylactide, granulate (GLO) production | Cut-off, S
- Transport, freight, light commercial vehicle (Europe without Switzerland) | processing | Cut-off, S
- Argon, liquid (RoW) production | Cut-off, S
- Electricity, low voltage (IT) electricity voltage transformation from medium to low voltage | Cut-off, S
- Municipal solid waste (IT) treatment of, incineration | Cut-off, S

Case 2



- Municipal solid waste (IT) market for municipal solid waste | Cut-off, S
- Synthetic rubber (RoW) production | Cut-off, S
- Epichlorohydrin (GLO) market for | Cut-off, S



In contrast, the results obtained using the IPCC 100a method are shown below (Table 26).

Table 26. IPCC 100a values obtained from the two case studies, considering both the assembly and end-of-life phases, with calculation of the percentage change of both phases.

Impact category	Unit	Innovative restoration case		Traditional restoration case		Percentage variance	
		Assembly	End-of-life	Assembly	End-of-life	Assembly	End-of-life
IPCC GWP 100a	kg CO2 eq	20,9	5,54	3,85E+03	810	4%	-17%

Again, to better visualise the data in the table, histograms are proposed with the percentage, for each case study, of carbon dioxide emitted in each phase (Figures 63 and 64).

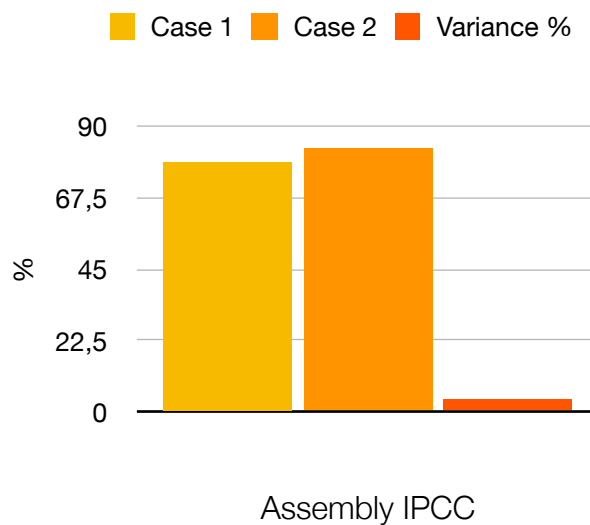


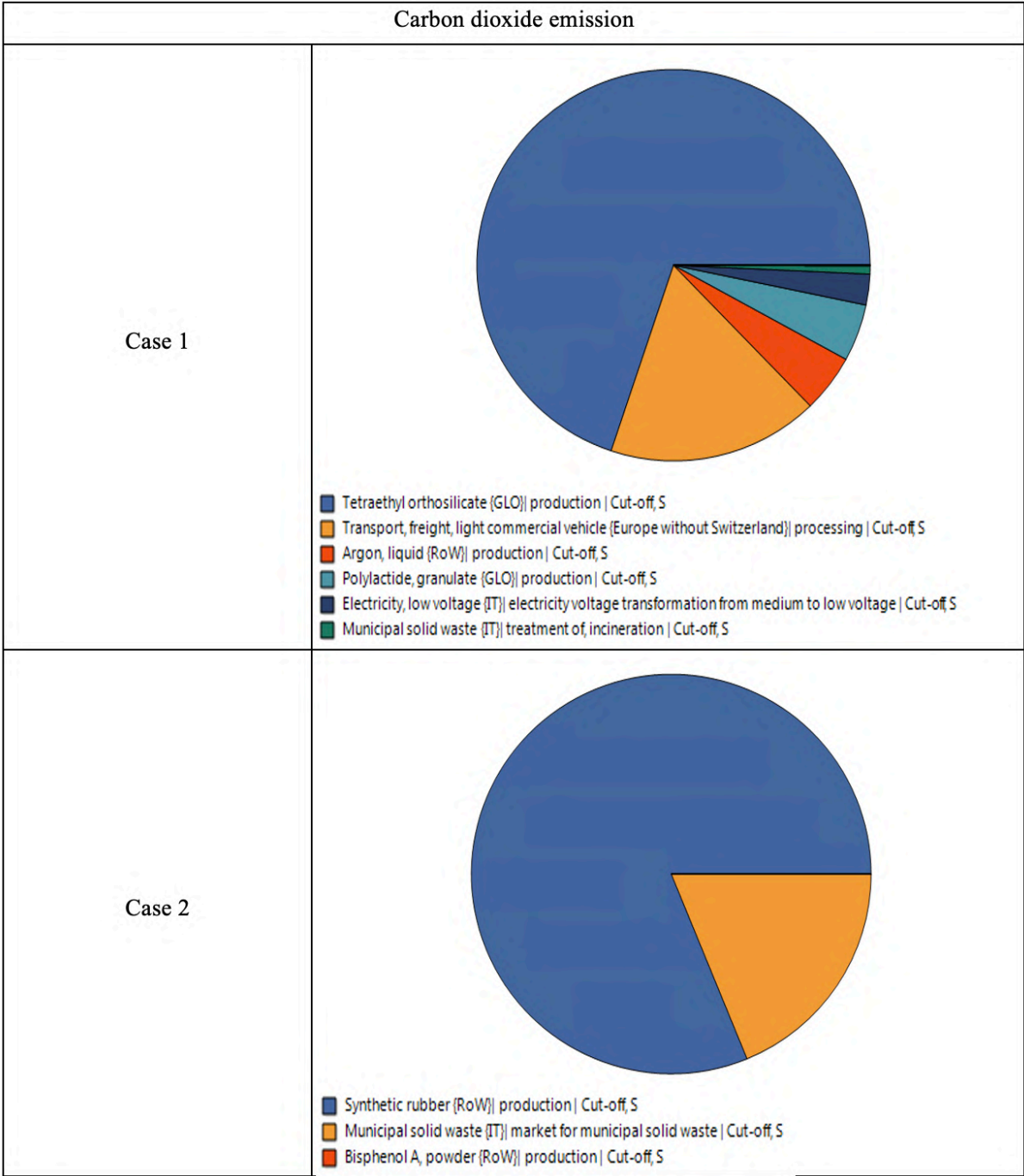
Figure 63. Histograms with variance % of the carbon dioxide emission on the assembly phase.



Figure 64. Histograms with variance % of the carbon dioxide emission on the end-of-life phase.

Below are pie charts, for both the cases, useful in determining which inputs mostly contributed to the specific impact category considered (Table 27).

Table 27. Impact category and total influence of different inputs.



4.4 Life Cycle Interpretation

With regard to the *Recipe Midpoint (H)* method, it can be seen from the histogram graphs (Figs. 61 and 62) that the percentage values on the assembly phase of the various impact categories are generally higher in the case of integrative restorations made with conventional methods than in the case of restorations made with innovative methods and materials. It is assumed that this trend is dictated by the use of materials of synthetic origin, such as silicone rubber and epoxy resin, which, unlike PLA, which is obtained by fermentation and synthesis processes from biomass, are subject to long industrial processing from synthetic substances.

The only impact categories higher in the former than in the latter case are: 'Marine eutrophication', 'Freshwater ecotoxicity', 'Marine ecotoxicity' and 'Human non-carcinogenic toxicity'.

Looking at the percentage contributions of the end-of-life phase, however, a higher impact is recorded for products included in the first case study. In particular, it is referred to the formation of ozone and atmospheric particulates, probably due to the deposition of the siloxane precursor between the layers of 3D printed polylactic acid.

In order to discuss in more detail the influence of individual inputs and determine how they contributed, it was decided to analyse a number of impact categories (Table 25).

In the first case of integrative restoration, most of the impact in 'ozone formation - human health', which assesses the destruction of the stratospheric ozone layer by anthropogenic emissions, is from TEOS, followed by transport and argon; the same is true for 'particulate matter formation'. This is probably due to the emission of air pollutants and exhaust gases into the air from combustion processes. Even in the case of 'human non-carcinogenic toxicity', which characterises human toxicity by also assessing environmental persistence, the greatest impact is given not only by transport and transport but also by the incinerator. In the case of 'marine eutrophication', which considers the presence of inorganic nutrients such as phosphorus and nitrogen in marine waters, the main contribution is again made by TEOS, followed by PLA. As for the second case study carried out with traditional materials and methods, in all categories the biggest impact is always given by the incinerator and synthetic rubber.

In the case of the IPCC 100a method, the assembly phase turns out to be the most influential in assessing environmental impact (Table 26). However, while in the assembly phase the second case presents a greater percentage impact than the first, the same cannot be said for the end-of-life phase; in fact, the first case presents a greater impact (Figures 63 and 64). Observing the pie charts, it is also possible to observe that the highest contributions, for both case studies, are given by the same materials that also presented a high impact in the *ReCiPe Midpoint (H)* method: in the first case, TEOS and argon, for the processes of coating deposition between the polymer layers by means of nebulized gas, and transport; in the second case, silicone rubber and resin, being products of synthetic origin, require in fact industrial processes that involve a high production of carbon dioxide.

In the first case, moreover, the total contribution given by electrical energy is negligible.

Considering that, in the case of integrative restoration performed with innovative methods, the main contribution is given by the deposition process of the siloxane coating, it can be considered to switch off the plasma torch between the deposition of one layer of polymeric material and the other. By doing this, the consumption of TEOS, as well as of argon, would be halved.

Alternatively, the use of a more ecofriendly precursor could be evaluated. Recently, qualitative risk rankings have been developed to evaluate nanoparticles according to their toxicity, water solubility, bioaccumulation, flammability and emissions [168]. In the case of restoration carried out using traditional methods, the greatest impact is given by the use of silicone rubber for making the cast. Furthermore, given its versatility and performability, it is difficult to replace this material for the cast's realization.

Chapter 5. Conclusion

In recent years, digital fabrication technologies have rapidly diffused in many sectors of industry, becoming, also in the field of Cultural Heritage, a valid alternative for the accurate reproduction of art objects and as a support for restoration operations.

The aim of this thesis project is to study the physical-mechanical characteristics of a thermoplastic polymer, polylactic acid, extruded in the form of a filament and treated, in the printing phase, with a cold plasma source at atmospheric pressure. The plasma torch, installed on the print head and passed layer-by-layer over the printing layers, deposited a siloxane-based coating (TEOS) capable of implementing adhesion, wettability and resistance properties of the polymer. The aim, once the samples were printed, is to compare them in order to assess the effective improvement in properties given by the plasma treatment.

The samples, once printed, were subjected to accelerated ageing processes in relative humidity and under the direct action of ultraviolet radiation. These were characterised using spectroscopic investigation techniques (ATR-FTIR and Raman) that allowed the identification not only of the main constituent substances of the polymer matrix, but also of an inorganic additive (talc) and PLA stereocomplexes.

TG-DSC and dynamometric analyses were also carried out, with the aim of verifying the physical-mechanical behaviour of the samples, treated and untreated, before, during and after accelerated ageing.

The TG-DSC technique, in particular, made it possible to determine the polymer temperatures, which were then compared with those obtained following an annealing process performed on the PLA filament.

The intention was to eliminate the thermal history of the polymer and to assess if there were any differences between the filament directly extracted from the spool and the filament that had been annealed. A direct comparison of the results showed that the T_g of the annealed filament was lower, probably due to a chain scissoring process, while the melting temperature as well as the degree of crystallinity tended to increase, possibly due to a process of crystallite thickening.

If the spectroscopic tests carried out on the filament and on the samples in their initial state did not reveal substantial changes, those carried out on the treated and untreated samples at different ageing steps showed differences due to the photochemical and hydrolytic

degradation processes. These differences in the chemical composition of the polymer before and after ageing were also detected by the acquisition of colorimetric data, for which an oscillatory variation was found.

In addition, dynamometric tests showed that the non-plasma-treated samples had a higher tensile strength than the treated samples. This rather unexpected result may not be due to the ineffectiveness of the plasma treatment, but rather to excessive precursor deposition between the polymer layers during the printing process, which led to increased vitrification between the layers.

Finally, it was decided to subject the treated and untreated samples to resistance tests in acid in order to assess the adhesiveness of the polymeric material. The samples were therefore placed in nitric acid and then in acetic acid. In the specific case of acetic acid, which is chemically similar to the polymeric material, it caused the material to swell and dissolve, especially in the case of the treated samples. In this case, too, it is assumed that the defective result is due to excessive coating deposition.

The LCA methodology was also used to compare the environmental impact of two hypothetical cases of integrative restoration: the first involved the use of innovative techniques and materials, such as the plasma torch used on polymeric materials for their conservation in an outdoor environment, and the other based on the use of traditional techniques and materials, such as epoxy resin and silicone rubber for the creation of a cast. The results obtained confirmed the sustainable and ecological nature of the polymer, whose production and disposal resulted in a lower environmental impact compared to the use of more traditional materials.

References

- [1] Hyperlink "<https://www.nextrebrandt.com>" Accessed on 19th August.
- [2] G. Bigliardi, P. Dioni, G. Panico, *Restauro e innovazione al Palazzo Ducale di Mantova: la stampa 3D al servizio dei Gonzaga*, 2015, *Archeomatica*, 3, p. 40.
- [3] I. Greggio, *La stampa 3D nei Beni Culturali: analisi e caratterizzazione di materiali per la fabbricazione digitale di Beni Culturali*, 2018, Tesi di laurea magistrale Scienze Chimiche per la Conservazione e il Restauro, pp. 4-13.
- [4] U. Betocchi, N. Madeddu, *Stampa 3D: una nuova risorsa per gli allestimenti museali*, Conferenza "Allestire per comunicare nei Musei scientifici", Venezia, 13-15 novembre 2013, 2016, *Museologia scientifica memorie*, 15, pp. 152-153.
- [5] A. Reichinger, M. Neumüller, F. Rist, S. Maierhofer, W. Purgathofer, *Computer-Aided Design of Tactile Models. Computers Helping People with Special Needs*, 2012, Springer-Verlag Berlin Heidelberg, pp. 497-504.
- [6] Hyperlink "<https://www.e3dplusvet.eu/wp-content/docs/O1A1-IT.pdf>". Accessed on 12th June.
- [7] Hyperlink "<https://formlabs.com/it/produzione-additiva-e-produzione-sottrattiva-a-confronto>" Accessed on 12th June.
- [8] D. Cadeddu, *Prove sperimentali e simulazioni numeriche per la validazione della matrice dei coefficienti elastici ricavata per elementi strutturali polimerici stampati in FDM*, 2020, Tesi di laurea magistrale Ingegneria Aerospaziale, pp.10-22.
- [9] E. Bella, *La rivoluzione della Stampa 3D dalla prototipazione al consumatore finale: analisi delle prospettive di adozione*, 2014, Tesi di laurea magistrale in Marketing e Comunicazione, pp. 31-38.
- [10] C. Schmidleithner, D. M. Kalaskar, *Stereolithography*, 2018, IntechOpen ed., pp. 3-9.
- [11] X. Wang, M. Jiang, Z. Zhou, J. Gou, D. Hui, *3D printing of polymer matrix composites: A review and prospective. Composites. Part B*, 2017, *Engineering*, pp. 442-458.
- [12] P. Bartolo, J. Gaspar, *Metal filled resin for stereolithography metal part*, 2008, *CIRP Annals*, pp. 235-238.
- [13] J. Halloran, *Ceramic Stereolithography: Additive manufacturing for ceramics by photopolymerization*, 2016, *Annual Review of Materials Research*, pp. 19-40.
- [14] Hyperlink "<https://www.stratasys.com/polyjet-technology>" Accessed on 17th July.

- [15] Hyperlink "<https://www.protiq.com/it/stampa-3d/processi/polyJet-multijet/>" Accessed on 17th July.
- [16] M. Eslamian, N. Ashgriz, *Drop-on-Demand Drop Generators. Handbook of atomization and sprays*, 2011, Springer Science and Business Media, pp. 581-582.
- [17] D. Dimitrov, K. Schreve, N. de Beer, *Advances in three dimensional printing - state of the art and future perspectives*, 2006, Rapid prototyping Journal, vol. 12, p. 137.
- [18] G. Zhu, Y. Hou, J. Xu, N. Zhao, *Reprintable Polymers for Digital Light Processing 3D Printing*, 2020, Advanced Functional Materials Journal, p. 1.
- [19] R. Scopigno, P. Cignoni, N. Pietroni, M. Callieri, M. Dellepiane, *Digital fabrication techniques for Cultural Heritage: A survey*, 2015, Computer Graphics Forum, vol. 20, pp. 1-17.
- [20] L. Novakova-Marcincinova, I. Kuric, *Basic and Advanced Materials for Fused Deposition Modeling Rapid Prototyping Technology*, 2012, Materials Science, 11(1), pp. 24-27.
- [21] S. Kumar, A. K. S. Choudhary, A. K. Singh, A. K. Gupta, *A Comparison of Additive Manufacturing Technologies*, 2016, International Journal for Innovative Research in Science & Technology, vol. 3, pp. 147-152.
- [22] Hyperlink "<https://www.protiq.com/it/stampa-3d/processi/sinterizzazione-laser-selettiva/>" Accessed on 17 July.
- [23] M. Grotto, *Prototipazione rapida. Lom Helisys 1015*, 2013, Tesi di laurea triennale in Ingegneria Meccanica e Meccatronica, p. 15.
- [24] U. Bathia, *3D Printing Technology*, 2015, International Journal of Engineering and Technical Research (IJETR), vol. 3, n. 2, p. 328.
- [25] G. N. Levy, R. Schindel, J. Kruth, *Rapid Manufacturing and Rapid Tooling with Layer Manufacturing (LM) Technologies, State of the Art and Future Perspectives*, 2003, CIRP Annals - Manufacturing Technology, vol. 52, n. 2, p. 598.
- [26] Hyperlink "<https://all3dp.com/2/electron-beam-melting-ebm-3d-printing-simply-explained/>" Accessed on 17th July.
- [27] V. Kaufui, A. Hernandez, *A Review of Additive Manufacturing*, 2012, International Scholarly Research Network (ISRN) Mechanical Engineering, p. 5.

- [28] Hyperlink “<https://formlabs.com/it/produzione-additiva-e-produzione-sottrattiva-a-confronto>”. Accessed on 12th June.
- [29] G. Pavlidis, A. Koutsoudis, F. Arnaoutoglou, V. Tsioukas, C. Chamzas, *Methods for 3D digitalization of Cultural Heritage*, 2007, *Journal of Cultural Heritage*, vol. 8, pp. 93-98.
- [30] Hyperlink “<https://stampa3d.valorebf.it/manifattura-additiva-vs-sottrattiva/>” Accessed on 20th June.
- [31] Hyperlink “3D Printing & Additive Manufacturing - A Complete Overview (hubs.com)” Accessed on 26th June.
- [32] K.H. Ho, S.T. Newman, *State of the art electrical discharge machining (EDM)*, 2003, *International Journal of Machine Tools & Manufacture*, 43, p. 1288.
- [33] Hyperlink “<https://www.etmm-online.com/water-jet-cutting-function-methods-and-application>” Accessed on 18th July.
- [34] A. K. Dubey, V. Yadava, *Laser beam machining - A review*, 2008, *International Journal of Machine Tools & Manufacture* 43, pp. 610-615.
- [35] S. Tofail, E. P. Koumoulos, A. Bandyopadhyay, S. Bose, L. O’Donoghue, C. Charitidis, *Additive manufacturing: scientific and technological challenges, market uptake and opportunities*, 2018, *Materials Today*, 22-37.
- [36] M. K. Niaki, S. A. Torabi, F. Nonino, *Why manufacturers adopt additive manufacturing technologies: The role of sustainability*, 2019, *Journal of Cleaner Production*, pp. 381-382.
- [37] F. Auricchio, G. Alaimo, A. Cattenone, S. Marconi, S. Morganti, *La stampa 3D: una tecnologia abilitante ed affascinante. Dalla scienza dei materiali alla modellistica, dalla chirurgia all’ingegneria civile*, 2018, *Rendiconti - Accademia Nazionale delle Scienze detta dei XL - Memorie di Scienze Fisiche e Naturali*, 136°, Vol. XLII, Parte II, Tomo I, pp. 19-33.
- [38] J. R. C. Dizon, A. H. Espera Jr., Q. Chen, R. C. Advincula, *Mechanical characterization of 3D-printed polymers*, 2017, *Additive Manufacturing*, p. 57-58.
- [39] M. Anni, *3D Printing: analisi della tecnologia e studio delle potenzialità del mercato*, 2016, *Tesi di Laurea Magistrale in Ingegneria Gestionale*, p. 13.
- [40] S. Rossini, *Acido Polilattico (PLA): miglioramento delle proprietà barriera e sviluppo di compositi ecosostenibili*, 2014, *Tesi di Laurea Magistrale in Ingegneria Chimica e dei Processi Industriali*, pp. 13-15.

- [41] Hyperlink “https://docs.europeanbioplastics.org/publications/fsEuBP_FS_What_are_bioplastics” Accessed on 16th August.
- [42] Hyperlink “<http://store.uni.com/catalogo/uni-en-iso-14855-2-2018>” Accessed on 16th August.
- [43] Hyperlink “<https://www.3dcraft.it/manuale-sui-filamenti-per-stampa-3d/>” Accessed on 28th July.
- [44] N. Guo, M. C. Leu, Additive manufacturing: technology, applications and research needs, 2013, *Frontiers of Mechanical Engineering*, pp. 215-243.
- [45] N. Paiola, *La Fabbrica 4.0: alla scoperta del nuovo paradigma produttivo e delle tecnologie che lo supportano. Il caso WASP*, 2016, Tesi di laurea magistrale in Economia Internazionale, pp. 36-39.
- [46] Hyperlink “<https://felfil.com/it/abs-mini-guida-del-filamento-plastico-per-stampanti-3d/>” Accessed on 5th July.
- [47] Hyperlink “<http://www.paperdifferent.com/abs---stampa-e-post-lavorazione.html>” Accessed on 18th July.
- [48] M. Feygin, B. Hsieh, *Laminated object manufacturing (LOM): a simpler process*, 1991, *Proceedings of Solid Freeform Fabrication Symposium*, pp. 123-130.
- [49] B. Caulfield, P. E. McHugh, S. Lohfeld, *Dependence of mechanical properties of polyamide components on build parameters in the SLS process*, 2007, *Journal of Materials Processing Technology*, 182, pp. 477-488.
- [50] Hyperlink “<https://www.beamler.com/it/qual-e-la-differenza-tra-tpe-e-tpu-nellastampa-3d>” Accessed on 5th July.
- [51] Hyperlink “<https://filament.nu/gb/content/17-pet>” Accessed on 18th July.
- [52] Hyperlink “<http://www.inkamprinting.com/tutto/filamenti-per-la-stampa-3d-tpu-e-policarbonato-3445.html>” Accessed on 18th July.
- [53] Hyperlink “<https://stampoin3d.blogspot.com/2017/08/tipologie-di-filamenti-in-pva-per.html>” Accessed on 18th July.

- [54] Hyperlink "<https://www.nuovamacut.it/blog/materiali-per-la-stampa-3d-i-materiali-compositi/>" Accessed on 18th July.
- [55] F. Pignatelli, *L'evoluzione della stampa 3D e le applicazioni in campo museale*, 2013, Ricerca Scientifica e Tecnologie dell'Informazione, Vol 3, Issue 2, 143-158.
- [56] M. Neumüller, A. Reichinger, F. Rist and C. Kern, *3D Printing for Cultural Heritage: Preservation, Accessibility, Research and Education*, 2014, Springer-Verlag Berlin Heidelberg, p. 121.
- [57] Hyperlink "<https://www.martalab.com/post/tecnologie-3d-per-i-beni-culturali/>" Accessed on 7th July.
- [58] Hyperlink "<https://artemagazine.it/attualita/item/12932-tecnologie-e-materiali-per-i-beni-culturali-il-progetto-temart>" Accessed on 19th July.
- [59] Hyperlink "<https://www.3d-archeolab.it/servizi/musei-tattili/>" Accessed on 7th July.
- [60] Hyperlink "<https://acme3.it/2018/03/05/restauro-opere-3d/>" Accessed on 10th July.
- [61] A. Gebhardt, *AM-Based Evaluation, Reconstruction and Improvement of Cultural Heritage Artifacts - Mixed reality and gamification for Cultural Heritage*, 2017, Springer International Publishing, pp. 527-548.
- [62] A. Gebhardt, *Understanding Additive Manufacturing: Rapid Prototyping - Rapid Tooling - Rapid Manufacturing*, 2011, Hanser Publications, pp. 83-91.
- [63] Hyperlink "<https://www.treccani.it/enciclopedia/plasma>" Accessed on 10th July.
- [64] M. I. Boulos, P. Fauchais, & P. Fender, *Thermal plasmas: fundamentals and applications*, 2013, Springer Science & Business Media, pp. 133-183.
- [65] F. Marani, *Realizzazione e caratterizzazione chimico-fisica di una sorgente al plasma di non equilibrio operante a pressione atmosferica per la modifica superficiale di materiali polimerici in ambiente controllato*, 2013, Tesi di laurea magistrale in Ingegneria Energetica, pp. 7-21.
- [66] C. Tendero, C. Tixier, P. Tristant, J. Desmaison, P. Leprince, *Atmospheric pressure plasmas: A review*, 2016, Spectrochimica Acta Part B: Atomic Spectroscopy, Vol. 61, Issue 1, pp. 2-30.
- [67] L. Fontanili, *Studio dell'interazione tra un plasma jet nanopulsato con substrati metallici, dielettrici e liquidi*, 2015, Tesi di laurea triennale in Ingegneria Clinica, pp. 4-7.

- [68] T. L. Eddy, *Electron temperature determination in LTE and non-LTE plasmas*, 1985, *Journal of Quantitative Spectroscopy and Radiative Transfer*, 33(3), pp. 197-211.
- [69] C. Dalla Pria, *Ottimizzazione del trattamento su materiali industriali tramite jet a plasma freddo a pressione atmosferica*, 2019, Tesi di laurea magistrale in Ingegneria dell'energia elettrica, p.6.
- [70] Hyperlink "<https://www.igi.cnr.it/innovation/tecnologie/plasma-freddo/>" Accessed on 10th July.
- [71] Hyperlink "http://www.plasmaprometeo.unimib.it/wp-content/uploads/2013/03/industria_carta_2.pdf" Accessed on 10th July.
- [72] Hyperlink "<https://www.notiziariochimicofarmaceutico.it/2019/09/29/plasma-freddo-per-sterilizzare-i-prodotti-biomedicali/>" Accessed on 10th July.
- [73] D. Dudek, N. Bibinov, J. Engemann, P. Awakowicz, *Direct current plasma jet needle source*, 2007, *Journal of Physics D: Applied Physics*, Volume 40, Number 23, pp. 7367-7371.
- [74] J. T. Gudmundsson, A. Hecimovic, *Foundations of DC plasma sources*, 2017, *Plasma Sources Science and Technology*, Volume 26, Number 12, pp. 1-20.
- [75] A. Yehia, *Characteristics of the dielectric barrier corona discharges*, 2019, *AIP Advances*, pp. 1-11.
- [76] G. Vergari, *Review sui plasmi a pressione atmosferica*, 2009, Tesi di laurea triennale in Scienza dei Materiali, pp. 7-15.
- [77] A. Lagăr, C. M. Diniş, G. N. Popa, *Experimental analysis of direct current corona discharge*, 2007, *IOP Conference Series: Materials Science and Engineering*, 163, pp. 1-9.
- [78] V. I. Kolobov, R. R. Arslanbekov, D. Levko, V. A. Godyak, *Plasma Stratification in Radio-Frequency Discharges in Argon Gas*, 2020, *Journal of Physics D: Applied Physics*, Volume 53, Number 25, pp. 1-5.
- [79] A. Schutze, J. Y. Jeong, S. E. Babayan, P. Jaeyoung, G. S. Selwyn, R. F. Hicks, *The atmospheric-pressure plasma jet: a review and comparison to other plasma sources*, 1998, *IEEE Transactions on Plasma Science*, pp. 1685–1694.
- [80] M. C. Kim, S. H. Yang, J. H. Boo, J. G. Han, *Surface treatment of metals using an atmospheric pressure plasma jet and their surface characteristics*, 2003, *Surface and Coatings Technology*, pp. 174-175.

- [81] R. J. Soukup, N. J. Ianno, J. L. Huguenin-Love, *Analysis of semiconductor thin films deposited using a hollow cathode plasma torch*, 2007, *Solar Energy Materials and Solar Cells*, pp. 1383–1387.
- [82] R. D. Deutsch, G. M. Hieftje, *Development of a Microwave-Induced Nitrogen Discharge at Atmospheric Pressure (MINDAP)*, 1985, *Applied Spectroscopy*, Volume 39, pp. 214-222.
- [83] L. L. Alves, R. Álvarez, L. Marques, S. J. Rubio, A. Rodero, M. C. Quintero, *Modeling of an axial injection torch*, 2009, *The European Physical Journal: Applied Physics*, Volume 46, pp. 1-10.
- [84] H. S. Uhm, Y. C. Hong, D. H. Shin, *A microwave plasma torch and its applications*, 2006, *Plasma Sources Science and Technology*, pp. 26-34.
- [85] T. Monetta, F. Bellucci, *Applicazioni industriali delle tecnologie al plasma*, 2018, Dipartimento di Ingegneria dei Materiali e della Produzione, pp. 1-4.
- [86] R. Tiño, K. Vizárová, K. Krčma, *Plasma Surface Cleaning of Cultural Heritage Objects*, 2019, *Nanotechnologies and Nanomaterials for Diagnostic, Conservation and Restoration of Cultural Heritage*, pp. 239-275.
- [87] Hyperlink “<https://www.nadir-tech.it/it/tecnologie/plasma-2/applicazioni/beni-culturali/>” Accessed on 21th July.
- [88] C. Rodríguez-Villanueva, N. Encinas, J. Abenojar, M.A. Martínez, *Assessment of atmospheric plasma treatment cleaning effect on steel surfaces*, 2013, *Surface and Coatings Technology*, pp. 450-456.
- [89] S. Voltolina, L. Nodari, C. Aibéo, E. Egel, M. Pamplona, S. Simon, E. Verga Falzacappa, P. Scopece, A. Gambirasi, M. Favaro, A. Patelli, *Assessment of plasma torches as innovative tool for cleaning of historical stone materials*, 2016, *Journal of Cultural Heritage*, 22, 940-950.
- [90] W. Klöpffer, *Life cycle assessment - from the beginning to the current state*, 1997, *Environmental Science and Pollution research*, pp. 223-228.
- [91] Personal communications.
- [92] Hyperlink “<https://www.reteclima.it/lca-life-cycle-assessment-analisi-del-ciclo-di-vita/>” Accessed on 12th August.
- [93] Hyperlink “<https://www.lca-ambiente.com/la-metodologia/>” Accessed on 12th August.

- [94] Hyperlink "http://www.ciriaf.it/ft/File/Didattica/lezioni/asdrubali_IA_Mod_PE_2/24_LCA" Accessed on 12th August.
- [95] A. Bjørn, A. Laurent, M. Owsianiak, S. I. Olsen, *Life Cycle Assessment*, 2018, Springer, pp. 59-423.
- [96] G.Finnveden, M. Z. Hauschild, T. Ekvall, J. Guinée, R. Heijungs, S. Hellweg, S. Hellwege, A. Koehler, D. Pennington, S. Suh, *Recent developments in Life Cycle Assessment*, 2009, Journal of Environmental Management, pp. 1-21.
- [97] J. B. Guinée, *Selection of Impact Categories and Classification of LCI Results to Impact Categories*, 2015, LCA Compendium - The Complete World of Life Cycle Assessment, pp. 17-37.
- [98] Personal communication: technical data sheet '67C1WR-N_iniezione_IT_Rev.1.0.pdf'.
- [99] Hyperlink "<https://www.nadir-tech.it/it/tecnologie/plasma-2/prodotti-plasma/stylus-plasma-noble/>" Accessed on 12th August.
- [100] A. Patelli, E. Verga, L. Nodari, S. M. Petrillo, A. Delva, P. Ugo, P. Scopece, *A customised atmospheric pressure plasma jet for conservation requirements*, 2017, Materials Science and Engineering, Volume 384, pp. 1-9.
- [101] M. Di Foggia, *Studio di bio-materiali usati come scaffold per Tissue Engineering e loro caratterizzazione con tecniche spettroscopiche vibrazionali e di analisi termica*, 2008, Tesi di Dottorato in Biotecnologie Mediche, pp. 22-38.
- [102] M. M. Blum, H. John, *Historical perspective and modern applications of Attenuated Total Reflectance - Fourier Transform Infrared Spectroscopy (ATR-FTIR)*, 2011, Drug Testing and Analysis, 4(3-4), pp. 298-302.
- [103] Hyperlink "<http://www.ipac.regione.fvg.it/userfiles/file/gorassini.pdf>" Accessed on 16th August.
- [104] V. G. Gregoriou, *Fourier Transform Infrared Spectroscopy of polymers*, 2000, Applied Polymer Science, pp. 709-757.
- [105] M. Harris, J. Potgieter, R. Archer, K. M. Arif, *In-process thermal treatment of polylactic acid in fused deposition modelling*, 2019, Materials and Manufacturing Processes, pp. 1-13.
- [106] Hyperlink "<https://www.ecotogo.it/post/58c7da4affe48e975936b84a/materiali-la-bioplastica-pla.html>" Accessed on 1st September.

- [107] K. F. Lim, S. W. Lewis, *Spectroscopic Techniques*, 2013, Encyclopedia of Forensic Sciences, pp. 627-634.
- [108] H. Tsuji, Y. Echizen, Y. Nishimura, *Photodegradation of biodegradable polyesters: A comprehensive study on poly(L-lactide) and poly(3-caprolactone)*, 2006, Polymer degradation and stability, pp. 1128-1137.
- [109] M. C. Mistretta, F. P. La Mantia, V. Titone, B. Megna, L. Botta and M. Morreale, *Durability of biodegradable polymers for the conservation of Cultural Heritage*, 2019, Frontiers in materials, pp. 1-12.
- [110] M. G. M. Van Der Vis, E. H. P. Cordfunke, R. J. M. Konings, *The thermodynamic properties of tetraethoxysilane (TEOS) and an infrared study of its thermal decomposition*, 1993, Journal de Physique, pp. 75-82.
- [111] M. Gnyba, M. J-Szczerska, M. Keränen, J. Suhonen, Sol-Gel materials investigation by means of Raman Spectroscopy, 2003, XVII IMEKO World Congress Metrology in the 3rd Millennium, pp. 237-240.
- [112] M-Y. Jo, Y. J. Ryu, J. H. Ko, J-S. Yoon, *Hydrolysis and Thermal Degradation of Poly(L-Lactide) in the Presence of Talc and Modified Talc*, 2012, Journal of Applied Polymer Science, 1019-1025.
- [113] J. Madejová, W.P. Gates, S. Petit, *IR Spectra of Clay Minerals*, 2017, Development in Clay Science, pp. 107-149.
- [114] M. Gardette, S. Thérias, J-L. Gardette, M. Murariu, P. Dubois, *Photooxidation of polylactide/calcium sulphate composites*, 2011, Polymer Degradation and Stability, pp. 616-623.
- [115] L.L. Lizárraga-Laborín, J.M. Quiroz-Castillo, J.C. Encinas-Encinas, M.M. Castillo-Ortega, S.E. Burruel-Ibarra, J. Romero-García, J.A. Torres-Ochoa, D. Cabrera-German, D.E. Rodríguez-Félix, *Accelerated weathering study of extruded polyethylene/poly (lactic acid)/chitosan films*, 2018, Polymer Degradation and Stability, pp. 2-21.
- [116] L. Zaidi, M. Kaci, S. Bruzaud, A. Bourmaud, Y. Grohens, *Effect of natural weather on the structure and properties of polylactide/Cloisite 30B nanocomposites*, 2010, Polymer Degradation and Stability, pp. 1751-1758.
- [117] G.I. Bolio-Lo'pez, L. Veleza, A. Valadez-González and P. Quintana-Owen, *Weathering and biodegradation of polylactic acid composite reinforced with cellulose-whiskers*, 2012, Revista Mexicana de Ingeniería Química, pp.143-153.

- [118] J. R. Rocca-Smith, O. Whyte, CH. Brachais, D. Champion, F. Piasente, E. Marcuzzo, A. Sensidoni, F. Debeaufort, T. Karbowski, *Beyond Biodegradability of Poly(lactic acid): Physical and Chemical Stability in Humid Environments*, 2017, ACS Sustainable Chemistry and Engineering, pp. 2751-2762.
- [119] A. Porfyrus, S. Vasilakos, C. Zotiadis, C. Papaspyrides, K. Moser, L. Van der Schueren, G. Buyle, S. Pavlidou, S. Vouyiouka, *Accelerated ageing and hydrolytic stabilization of poly(lactic acid) (PLA) under humidity and temperature conditioning*, 2018, Polymer Testing, 315-332.
- [120] S. J. de Jong, E. R. Arias, D.T.S. Rijkers, C.F van Nostrum, J.J. Kettenes-van den Bosch, W.E. Hennink, *New insights into the hydrolytic degradation of poly(lactic acid): participation of the alcohol terminus*, Polymer, vol. 42, 2001, pp. 2795-2802.
- [121] R. Lenz, K. Enders, C. A. Stedmon, D. M. A. Mackenzie, T. G. Nielsen, *A critical assessment of visual identification of marine microplastic using Raman spectroscopy for analysis improvement*, 2015, Marine Pollution Bulletin, pp. 82-91.
- [122] G. Kister, G. Cassanas, M. Vert, *Effects of Morphology, Conformation and Configuration on the IR and Raman Spectra of Various Poly(lactic acid)s*, 1998, Polymers, vol. 39, pp. 267-273.
- [123] D. Wolverson, *Raman spectroscopy. Characterization of Semiconductor Heterostructures and Nanostructures*, 2008, Elsevier, pp. 249-288.
- [124] L. Cai, J. Wang, J. Peng, Z. Wu, X. Tan, *Observation of the degradation of three types of plastic pellets exposed to UV irradiation in three different environments*, 2018, Science of the Total Environment, pp. 740-747.
- [125] K. Vano-Herrera, A. Misiun, C. Vogt, *Preparation and characterization of poly(lactic acid)/poly(methyl-methacrylate) blend tablets for application in quantitative analysis by micro Raman spectroscopy*, 2015, Journal of Raman Spectroscopy, vol. 46, pp. 273-279.
- [126] R. B. Prime, H. E. Bair, S. Vyazovkin, P. K. Gallagher, A. Riga, *Thermal Analysis of Polymers: Fundamentals and Applications*, 2009, John Wiley & Sons, pp. 7-318.
- [127] Hyperlink "<http://dspace.unive.it/bitstream/handle/10579/7950/831990-1192110.pdf?sequence=2>" Accessed on 21th August.
- [128] Hyperlink "<https://www.zetalab.it/offerte-colorimetro-nozioni-colorimetro-htm/>" Accessed on 21th August.
- [129] Hyperlink "<http://www00.unibg.it/dati/corsi/60057/70709-UNI11182.pdf>" Accessed on 21th August.

[130] Hyperlink "https://www.unirc.it/documentazione/materiale_didattico/597_2011_290_12981.pdf" Accessed on 21th August.

[131] Hyperlink "<https://rdlab137.it/it/2019-06-06-09-01-40/invecchiamento-accelerato-e-normative.html>" Accessed on 14th August.

[132] A. Chabas, A. Fouqueau, M. Attoui, S. C. Alfaro, A. Petitmangin, A. Bouilloux, M. Saheb, A. Coman, T. Lombardo, N. Grand, ... S. Nowak, *Characterisation of CIME, an experimental chamber for simulating interactions between materials of the cultural heritage and the environment*, 2015, Environmental Science and Pollution Research, Volume 22, pp. 19170–19183.

[133] Hyperlink "<https://www.ensingerplastics.com/it-it/semilavorati/soluzioni-in-materiale-plastico/resistenza-chimica>" Accessed on 20th August.

[134] Hyperlink "https://www.sigmaaldrich.com/specification-sheets/182/275/438073-6X2.5L-PW_SIGALD.pdf" Accessed on 26th September.

[135] Hyperlink "<https://www.sigmaaldrich.com/IT/it/substance/glacialaceticacid600564197?context=product>" Accessed on 26th September.

[136] Hyperlink "<https://www.iso.org/standard/75824.html>" Accessed on 17th August.

[137] Hyperlink "<https://www.iso.org/standard/77424.html>" Accessed on 17th August.

[138] Hyperlink "<https://www.astm.org/Standards/D638>" Accessed on 17th August.

[139] G. Favaro, *Caratterizzazione meccanica sperimentale di materiali polimerici: confronto tra polimeri e biopolimeri*, 2010, Tesi di laurea triennale in Ingegneria Biomedica, pp. 43-49.

[140] Hyperlink "<https://www.zwickroell.com/it/settori-industriali/plastiche/materiali-termoplastici-e-termoindurenti-da-stampaggio/prove-di-trazione-iso-527-1-2/>" Accessed on 17th August.

[141] F. Carrasco, P. Pages, J. Gamez-Perez, O.O Santana, M.L. Maspoch, *Processing of poly(lactic acid): Characterization of chemical structure, thermal stability and mechanical properties*, 2010, Polymer Degradation and Stability, vol. 95, pp. 116-125.

[142] J.K. Lee, K.H. Lee, B.S. Jin, *Structure development and biodegradability of uniaxially stretched poly(L-lactide)*, 2001, European Polymer Journal, vol. 37, pp. 907-914.

- [143] J.Zhang, Y. Duan, H. Sato, H. Tsuji, I. Noda, S. Yan, Y. Ozaki, *Crystal Modifications and Thermal Behavior of Poly(L-lactic acid) Revealed by Infrared Spectroscopy*, 2005, *Macromolecules*, pp. 8012-8021.
- [144] D. Bermudez, P.A. Quinonez, E.J. Vasquez, I.A. Carrete, T.J. Word, D.A. Roberson, *A comparison of the physical properties of two commercial 3D printing PLA grades*, *Virtual and Physical Prototyping*, 2021, pp. 178-195.
- [145] E. Ferreira, C.B.B. Luna, D.D. Siqueira, E. M. Araujo, D. C. de Franca, R.M.R. Wellen, *Annealing effect on Pla/Eva performance*, 2021, *Journal of Polymers and the Environment*, pp. 1-14.
- [146] Hyperlink "https://people.unica.it/michelesaba/files/2018/09/Energia_di_superficie.pdf" Accessed on 21th August.
- [147] O. Laput, I. Vasenina, M. C. Salvadori, K. Savkin, D. Zuza, I. Kurzina, *Low-temperature plasma treatment of polylactic acid and PLA/HA composite material*, 2019, *Journal of Materials Science*, pp. 11726-11738.
- [148] E. A. S. González, D. Olmos, M. Á. Lorente, I Vélaz, J. González-Benito, *Preparation and Characterization of Polymer Composite Materials Based on PLA/TiO₂ for Antibacterial Packaging*, 2018, *Polymers*, pp. 2-14.
- [149] M. Ł. Maminski, I. Novák, M. Mičušík, A. Małolepszy, R. Toczyłowska-Maminska, *Discharge Plasma Treatment as an Efficient Tool for Improved Poly(lactide) Adhesive–Wood Interactions*, 2021, *Materials*, pp. 1-12.
- [150] M. Maiza, M.T. Benaniba, V. Massardier-Nageotte, *Plasticizing effects of citrate esters on properties of poly(lactic acid)*, 2006, *Journal Polymers Engineer*, pp. 371-380.
- [151] K. Yuniarto, Y. A. Purwanto, S. Purwanto, B. A. Welt, H. K. Purwadaria, T. C. Sunarti, *Infrared and Raman studies on polylactide acid and polyethylene glycol-400 blend*, 2016, *AIP Conference Proceedings*, pp. 1-6.
- [152] C. Chaiwong, P. Rachtanapun, P. Wongchaiya, R. Auras, D. Boonyawan, *Effect of plasma treatment on hydrophobicity and barrier property of polylactic acid*, 2010, *Surface & Coatings Technology*, pp. 2933-2939.
- [153] M. A. Cuiffo, J. Snyder, A. M. Elliott, N. Romero, S. Kannan, G. P. Halada, *Impact of the Fused Deposition (FDM) Printing Process on Polylactic Acid (PLA) Chemistry and Structure*, 2017, *Applied Sciences*, pp. 1-14.

- [154] J-C. Lee, D-H. Choi, J-Y. Choi, C-S. Ha, *Poly(lactic acid)/Functionalized Silica Hybrids by Reactive Extrusion: Thermal, Rheological, and Degradation Behavior*, 2019, Macromolecular Research, pp. 327-335.
- [155] S. Mallick, Z. Ahmad, F. Touati, J. Bhadra, R. Shakoor, N. Al-T., *PLA-TiO₂ nanocomposites: Thermal, morphological, structural, and humidity sensing properties*, 2018, Ceramics International, pp. 1-7.
- [156] C. Huang, C-H. Liu, S-Y. Wu, *Surface characterization of the SiO films prepared by a remote atmospheric pressure plasma jet*, 2008, Surface and interface analysis, pp. 44-48.
- [157] J. Shao, S. Xiang, X. Bian, J. Sun, G. Li, X. Chen, *Remarkable Melting Behavior of PLA Stereocomplex in Linear PLLA/PDLA Blends*, 2015, Industrial and Engineering Chemistry, pp. 2246-2253.
- [158] Y. Srisuwan, Y. Baimark, *Controlling stereocomplexation, heat resistance and mechanical properties of stereocomplex polylactide films by using mixtures of low and high molecular weight poly(D-lactide)s*, 2018, De Gruyter, pp. 485-490.
- [159] J. Narita, M. Katagiri, H. Tsuji, *Highly enhanced accelerating effect of melt-recrystallized stereocomplex crystallites on poly(L-lactic acid) crystallization: effects of molecular weight of poly(D-lactic acid)*, Society of Chemical Industry, pp. 936-948.
- [160] D. Rasselet, A. Ruellan, A. Guinault, G. Miquelard-Garnier, C. Sollogoub, B. Fayolle, *Oxidative degradation of polylactide (PLA) and its effects on physical and mechanical properties*, 2014, European Polymer Journal, pp. 109-116.
- [161] H. Abourayana, P. Dobbyn, D. Dowling, *Enhancing the mechanical performance of additive manufactured polymer components using atmospheric plasma pre-treatments*, 2017, Plasma Processes and Polymers, pp. 1-8.
- [162] J-W. Wee, M-S. Choi, H-C. Hyun, J-H. Hwang, B-H. Choi, *Effect of weathering-induced degradation on the fracture and fatigue characteristics of injection-molded polypropylene/talc composites*, 2018, International Journal of Fatigue, pp. 111-120.
- [163] M-Y. Jo, Yeon J. Ryu, J. H. Ko, J-S. Yoon, *Hydrolysis and Thermal Degradation of Poly(L-Lactide) in the Presence of Talc and Modified Talc*, 2012, Journal of Applied Polymers Science, pp. 1019-1025.
- [164] P. B. Linares, L. A. Castillo, S. E. Barbosa, *Pro-Degradant Effect of Talc Nanoparticles on Polypropylene Films*, 2019, Journal of Polymers and the Environment, pp. 1666-1676.

- [165] A. Belbella, C. Vauthier, H. Fessi, J.P. Devissaguet, F. Puisieux, *In vitro degradation of nanospheres from poly(D,L-lactides) of different molecular weights and polydispersities*, International Journal of Pharmaceutics, vol. 129, 2005, pp. 95-102.
- [166] Hyperlink "http://instructor.physics.lsa.umich.edu/adv-labs/Raman_Spectroscopy/Raman_spect.pdf" Accessed on 13th August.
- [167] Y. Qiu, X. Shao, C. Jensen, Y.J. Hwang, C. Zhang, M. G. McCord, *The effects of atmospheric pressure plasma treatments on adhesion and mechanical properties of high-performance fibers for composites*, Polymer Surface Modification: Relevance to Adhesion, Volume 3, pp. 3-24.
- [168] U. Schulz & G. Tjandraatmadja, *The Influence Of Rain And Humidity On The Lifetime Of Transparent Polymeric Roof Materials*, CSIRO Building Construction and Engineering Australia, pp. 2-10.
- [169] A. Güzel, *Photo-oxidative degradation of ABS copolymer*, Final thesis in Natural and Applied Science, 2009, p. 24.
- [170] C. Shih, *Chain-end scission in acid catalyzed hydrolysis of poly (d,l-lactide) in solution*, 1995, Journal of Controlled Release, pp. 9-15.
- [171] M. R. M. Saade, A. Yahia, B. Amor, *How has LCA been applied to 3D printing? A systematic literature review and recommendations for future studies*, 2019, Journal of Cleaner Production, pp. 1-23.
- [172] D. Hartwig, *Originali ricongiunti e copie tra Roma e Ann Arbor - Ipotesi per il Templum Gentis Flaviae*, 1994, Giunti Editore, pp. 149-158.
- [173] Hyperlink '<https://www.icdp.ucar.edu/using-pla-for-long-term-outdoor-applications/>' Accessed on 20th September.
- [174] J. Ren, *Biodegradable Poly(Lactic Acid): Synthesis, Modification, Processing and Applications*, 2010, Springer, pp. 208-239.
- [175] Hyperlink '<https://www.icdp.ucar.edu/using-pla-for-long-term-outdoor-applications/>' Accessed on 20th September.

